Third-Generation Systems and Intelligent Wireless Networking: Smart Antennas and Adaptive Modulation

by

©J.S. Blogh, L. Hanzo
Department of Electronics and Computer Science,
University of Southampton, UK

Contents

Introduction

Background and Overview

Wireless communications is experiencing an explosive growth rate. This high demand for wireless communications services requires increased system capacities. The simplest solution would be to allocate more bandwidth to these services, but the electromagnetic spectrum is a limited resource, which is becoming increasingly congested [1]. Furthermore, the frequency bands to be used for the Third Generation (3G) wireless services have been auctioned in various European countries, such as Germany and the UK at an extremely high price. Therefore, the efficient use of the available frequencies is paramount [1, 2].

The digital transmission techniques of the Second Generation (2G) mobile radio networks have already improved upon the capacity and voice quality attained by the analogue mobile radio systems of the first generation. However, more efficient techniques allowing multiple users to share the available frequencies are necessary. Classic techniques of supporting a multiplicity of users are frequency, time, polarisation, code or spatial division multiple access [3]. In Frequency Division Multiple Access [4,5] the available frequency spectrum is divided into frequency bands, each of which is used by a different user. Time Division Multiple Access (TDMA) [4, 5] allocates each user a given period of time, referred to as a time slot, over which their transmission may take place. The transmitter must be able to store the data to be transmitted and then transmit it at a proportionately increased rate during its time slot constituting a fraction of the TDMA frame duration. Alternatively, Code Division Multiple Access (CDMA) [4, 5] allocates each user a unique code. This code is then used to spread the data over a wide bandwidth shared with all users. For detecting the transmitted data the same unique code, often referred to as the user signature, must be used.

The increasing demand for spectrally efficient mobile communications systems motivates our quest for more powerful techniques. With the aid of spatial processing at a cell site, optimum receive and transmit beams can be used for improving the system's performance in terms of the achievable capacity and the quality of service measures. This approach is usually referred to as Spatial Division Multiple Access (SDMA) [3,6] which enables multiple users in the same cell to be accommodated on the same frequency and time slot by exploiting the spatial selectivity properties offered by adaptive antennas [7]. By contrast, if the desired signal and interferers occupy the same frequency band and time slot, then "temporal filtering" cannot be used for separating the signal from the interference. However, the desired and interfering signal usually originate from different spatial locations and this spatial separation may be exploited, in order to separate the desired signal from the interference using a

"spatially selective filter" at the receiver [8–10]. As a result, given a sufficiently large distance between two users communicating in the same frequency band, there will be negligible interference between them. The higher the number of cells in a region, due to using small cells, the more frequently the same frequency is re-used and hence higher teletraffic density per unit area can be carried.

However, the distance between co-channel cells must be sufficiently high, so that the intra-cell interference becomes lower than its maximum acceptable limit [3]. Therefore, the number of cells in a geographic area is limited by the base stations' transmission power level. A method of increasing the system's capacity is to use 120° sectorial beams at different carrier frequencies [11]. Each of the sectorial beams may serve the same number of users as supported in ordinary cells, while the Signal-to-Interference Ratio (SIR) can be increased due to the antenna's directionality. The ultimate solution, however, is to use independently steered high gain beams for supporting individual users [3].

Adaptive Quadrature Amplitude Modulation (AQAM) [12, 13] is another technique that is capable of increasing the spectral efficiency that may be achieved. The philosophy behind adaptive modulation is to select a specific modulation mode, from a set of modes, according to the instantaneous radio channel quality [12, 13]. Thus, if the channel quality exhibits a high instantaneous SINR, then a high-order modulation mode may be employed, enabling the exploitation of the temporarily high channel capacity. By contrast, if the channel has a low instantaneous SINR, using a high-order modulation mode would result in an unacceptable Frame Error Ratio (FER), and hence a more robust, but lower throughput modulation mode would be invoked. Hence, adaptive modulation not only combats the effects of a poor quality channel, but also attempts to maximise the throughput, whilst maintaining a given target FER. Thus, there is a trade-off between the mean FER and the data throughput, which is governed by the modem mode switching thresholds. These switching thresholds define the SINRs, at which the instantaneous channel quality requires changing the current modulation mode, i.e. where an alternative AQAM mode must be invoked.

A more explicit representation of the wideband AQAM regime is shown in Figure 1, which displays the variation of the modulation mode with respect to the pseudo SNR at channel SNRs of 10 and 20dB. In these figures, it can be seen explicitly that the lower-order modulation modes were chosen, when the pseudo SNR was low. In contrast, when the pseudo SNR was high, the higher-order modulation modes were selected in order to increase the transmission throughput. These figures can also be used to exemplify the application of wideband AQAM in an indoor and outdoor environment. In this respect, Figure 1(a) can be used to characterise a hostile outdoor environment, where the perceived channel quality was low. This resulted in the utilization of predominantly more robust modulation modes, such as BPSK and 4QAM. Conversely, a less hostile indoor environment is exemplified by Figure 1(b), where the perceived channel quality was high. As a result, the wideband AQAM regime can adapt suitably by invoking higher-order modulation modes, as evidenced by Figure 1(b). Again, this simple example demonstrated that wideband AQAM can be utilized, in order to provide a seamless, near-instantaneous reconfiguration between for example indoor and outdoor environments.

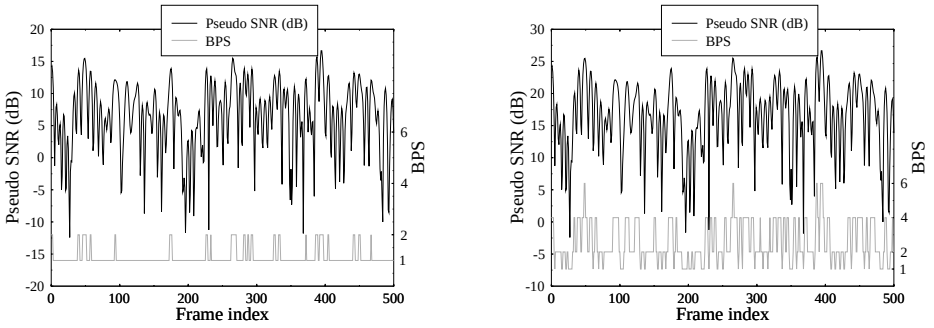

(a) Channel SNR of 10dB **(b)** Channel SNR of 20dB

Figure 1: Modulation mode variation with respect to the pseudo SNR evaluated at the output of the channel equaliser of a wideband AQAM modem for transmission over the **TU Rayleigh fading channel**. The BPS throughputs of 1, 2, 4 and 6 represent BPSK, 4QAM, 16QAM and 64QAM, respectively.

This book studies the network capacity gains that may be achieved with the advent of adaptive antenna arrays and adaptive modulation techniques in both FDMA / TDMA and CDMA based mobile cellular networks. The advantages of employing adaptive antennas are multifold, as outlined below.

Reduction of Co-channel Interference: Antenna arrays employed by the base station allow the implementation of spatial filtering, as shown in Figure 2, which may be exploited in both transmitting as well as receiving modes in order to reduce co-channel interferences [1, 2, 14, 15] experience in the uplink (UL) and downlink (DL) of wireless systems. When transmitting with an increased antenna gain in a certain direction of the DL, the base station's antenna is used to focus the radiated energy in order to form a high-gain directive beam in the area, where the mobile receiver is likely to be. This in turn implies that there is a reduced amount of radiated energy and hence reduced interference inflicted upon the mobile receivers roaming in other directions, where the directive beam has a lower gain. The co-channel interference generated by the base station in its transmit mode may be further reduced by forming beams exhibiting nulls in the directions of other receivers [6, 16]. This scheme deliberately reduces the transmitted energy in the direction of co-channel receivers and hence requires prior knowledge of their positions.

The employment of antenna arrays at the base station for reducing the co-channel interference in its receive mode has been also reported widely [1, 2, 6, 16–18]. This technique does not require explicit knowledge of the co-channel interference signal itself, however, it has to possess information concerning the desired signal, such as the direction of its source, a reference signal, such as a channel sounding sequence, or a signal that is higly correlated with the desired signal.

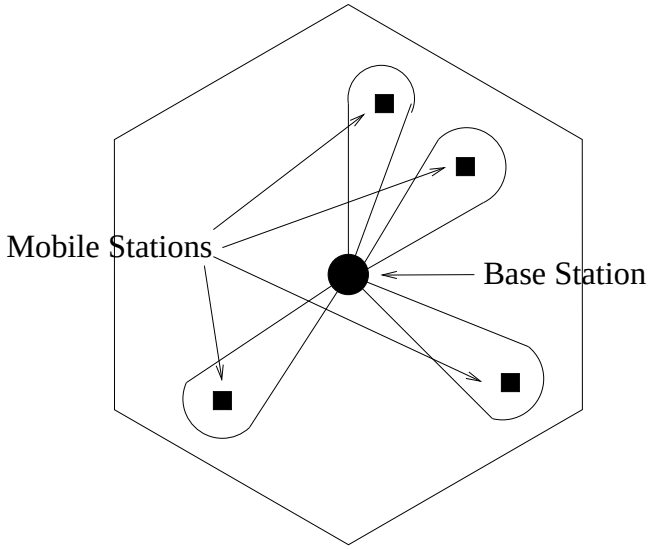

Figure 2: A cell layout showing how an antenna array can support many users on the same carrier frequency and timeslot with the advent of spatial filtering or Space Division Multiple Access (SDMA).

Capacity Improvement and Spectral Efficiency: The spectral efficiency of a wireless network refers to the amount of traffic a given system having a certain spectral allocation could handle. An increase in the number of users of the mobile communications system without a loss of performance increases the spectral efficiency. Channel capacity refers to the maximum data rate a channel of a given bandwidth can sustain. An improved channel capacity leads to an ability to support more users of a specified data rate, implying a better spectral efficiency. The increased quality of service that results from the reduced co-channel interference and reduced multipath fading [18,19] upon using smart antennae may be exchanged for an increased number of users [2,20].

Increase of Transmission Efficiency: An antenna array is directive in its nature, having a high gain in the direction where the beam is pointing. This property may be exploited in order to extend the range of the base station, resulting in a larger cell size or may be used to reduce the transmitted power of the mobiles. The employment of a directive antenna allows the base station to receive weaker signals than an omni-directional antenna. This implies that the mobile can transmit at a lower power and its battery recharge period becomes longer, or it would be able to use a smaller battery, resulting in a smaller size and weight, which is important for hand-held mobiles. A corresponding reduction in the power transmitted from the base station allows the use of electronic components having lower power ratings and therefore, lower cost.

Reduction of the Number of Handovers: When the amount of traffic in a cell

exceeds the cell's capacity, cell splitting is often used in order to create new cells [2], each with its own base station and frequency assignment. The reduction in cell size leads to an increase in the number of handovers performed. By using antenna arrays for increasing the user capacity of a cell [1] the number of handovers required may actually be reduced. More explicitly, since each antenna beam tracks a mobile [2], no handover is necessary, unless different beams using the same frequency cross each other.

Avoiding Transmission Errors: When the instantaneous channel quality is low, conventional fixed-mode transceivers typically inflict a burst of transmission errors. By contrast, adaptive transceivers avoid this problem by reducing the number of transmitted bits per symbol, or even by disableing transmissions temporarily. The associated throughput loss can be compensated by transmitting a higher number of bits per symbol during the periods of relatively high channel qualities. This advantageous property manifests itself also in terms of an improved service quality, which is quantified in the book in terms of the achievable video quality.

However, realistic propagation scenarios are significantly more complex than that depicted in Figure 2. Specifically, both the desired signal and the interference sources experience **multipath propagation**, resulting in a high number of received up-link signals impinging upon the base station's receiver antenna array. A result of the increased number of received up-link signals is that the limited degrees of freedom of the base station's adaptive antenna array are exhausted, resulting in reduced nulling of the interference sources. A solution to this limitation is to increase the number of antenna elements in the base station's adaptive array, although this has the side effect of raising the cost and complexity of the array. In a macro-cellular system it may be possible to neglect multipath rays arriving at the base station from interfering sources, since the majority of the scatterers are located close to the mobile station [21]. By contrast, in a micro-cellular system the scatterers are located in both the region of the reduced-elevation base station and that of the mobile, and hence multipath propagation must be considered. Figure 3 shows a realistic propagation environment for both the up- and the downlink, with the multipath components of the desired signal and interference signals clearly illustrated, where the up- and downlink multipath components were assumed to be identical for the sake of simplicity. Naturally, this is not always the case and hence we will investigate the potential performance gains, when the up- and downlink beamforms are determined independently.

The Outline of the Book

- **Chapter 1:** We commence by reviewing the state-of-the-art in near-instantaneously adaptive modulation and introduce the associated principles. We then apply the AQAM philosophy in the context of CDMA as well as OFDM and quantify the service-related benefits of adaptive transceivers in terms of the achievable video quality.

- **Chapter 2:** Following a brief introduction to the principles of CDMA the three most important 3G wireless standards, namely UTRA, IMT 2000 and cdma 2000 are characterised. The range of various transport and physical channels, the

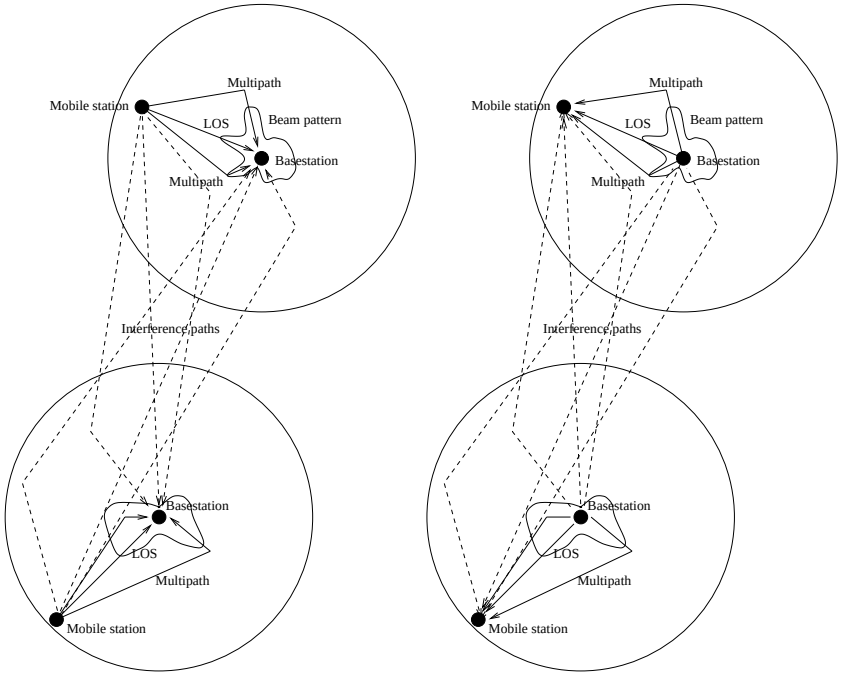

(a) Uplink. **(b)** Downlink.

Figure 3: The multipath environments of both the uplink and downlink, showing the multipath components of the desired signals, the line-of-sight interference and the associated base station antenna array beam patterns.

multiplexing of various services for transmission, the aspects of channel coding are discussed. The various options available for supporting variable-rates and a range quality of service are highlighted. The uplink and downlink modulation and spreading schemes are described and UTRA and IMT 2000 are compared in terms of the various solutions standardised. The chapter is closed with a similar portrayal of the pan-American cdma 2000 system.

- **Chapter 3:** The principles behind beamforming and the various techniques by which it may be implemented are presented. From this the concept of adaptive beamforming is developed, and temporal as well as spatial reference techniques are examined. Performance results are then presented for three different temporal-reference based adaptive beamforming algorithms, namely the Sample Matrix Inversion (SMI), Unconstrained Least Mean Squares (ULMS) and the Normalised Least Mean Squares (NLMS) algorithms.

- **Chapter 4:** A brief summary of possible methods used for modelling the performance of an adaptive antenna array is provided. This is followed by an overview

of fixed and dynamic channel allocation. Multipath propagation models are then considered for use in our network simulations. Metrics are then developed for characterising the performance of mobile cellular networks and our results are presented for simulations conducted under Line-Of-Sight (LOS) propagation conditions, both with and without adaptive antennas. Further results are then given for identical networks under multipath propagation conditions, which are then extended to power-controlled scenarios using both fixed and adaptive QAM techniques. These network capacity results were obtained for both "island" type simulation areas, and for an infinite plane, using wraparound techniques.

- **Chapter 5:** This chapter provides a brief description of the 3rd generation mobile cellular network, known as UTRA - the UMTS Terrestrial Radio Access - network, and then presents network capacity results obtained under various propagation conditions, in conjunction with different soft handover threshold metrics. The performance benefits of adaptive antenna arrays are then analysed, both in a non-shadowed environment, and inflicted by log-normal shadow fading having a frequencies of 0.5 Hz and 1.0 Hz . This work was then extended by the invoking of adaptive modulation techniques, which were studied when the channel conditions were impaired by shadow fading.
- **Chapter 6:** Conclusions and further work.

Contributions of the Book

- Providing an introduction to near-instantaneously adaptive modulation invoked in the context of both single- and multi-carrier modulation or OFDM, as well as CDMA.
- Quantifying the service-related benefits of adaptive transceivers in the context of wireless video telephony.
- Providing an overview of the various CDMA based 3G wireless standards.
- Study of the network performance gains using adaptive antenna arrays at the base station in an FDMA / TDMA cellular mobile network [22, 23].
- Study of the network performance gains using adaptive antenna arrays in conjunction with power control at the base station in an FDMA/TDMA cellular mobile network [24, 25].
- Design of a combined power control and adaptive modulation assisted channel allocation algorithm, and characterisation of its performance in an FDMA / TDMA cellular mobile network [25, 26].
- Comparing the performance of various UTRA soft-handover techniques.
- Quantifying the UTRA network capacity under various channel conditions.
- Evaluating the network performance of UTRA with the aid of adaptive antenna arrays.

- Demonstrating the benefits of adaptive modulation in the context of both FDMA / TDMA and CDMA cellular mobile networks.

Our hope is that the book offers you a range of interesting topics in the era of the imminent introduction of 3G wireless networks. We attempted to provide an informative technological roadmap, allowing the reader to quantify the achievable network capacity gains with the advent of introducing more powerful enabling technologies in the phisical layer. Analyzing the associated system design trade-offs in terms of network complexity and network capacity is the basic aims of this book. We aimed for underlining the range of contradictory system design trade-offs in an unbiased fashion, with the motivation of providing you with sufficient information for solving your own particular wireless networking problems. Most of all however we hope that you will find this book an enjoyable and relatively effortless reading, providing you with intellectual stimulation.

Jonathan Blogh and Lajos Hanzo
Department of Electronics and Computer Science
University of Southampton

Acknowledgments

We are indebted to our many colleagues who have enhanced our understanding of the subject, in particular to Prof. Emeritus Raymond Steele. These colleagues and valued friends, too numerous to be mentioned, have influenced our views concerning various aspects of wireless multimedia communications. We thank them for the enlightenment gained from our collaborations on various projects, papers, and books. We are grateful to Jan Brecht, Jon Blogh, Marco Breiling, Marco del Buono, Peter Cherriman, Stanley Chia, Byoung Jo Choi, Joseph Cheung, Peter Fortune, Sheyam Lal Dhomeja, Lim Dongmin, Dirk Didascalou, Stephan Ernst, Eddie Green, David Greenwood, Hee Thong How, Thomas Keller, Ee Lin Kuan, W. H. Lam, Matthias Münster, C. C. Lee, M. A. Nofal, Xiao Lin, Chee Siong Lee, Tong-Hooi Liew, Vincent Roger-Marchart, Redwan Salami, David Stewart, Clare Sommerville, Jeff Torrance, Spyros Vlahoyiannatos, William Webb, John Williams, Jason Woodard, Choong Hin Wong, Henry Wong, James Wong, Lie-Liang Yang, Bee-Leong Yeap, Mong-Suan Yee, Kai Yen, Andy Yuen, and many others with whom we enjoyed an association.

We also acknowledge our valuable associations with the Virtual Centre of Excellence in Mobile Communications, in particular with its chief executives, Dr. Tony Warwick and Dr. Walter Tuttlebee, and other members of its Executive Committee, namely Dr. Keith Baughan, Prof. Hamid Aghvami, Prof. Ed Candy, Prof. John Dunlop, Prof. Barry Evans, Dr. Mike Barnard, Prof. Joseph McGeehan, Prof. Peter Ramsdale and many other valued colleagues. Our sincere thanks are also due to the EPSRC, UK for supporting our research. We would also like to thank Dr. Joao Da Silva, Dr Jorge Pereira, Bartholome Arroyo, Bernard Barani, Demosthenes Ikonomou, and other valued colleagues from the Commission of the European Communities, Brussels, Belgium, as well as Andy Aftelak, Mike Philips, Andy Wilton, Luis Lopes, and Paul Crichton from Motorola ECID, Swindon, UK, for sponsoring some of our recent research. Further thanks are due to Tim Wilkinson at HP in Bristol for funding some of our research efforts.

Similarly, our sincere thanks are due to our Senior Editor, Mark Hammond and his colleagues at Wiley in Chichster, UK, who assisted us during the production of the book. Finally, our sincere gratitude is due to the numerous authors listed in the Author Index — as well as to those, whose work was not cited due to space limitations — for their contributions to the state of the art, without whom this book would not have materialized.

Jonathan Blogh and Lajos Hanzo
Department of Electronics and Computer Science
University of Southampton

Chapter 1

Burst-by-Burst Adaptive Wireless Transceivers

L. Hanzo, P.J. Cherriman, C.H. Wong, E.L. Kuan, T. Keller[1]

1.1 Motivation

In recent years the concept of intelligent multi-mode, multimedia transceivers (IMMT) has emerged in the context of wireless systems [27] and the range of various existing solutions that have found favour in existing standard systems was summarised in the excellent overview by Nanda *et al.* [28]. *The aim of these adaptive transceivers is to provide mobile users with the best possible compromise amongst a number of contradicting design factors, such as the power consumption of the hand-held portable station (PS), robustness against transmission errors, spectral efficiency, teletraffic capacity, audio/video quality and so forth [27].* In this introductory chapter we have to limit our discourse to a small subset of the associated wireless transceiver design issues, referring the reader for a deeper exposure to the literature cited [29]. A further advantage of the IMMTs of the near future is that due to their flexibility they are likely to be able to reconfigure themselves in various operational modes in order to ensure backwards compatibility with existing, so-called second generation standard wireless systems, such as the Japanese Digital Cellular [30], the Pan-American IS-54 [31] and IS-95 [32] systems, as well as the Global System of Mobile Communications (GSM) [11] standards.

[1] This chapter is based on L. Hanzo, C.H. Wong, P.J. Cherriman: Channel-adaptive wideband wireless video telephony, ©IEEE Signal Processing Magazine, July 2000; Vol. 17., No. 4, pp 10-30 and on
L. Hanzo, P.J. Cherriman, Ee Lin Kuan: Interactive cellular and cordless video telephony: State-of-the-art, system design principles and expected performance, ©IEEE Proceedings of the IEEE, Sept. 2000, pp 1388-1413

The fundamental advantage of burst-by-burst adaptive IMMTs is that - regardless of the propagation environment encountered - when the mobile roams across different environments subject to pathloss, shadow- and fast-fading, co-channel-, intersymbol- and multi-user interference, while experiencing power control errors, the system will always be able to configure itself in the highest possible throughput mode, whilst maintaining the required transmission integrity. Furthermore, whilst powering up under degrading channel conditions may disadvantage other users in the system, invoking a more robust - although lower throughput - transmission mode will not. The employment of the above burst-by-burst adaptive modems in the context of Code Division Multiple Access (CDMA) is fairly natural and it is motivated by the fact that all three third-generation mobile radio system proposals employ CDMA [11, 33, 34].

1.2 Narrowband Burst-by-Burst Adaptive Modulation

In burst-by-burst Adaptive Quadrature Amplitude Modulation (BbB-AQAM) a high-order, high-throughput modulation mode is invoked, when the instantaneous channel quality is favourable [13]. By contrast, a more robust lower order BbB-AQAM mode is employed, when the channel exhibits inferior quality, for improving the average BER performance. In order to support the operation of the BbB-AQAM modem, a high-integrity, low-delay feedback path has to be invoked between the transmitter and receiver for signalling the estimated channel quality perceived by the receiver to the remote transmitter. This strongly protected message can be for example superimposed on the reverse-direction messages of a duplex interactive channel. The transmitter then adjusts its AQAM mode according to the instructions of the receiver, in order to be able to meet its BER target.

A salient feature of the proposed BbB-AQAM technique is that regardless of the channel conditions, the transceiver achieves always the best possible multi-media source-signal representation quality - such as video, speech or audio quality - by automatically adjusting the achievable bitrate and the associated multimedia source-signal representation quality in order to match the channel quality experienced. The AQAM modes are adjusted on a near-instantaneous basis under given propagation conditions in order to cater for the effects of path-loss, fast-fading, slow-fading, dispersion, co-channel interference (CCI), multi-user interference, etc. Furthermore, when the mobile is roaming in a hostile out-door - or even hilly terrain - propagation environment, typically low-order, low-rate modem modes are invoked, while in benign indoor environments predominantly the high-rate, high source-signal representation quality modes are employed.

BbB-AQAM has been originally suggested by Webb and Steele [35], stimulating further research in the wireless community for example by Sampei *et al.* [36], showing promising advantages, when compared to fixed modulation in terms of spectral efficiency, BER performance and robustness against channel delay spread. Various systems employing AQAM were also characterised in [13]. The numerical upper bound performance of narrow-band BbB-AQAM over slow Rayleigh flat-fading channels was evaluated by Torrance *et al.* [37], while over wide-band channels by Wong *et*

al. [38]. Following these developments, the optimization of the BbB-AQAM switching thresholds was carried employing Powell-optimization using a cost-function, which was based on the combination of the target BER and target Bit Per Symbol (BPS) performance [39]. Adaptive modulation was also studied in conjunction with channel coding and power control techniques by Matsuoka *et al.* [40] as well as Goldsmith and Chua [41].

In the early phase of research more emphasis was dedicated to the system aspects of adaptive modulation in a narrow-band environment. A reliable method of transmitting the modulation control parameters was proposed by Otsuki *et al.* [42], where the parameters were embedded in the transmission frame's mid-amble using Walsh codes. Subsequently, at the receiver the Walsh sequences were decoded using maximum likelihood detection. Another technique of estimating the required modulation mode used was proposed by Torrance *et al.* [43], where the modulation control symbols were represented by unequal error protection 5-PSK symbols. The adaptive modulation philosophy was then extended to wideband multi-path environments by Kamio *et al.* [44] by utilizing a bi-directional Decision Feedback Equaliser (DFE) in a micro- and macro-cellular environment. This equalization technique employed both forward and backward oriented channel estimation based on the pre-amble and post-amble symbols in the transmitted frame. Equalizer tap gain interpolation across the transmitted frame was also utilized, in order to reduce the complexity in conjunction with space diversity [44]. The authors concluded that the cell radius could be enlarged in a macro-cellular system and a higher area-spectral efficiency could be attained for micro-cellular environments by utilizing adaptive modulation. The latency effect, which occurred, when the input data rate was higher than the instantaneous transmission throughput was studied and solutions were formulated using frequency hopping [45] and statistical multiplexing, where the number of slots allocated to a user was adaptively controlled.

In reference [46] symbol rate adaptive modulation was applied, where the symbol rate or the number of modulation levels was adapted by using $\frac{1}{8}$-rate 16QAM, $\frac{1}{4}$-rate 16QAM, $\frac{1}{2}$-rate 16QAM as well as full-rate 16QAM and the criterion used to adapt the modem modes was based on the instantaneous received signal to noise ratio and channel delay spread. The slowly varying channel quality of the uplink (UL) and downlink (DL) was rendered similar by utilizing short frame duration Time Division Duplex (TDD) and the maximum normalised delay spread simulated was 0.1. A variable channel coding rate was then introduced by Matsuoka *et al.* in conjunction with adaptive modulation in reference [40], where the transmitted burst incorporated an outer Reed Solomon code and an inner convolutional code in order to achieve high-quality data transmission. The coding rate was varied according to the prevalent channel quality using the same method, as in adaptive modulation in order to achieve a certain target BER performance. A so-called channel margin was introduced in this contribution, which adjusted the switching thresholds in order to incorporate the effects of channel quality estimation errors. As mentioned above, the performance of channel coding in conjunction with adaptive modulation in a narrow-band environment was also characterised by Chua and Goldsmith [41]. In this contribution, trellis and lattice codes were used without channel interleaving, invoking a feedback path between the transmitter and receiver for modem mode control purposes. The

effects of the delay in the feedback path on the adaptive modem's performance were studied and this scheme exhibited a higher spectral efficiency, when compared to the non-adaptive trellis coded performance.

Subsequent contributions by Suzuki *et al.* [47] incorporated space-diversity and power-adaptation in conjunction with adaptive modulation, for example in order to combat the effects of the multi-path channel environment at a 10Mbits/s transmission rate. The maximum tolerable delay-spread was deemed to be one symbol duration for a target mean BER performance of 0.1%. This was achieved in a Time Division Multiple Access (TDMA) scenario, where the channel estimates were predicted based on the extrapolation of previous channel quality estimates. Variable transmitted power was then applied in combination with adaptive modulation in reference [41], where the transmission rate and power adaptation was optimised in order to achieve an increased spectral efficiency. In this treatise, a slowly varying channel was assumed and the instantaneous received power required in order to achieve a certain upper bound performance was assumed to be known prior to transmission. Power control in conjunction with a pre-distortion type non-linear power amplifier compensator was studied in the context of adaptive modulation in reference [48]. This method was used to mitigate the non-linearity effects associated with the power amplifier, when QAM modulators were used.

Results were also recorded concerning the performance of adaptive modulation in conjunction with different multiple access schemes in a narrow-band channel environment. In a TDMA system, dynamic channel assignment was employed by Ikeda *et al.*, where in addition to assigning a different modulation mode to a different channel quality, priority was always given to those users in reserving time-slots, which benefitted from the best channel quality [49]. The performance was compared to fixed channel assignment systems, where substantial gains were achieved in terms of system capacity. Furthermore, a lower call termination probability was recorded. However, the probability of intra-cell hand-off increased as a result of the associated dynamic channel assignment (DCA) scheme, which constantly searched for a high-quality, high-throughput time-slot for the existing active users. The application of adaptive modulation in packet transmission was introduced by Ue, Sampei and Morinaga [50], where the results showed improved data throughput. Recently, the performance of adaptive modulation was characterised in conjunction with an automatic repeat request (ARQ) system in reference [51], where the transmitted bits were encoded using a cyclic redundant code (CRC) and a convolutional punctured code in order to increase the data throughput.

A recent treatise was published by Sampei, Morinaga and Hamaguchi [52] on laboratory test results concerning the utilization of adaptive modulation in a TDD scenario, where the modem mode switching criterion was based on the signal to noise ratio and on the normalised delay-spread. In these experimental results, the channel quality estimation errors degraded the performance and consequently a channel estimation error margin was devised, in order to mitigate this degradation. Explicitly, the channel estimation error margin was defined as the measure of how much extra protection margin must be added to the switching threshold levels, in order to minimise the effects of the channel estimation errors. The delay-spread also degraded the performance due to the associated irreducible BER, which was not compensated

by the receiver. However, the performance of the adaptive scheme in a delay-spread impaired channel environment was better, than that of a fixed modulation scheme. Lastly, the experiment also concluded that the AQAM scheme can be operated for a Doppler frequency of $f_d = 10$Hz with a normalised delay spread of 0.1 or for $f_d = 14$Hz with a normalised delay spread of 0.02, which produced a mean BER of 0.1% at a transmission rate of 1 Mbits/s.

Lastly, the latency and interference aspects of AQAM modems were investigated in [45, 53]. Specifically, the latency associated with storing the information to be transmitted during severely degraded channel conditions was mitigated by frequency hopping or statistical multiplexing. As expected, the latency is increased, when either the mobile speed or the channel SNR are reduced, since both of these result in prolonged low instantaneous SNR intervals. It was demonstrated that as a result of the proposed measures, typically more than 4dB SNR reduction was achieved by the proposed adaptive modems in comparison to the conventional fixed-mode benchmark modems employed. However, the achievable gains depend strongly on the prevalant co-channel interference levels and hence interference cancellation was invoked in [53] on the basis of adjusting the demodulation decision boundaries after estimating the interfering channel's magnitude and phase.

Having reviewed the developments in the field of narrowband AQAM, let us now consider wideband AQAM modems in the next section.

1.3 Wideband Burst-by-Burst Adaptive Modulation

In the above narrow-band channel environment, the quality of the channel was determined by the short-term SNR of the received burst, which was then used as a criterion in order to choose the appropriate modulation mode for the transmitter, based on a list of switching threshold levels, l_n [35–37]. However, in a wideband environment, this criterion is not an accurate measure for judging the quality of the channel, where the existence of multi-path components produces not only power attenuation of the transmission burst, but also intersymbol interference. Consequently, appropriate channel quality criteria have to be defined, in order to estimate the wideband channel quality for invoking the most appropriate modulation mode.

1.3.1 Channel quality metrics

The most reliable channel quality estimate is the BER, since it reflects the channel quality, irrespective of the source or the nature of the quality degradation. The BER can be estimated with a certain granularity or accuracy, provided that the system entails a channel decoder or - synonymously - Forward Error Correction (FEC) decoder employing algebraic decoding [11]. If the system contains a so-called soft-in-soft-out (SISO) channel decoder, such as a turbo decoder [54], the BER can be estimated with the aid of the Logarithmic Likelihood Ratio (LLR), evaluated either at the input or the output of the channel decoder. Hence a particularly attractive way of invoking LLRs is employing powerful turbo codecs, which provide a reliable indication of the confidence associated with a particular bit decision. The LLR is defined as the logarithm of the ratio of the probabilities associated with a specific bit

being binary zero or one. Again, this measure can be evaluated at both the input and the output of the turbo channel codecs and both of them can be used for channel quality estimation.

In the event that no channel encoder / decoder (codec) is used in the system, the channel quality expressed in terms of the BER can be estimated with the aid of the mean-squared error (MSE) at the output of the channel equaliser or the closely related metric, the Pseudo-Signal-to-noise-ratio (Pseudo-SNR) [38]. The MSE or pseudo-SNR at the output of the channel equaliser have the important advantage that they are capable of quantifying the severity of the inter-symbol-interference (ISI) and/or CCI experienced, in other words quantifying the Signal to Interference plus Noise Ratio (SINR).

In our proposed systems the wideband channel-induced degradation is combated not only by the employment of adaptive modulation but also by equalization. In following this line of thought, we can formulate a two-step methodology in mitigating the effects of the dispersive wideband channel. In the first step, the equalization process will eliminate most of the intersymbol interference based on a Channel Impulse Response (CIR) estimate derived using the channel sounding midamble and consequently, the signal to noise and residual interference ratio at the output of the equalizer is calculated.

We found that the residual channel-induced ISI at the output of the DFE is near-Gaussian distributed and that if there are no decision feedback errors, the pseudo-SNR at the output of the DFE, γ_{dfe} can be calculated as [38, 55]:

$$\begin{aligned} \gamma_{dfe} &= \frac{\text{Wanted Signal Power}}{\text{Residual ISI Power + Effective Noise Power}} \\ &= \frac{E\left[\left|S_k \sum_{m=0}^{N_f-1} C_m h_m\right|^2\right]}{\sum_{q=-(N_f-1)}^{-1} E\left[\left|f_q S_{k-q}\right|^2\right] + N_o \sum_{m=0}^{N_f-1} |C_m|^2}, \end{aligned} \tag{1.1}$$

where C_m and h_m denotes the DFE's feed-forward coefficients and the channel impulse response, respectively. The transmitted signal and the noise spectral density is represented by S_k and N_o. Lastly, the number of DFE feed-forward coefficients is denoted by N_f. By utilizing the pseudo-SNR at the output of the equalizer, we are ensuring that the system performance is optimised by employing equalization and AQAM [13] in a wideband environment according to the following switching regime:

$$\text{Modulation Mode} = \begin{cases} NoTX & \text{if } \gamma_{DFE} < f_0 \\ BPSK & \text{if } f_0 < \gamma_{DFE} < f_1 \\ 4QAM & \text{if } f_1 < \gamma_{DFE} < f_2 \\ 16QAM & \text{if } f_2 < \gamma_{DFE} < f_3 \\ 64QAM & \text{if } \gamma_{DFE} > f_3, \end{cases} \tag{1.2}$$

where $f_n, n = 0...3$ are the pseudo-SNR thresholds levels, which are set according to the system's integrity requirements and the modem modes may assume $0 \ldots 6$ bits/symbol transmissions corresponding to no transmissions (No TX), Binary Phase Shift Keying (BPSK), as well as 4- 16- and 64QAM [13]. We note, however that in

the context of the interactive BbB-AQAM videophone schemes introduced during our later discourse for quantifying the service-related benefits of such adaptive transceivers we refrained from employing the No Tx mode. This allowed us to avoid the associated latency of the buffering required for storing the information, until the channel quality improved sufficiently for allowing transmission of the buffered bits.

In references [56, 57] a range of novel Radial Basis Function (RBF) assisted BbB-AQAM channel equalisers have been proposed, which exhibit a close relationship with the so-called Bayesian schemes. Decision feedback was introduced in the design of the RBF equaliser in order to reduce its computational complexity. The RBF DFE was found to give similar performance to the conventional DFE over Gaussian channels using various BbB-AQAM schemes, while requiring a lower feedforward and feedback order. Over Rayleigh-fading channels similar findings were valid for binary modulation, while for higher order modems the RBF based DFE required an increased feedforward and feedback orders in order to outperform the conventional MSE DFE scheme. Then turbo BCH codes were invoked [56] for improving the associated BER and BPS performance of the scheme, which was shown to give a significant improvement in terms of the mean BPS performance compared to that of the uncoded RBF equaliser assisted adaptive modem. Finally, a novel turbo equalisation scheme was presented in [57], which employed an RBF DFE instead of the conventional trellis-based equaliser, which was advocated in most turbo equaliser implementations. The so-called Jacobian logarithmic complexity reduction technique was proposed, which was shown to achieve an identical BER performance to the conventional trellis-based turbo equaliser, while incurring a factor 4.4 lower 'per-iteration' complexity in the context of 4QAM.

In summary, in contrast to the narrowband, statically reconfigured multimode systems of [29], in this section wideband, near-instantaneously reconfigured or burst-by-burst adaptive modulation was invoked, in order to quantify the achievable service-related benefits, as perceived by users of such systems. More specifically, the achievable video performance benefits of wireless BbB-AQAM video transceivers will be quantified in this section, when using the H.263 video encoder [29]. Similar BbB-AQAM speech and audio transceivers were portrayed in [58].

It is an important element of the system that when the binary BCH [11] or turbo codes [54] protecting the video stream are overwhelmed by the plethora of transmission errors, the systems refrains from decoding the video packet in order to prevent error propagation through the reconstructed frame buffer [29]. Instead, these corrupted packets are dropped and the reconstructed frame buffer will not be updated, until the next packet replenishing the specific video frame area arrives. The associated video performance degradation is fairly minor for packet dropping or frame error rates (FER) below about 5%. These packet dropping events are signalled to the remote decoder by superimposing a strongly protected one-bit packet acknowledgement flag on the reverse-direction packet, as outlined in [29]. In the proposed scheme we also invoked the adaptive rate control and packetisation algorithm of [29], supporting constant Baud-rate operation.

Having reviewed the basic features of adaptive modulation, in the forthcoming section we will characterise the achievable service-related benefits of BbB-AQAM video transceivers, as perceived by the users of such systems.

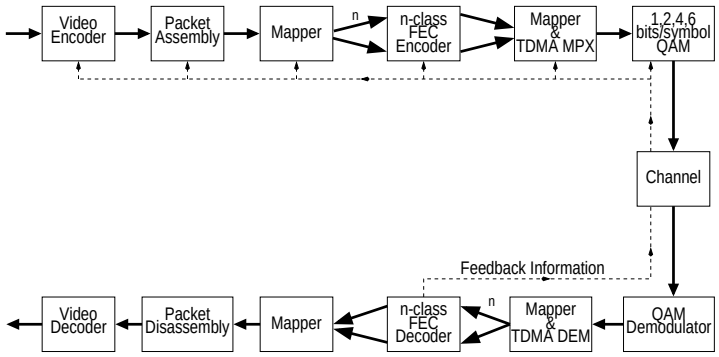

Figure 1.1: Reconfigurable transceiver schematic

1.4 Wideband BbB-AQAM Video Transceivers

Again, in this section we set out to demonstrate the service-quality related benefits of a wideband BbB-AQAM in the context of a wireless videophone system employing the programmable H.263 video codec in conjunction with an adaptive packetiser. The system's schematic is shown in Figure 1.1, which will be referred to in more depth during our further discourse.

In these investigations 176x144 pixel QCIF-resolution, 30 frames/s video sequences were transmitted, which were encoded by the H.263 video codec [29, 59] at bitrates resulting in high perceptual video quality. Table 1.1 shows the modulation- and channel parameters employed. The COST207 [60] four-path typical urban (TU) channel model was used, which is characterised by its CIR in Figure 1.2. We used the Pan-European FRAMES proposal [61] as the basis for our wideband transmission system, invoking the frame structure shown in Figure 1.3. Employing the FRAMES Mode A1 (FMA1) so-called non-spread data burst mode required a system bandwidth of 3.9MHz, when assuming a modulation excess bandwidth of 50% [13]. A range of other system parameters are shown in Table 1.2. Again, it is important to note that the proposed AQAM transceiver of Figure 1.1 requires a duplex system, since the AQAM mode required by the receiver during the next received video packet has to be signalled to the transmitter. In this system we employed TDD and the feedback path is indicated in dashed line in the schematic of Figure 1.1.

Again, the proposed video transceiver of Figure 1.1 is based on the H.263 video codec [59]. The video coded bitstream was protected by near-half-rate binary BCH coding [11] or by half-rate turbo coding [54] in all of the burst-by-burst adaptive wideband AQAM modes [13]. The AQAM modem can be configured either under network control on a more static basis, or under transceiver control on a near-instantaneous basis, in order to operate as a 1, 2, 4 and 6 bits/symbol scheme, while maintaining a constant signalling rate. This allowed us to support an increased throughput expressed in terms of the average number of bits per symbol (BPS, when the instantaneous channel quality was high, leading ultimately to an increased video quality in a constant bandwidth.

Parameter	Value
Carrier Frequency	1.9GHz
Vehicular Speed	30mph
Doppler frequency	85Hz
Norm. Doppler fr.	3.27×10^{-5}
Channel type	COST 207 Typ. Urban (Figure 1.2)
No. of channel paths	4
Data modulation	Adaptive QAM (BPSK, 4-QAM, 16-QAM, 64-QAM)
Receiver type	Decision Feedback Equalizer No. of Forward Filter Taps = 35 No. of Backward Filter Taps = 7

Table 1.1: Modulation and channel parameters

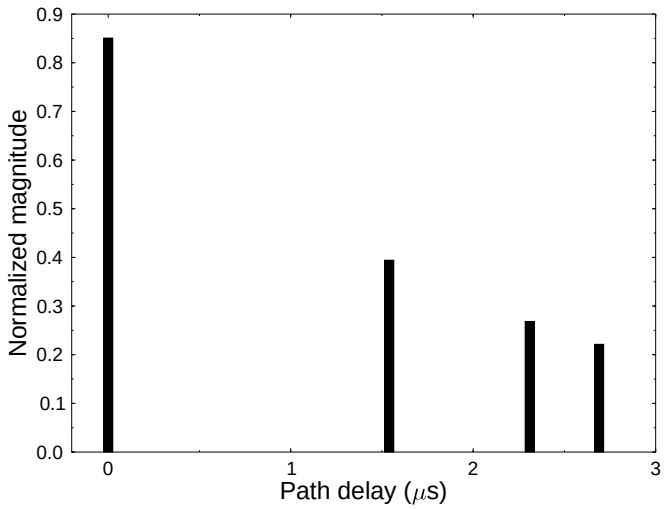

Figure 1.2: Normalized channel impulse response for the COST 207 [60] four-path Typical Urban (TU) channel.

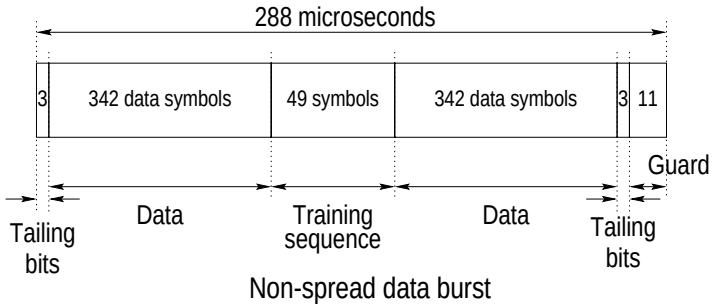

Figure 1.3: Transmission burst structure of the FMA1 non-spread data burst mode of the FRAMES proposal [61]

Features	**Value**
Multiple access	TDMA
Duplexing	TDD
No. of Slots/Frame	16
TDMA frame length	4.615ms
TDMA slot length	288μs
Data Symbols/TDMA slot	684
User Data Symbol Rate (KBd)	148.2
System Data Symbol Rate (MBd)	2.37
Symbols/TDMA slot	750
User Symbol Rate (KBd)	162.5
System Symbol Rate (MBd)	2.6
System Bandwidth (MHz)	3.9
Eff. User Bandwidth (kHz)	244

Table 1.2: Generic system features of the reconfigurable multi-mode video transceiver, using the non-spread data burst mode of the FRAMES proposal [61] shown in Figure 1.3.

The transmitted bitrate for all four modes of operation is shown in Table 1.3. The unprotected bitrate before approximately half-rate BCH coding is also shown in the table. The actual useful bitrate available for video is slightly less, than the unprotected bitrate due to the required strongly protected packet acknowledgement information and packetisation information. The effective video bitrate is also shown in the table.

In order to be able to invoke the inherently error-sensitive variable-length coded H.263 video codec in a high-BER wireless scenario, a flexible adaptive packetisation algorithm was necessary, which was highlighted in reference [29]. The technique proposed exhibits high flexibility, allowing us to drop corrupted video packets, rather than allowing errorneous bits to contaminate the reconstructed frame buffer of the H.263 codec. This measure prevents the propagation of errors to future video frames

Features	Multi-rate System			
Mode	BPSK	4QAM	16QAM	64QAM
Bits/Symbol	1	2	4	6
FEC	Near Half-rate BCH			
Transmission bitrate (kbit/s)	148.2	296.4	592.8	889.3
Unprotected bitrate (kbit/s)	75.8	151.7	303.4	456.1
Effective Video-rate (kbit/s)	67.0	141.7	292.1	446.4
Video fr. rate (Hz)	30			

Table 1.3: Operational-mode specific transceiver parameters

through the reconstructed frame buffer of the H.263 codec. More explicitly, corrupted video packets cannot be used by either the local or the remote H.236 decoder, since that would result in unacceptable video degradation over a prolonged period of time due to the error propagation inflicted by the associated motion vectors and run-length coding. Upon dropping the erroneous video packets, both the local and remote H.263 reconstruction frame buffers are updated by a blank packet, which corresponds to assuming that the video block concerned was identical to the previous one.

A key feature of our proposed adaptive packetisation regime is therefore the provision of a strongly error protected binary transmission packet acknowledgement flag [29], which instructs the remote decoder not to update the local and remote video reconstruction buffers in the event of a corrupted packet. This flag can be for example conveniently repetition-coded, in order to invoke Majority Logic Decision (MLD) at the decoder. Explicitly, the binary flag is repeated an odd number of times and at the receiver the MLD scheme counts the number of binary ones and zeros and opts for the logical value, constituting the majority of the received bits. These packet acknowledgement flags are then superimposed on the forthcoming reverse-direction packet in our advocated Time Division Duplex (TDD) regime [29] of Table 1.2, as seen in the schematic of Figure 1.1.

The proposed BbB-AQAM modem maximizes the system capacity available by using the most appropriate modulation mode for the current instantaneous channel conditions. As stated before, we found that the pseudo-SNR at the output of the channel equaliser was an adequate channel quality measure in our burst-by-burst adaptive wide-band modem. A more explicit representation of the wideband AQAM regime is shown in Figure 1.4, which displays the variation of the modulation mode with respect to the pseudo SNR at channel SNRs of 10 and 20dB. In these figures, it can be seen explicitly that the lower-order modulation modes were chosen, when the pseudo SNR was low. In contrast, when the pseudo SNR was high, the higher-order modulation modes were selected in order to increase the transmission throughput. These figures can also be used to exemplify the application of wideband AQAM in an indoor and outdoor environment. In this respect, Figure 1.4(a) can be used to characterise a hostile outdoor environment, where the perceived channel quality was

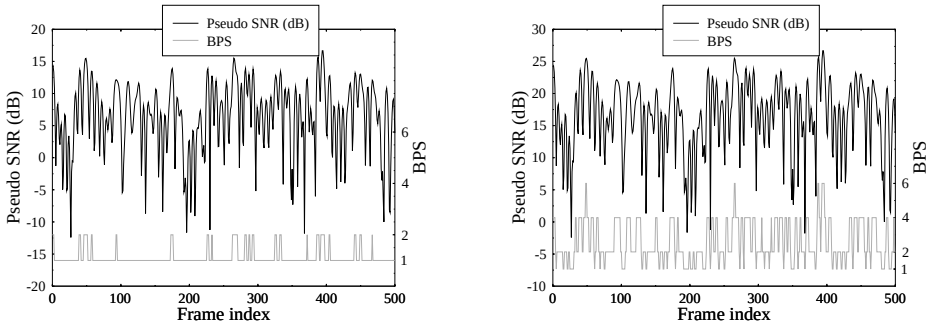

(a) Channel SNR of 10dB

(b) Channel SNR of 20dB

Figure 1.4: Modulation mode variation with respect to the pseudo SNR defined by Equation 1.1 over the **TU Rayleigh fading channel**. The BPS throughputs of 1, 2, 4 and 6 represent BPSK, 4QAM, 16QAM and 64QAM, respectively.

low. This resulted in the utilization of predominantly more robust modulation modes, such as BPSK and 4QAM. Conversely, a less hostile indoor environment is exemplified by Figure 1.4(b), where the perceived channel quality was high. As a result, the wideband AQAM regime can adapt suitably by invoking higher-order modulation modes, as evidenced by Figure 1.4(b). Again, this simple example demonstrated that wideband AQAM can be utilized, in order to provide a seamless, near-instantaneous reconfiguration between for example indoor and outdoor environments.

1.5 BbB-AQAM Performance

The mean BER and BPS performances were numerically calculated [38] for two different target BER systems, namely for the **High-BER** and **Low-BER** schemes, respectively. The results are shown in Figure 1.5 over the COST207 TU Rayleigh fading channel of Figure 1.2. The targeted mean BERs of the **High-BER** and **Low-BER** regime of 1% and 0.01% was achieved for all average channel SNRs investigated, since this scheme also invoked a no-transmission mode, when the channel quality was extremely hostile. In this mode only dummy data was transmitted, in order to facilitate monitoring the channel's quality.

At average channel SNRs below 20dB the lower-order modulation modes were dominant, producing a robust system in order to achieve the targeted BER. Similarly, at high average channel SNRs the higher-order modulation mode of 64QAM dominated the transmission regime, yielding a lower mean BER than the target, since no higher-order modulation mode could be legitimately invoked. This is evidenced by the modulation mode probability results shown in Figure 1.6 for the COST207 TU Rayleigh fading channel of Figure 1.2. The targeted mean BPS values for the

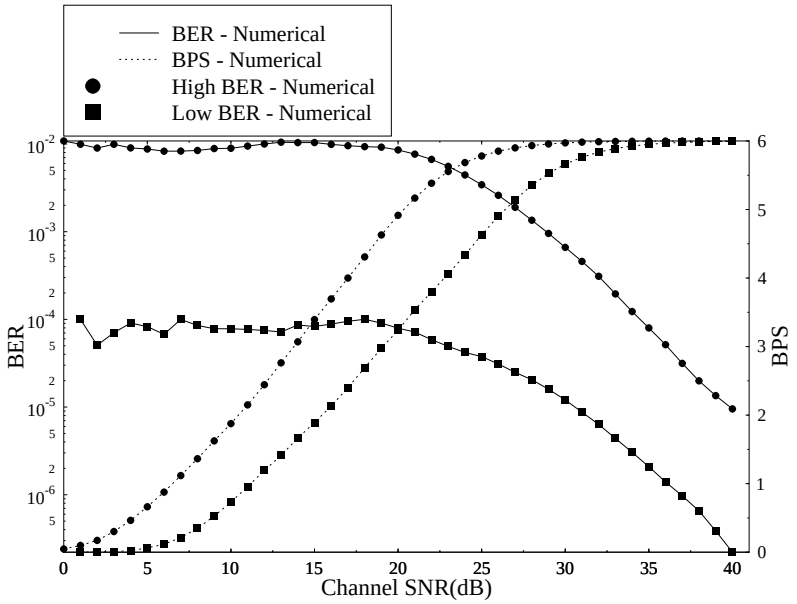

Figure 1.5: Numerical mean BER and BPS performance of the wideband equalized AQAM scheme for the **High-BER** and **Low-BER** regime over the COST207 TU Rayleigh fading channel.

High-BER and **Low-BER** regime of 4.5 and 3 were achieved at approximately 19dB channel SNR for the COST207 TU Rayleigh fading channels. However, at average channel SNRs below 3dB the above-mentioned no-transmission or transmission blocking mode was dominant in the **Low-BER** system and thus the mean BER performance was not recorded for that range of average channel SNRs.

The transmission throughput achieved for the **High-BER** and **Low-BER** transmission regimes is shown in Figure 1.7. The transmission throughput for the **High-BER** transmission regime was higher than that of the **Low-BER** transmission regime for the same transmitted signal energy due to the more relaxed BER requirement of the **High-BER** transmission regime, as evidenced by Figure 1.7. The achieved transmission throughput of the wideband AQAM scheme was higher than that of the BPSK, 4QAM and 16QAM schemes for the same average channel SNR. However, at higher average channel SNRs the throughput performance of both schemes converged, since 64QAM became the dominant modulation mode for the wideband AQAM scheme. SNR gains of $1-3$dB and $7-9$dB were recorded for the **High-BER** and **Low-BER** transmission schemes, respectively. These gains were considerably lower than those associated with narrow-band AQAM, where 5 - 7dB and 10 - 18dB of gains were reported for the **High-BER** and **Low-BER** transmission scheme, respectively [45, 53]. This was expected, since in the narrow-band environment the fluctuation of the instantaneous SNR was more severe, resulting in increased uti-

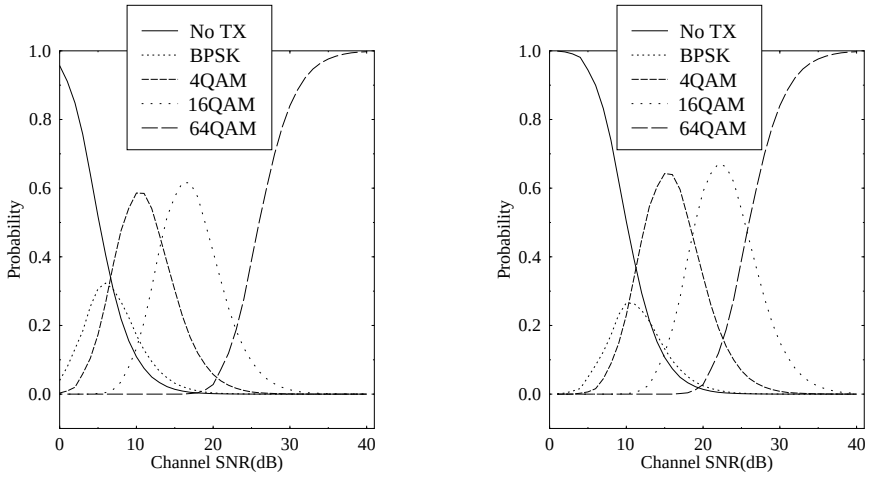

(a) High-BER transmission regime over the TU Rayleigh fading channel

(b) Low-BER transmission regime over the TU Rayleigh fading channel

Figure 1.6: Numerical probabilities of each modulation mode utilized for the wideband AQAM and DFE scheme over the **TU Rayleigh Fading channel** for the **(a) Low-BER Transmission** regime and **(b) Low-BER Transmission** regime.

lization of the modulation switching mechanism. Consequently, the instantaneous transmission throughput increased, whenever the fluctuations yielded a high received instantaneous SNR. Conversely, in a wideband channel environment the channel quality fluctuations perceived by the DFE were less severe due to the associated multi-path diversity, which was exploited by the equalizer.

Having characterised the wideband BbB-AQAM modem's performance, let us now consider the entire video transceiver of Figure 1.1 and Tables 1.1-1.3 in the next section.

1.6 Wideband BbB-AQAM Video Performance

As a benchmarker, the statically reconfigured modems of references [29] were invoked in Figure 1.8, in order to indicate, how a system would perform, which cannot act on the basis of the near-instantaneously varying channel quality. As it can be inferred from Figure 1.8, such a statically reconfigured transceiver switches its mode of operation from a lower-order modem mode, such as for example BPSK to a higher-order mode, such as 4QAM, when the channel quality has improved sufficiently for the

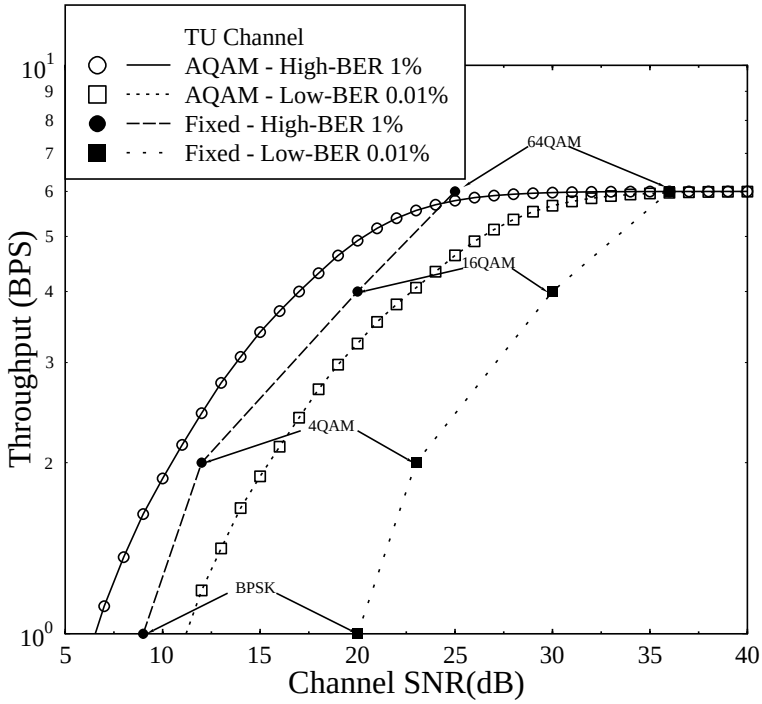

Figure 1.7: Transmission throughput of the wideband AQAM and DFE scheme and fixed modulation modes over the **TU Rayleigh Fading channel** for both the **High-BER** and **Low-BER** transmission regimes.

4QAM mode's FER to become lower than 5 % after reconfiguring the transceiver in this more long-term 4QAM mode.

In order to assess the effects of imperfect channel estimation on BbB-AQAM we considered two scenarios. In the first scheme the adaptive modem always chose the perfectly estimated AQAM modulation mode, in order to provide a maximum upper bound performance. In the second scenario the modulation mode was based upon the perfectly estimated AQAM modulation mode for the previous burst, which corresponded to a delay of one TDMA frame duration of 4.615ms. This second scenario represents a practical burst-by-burst adaptive modem, where the one-frame channel quality estimation latency is due to superimposing the receiver's required AQAM mode on a reverse-direction packet, for informing the transmitter concerning the best mode to be used for maintaining the target performance.

Figure 1.8 demonstrates on a logarithmic scale that the 'one-frame channel estimation delay' AQAM modem manages to maintain a similar FER performance to

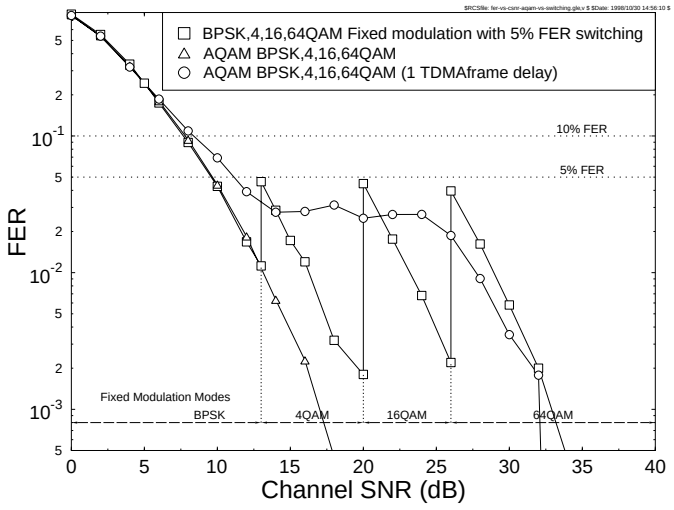

Figure 1.8: Transmission FER (or packet loss ratio) versus Channel SNR comparison of the four fixed modulation modes (BPSK, 4QAM, 16QAM, 64QAM) with 5% FER switching and adaptive burst-by-burst modem (AQAM). AQAM is shown with a realistic one TDMA frame delay between channel estimation and mode switching, and a zero delay version is included as an upper bound. The channel parameters were defined in Table 1.1 and near-half-rate BCH coding was employed [62] Cherriman, Wong, Hanzo, 2000 ©IEEE.

the fixed rate BPSK modem at low SNRs, although we will see during our further discourse that AQAM provides increasingly higher bitrates, reaching six times higher values than BPSK for high channel SNRs, where the employment of 64QAM is predominant. In this high-SNR region the FER curve asymptotically approaches the 64QAM FER curve for both the realistic and the ideal AQAM scheme, although this is not visible in the figure for the ideal scheme, since this occures at SNRs outside the range of Figure 1.8. Again, the reason for this performance discrepancy is the occasionally misjudged channel quality estimates of the realistic AQAM scheme. Additionally, Figure 1.8 indicates that the realistic AQAM modem exhibits a near-constant 3% FER at medium SNRs. The issue of adjusting the switching thresholds in order to achieve the target FER will be addressed in detail at a later stage in this section and the thresholds invoked will be detailed with reference to Table 1.4. Suffice to say at this stage that the average number of bits per symbol - and potentially also the associated video quality - can be increased upon using more "aggressive" switching thresholds. However, this results in an increased FER, which tends to decrease the video quality, as it will be discussed later in this section. Having shown the effect of the BbB-AQAM modem on the transmission FER, let us now demonstrate the effects of the AQAM switching thresholds on the system's performance in terms of the associated FER performance.

	BPSK	4QAM	16QAM	64QAM
Standard	<10dB	≥10dB	≥18dB	≥24dB
Conservative	<13dB	≥13dB	≥20dB	≥26dB
Aggressive	<9dB	≥9dB	≥17dB	≥23dB

Table 1.4: SINR estimate at output of the equaliser required for each modulation mode in Burst-by-Burst Adaptive modem, ie. switching thresholds

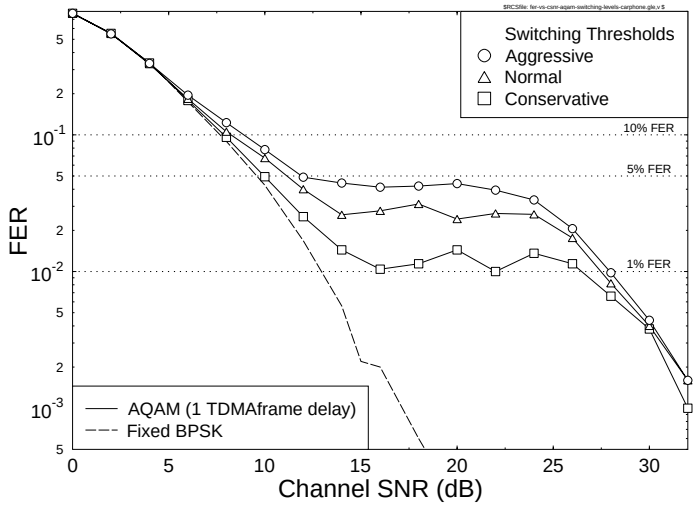

Figure 1.9: Transmission FER (or packet loss ratio) versus Channel SNR comparison of the fixed BPSK modulation mode and the adaptive burst-by-burst modem (AQAM) for the three sets of switching thresholds described in Table 1.4. AQAM is shown with a realistic one TDMA frame delay between channel estimation and mode switching. The channel parameters were defined in Table 1.1 [62] Cherriman, Wong, Hanzo, 2000 ©IEEE.

1.6.1 AQAM Switching Thresholds

The set of switching thresholds used in all the previous graphs was the "standard" set shown in Table 1.4, which was determined on the basis of the required channel SINR for maintaining the specific target video FER. In order to investigate the effect of different sets of switching thresholds, we defined two new sets of thresholds, a more "conservative" set, and a more "aggressive" set, employing less robust, but more bandwidth-efficient modem modes at lower SNRs. The more conservative switching thresholds reduced the transmission FER at the expense of a lower effective video bitrate. By contrast, the more aggressive set of thresholds increased the effective video bitrate at the expense of a higher transmission FER. The transmission FER performance of the realistic burst-by-burst adaptive modem, which has a one TDMA frame delay between channel quality estimation and mode switching is shown in Fig-

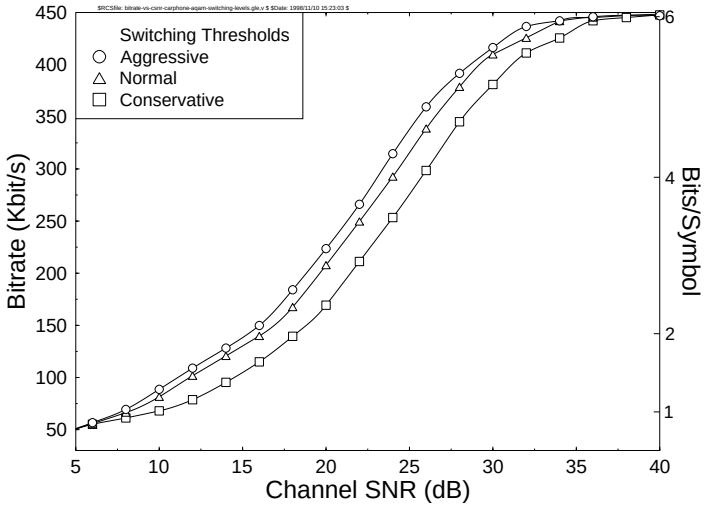

Figure 1.10: Video bitrate versus channel SNR comparison for the adaptive burst-by-burst modem (AQAM) with a realistic one TDMA frame delay between channel estimation and mode switching for the three sets of switching thresholds as described in Table 1.4. The channel parameters were defined in Table 1.1 [62] Cherriman, Wong, Hanzo, 2000 ©IEEE.

ure 1.9 for the three sets of switching thresholds of Table 1.4. It can be seen that the more "conservative" switching thresholds reduce the transmission FER from about 3% to about 1% for medium channel SNRs, while the more "aggressive" thresholds increase the transmission FER from about 3% to 4-5%. However, since FERs below 5% are not objectionable in video quality terms, this FER increase is an acceptable compromise for attaining a higher effective video bitrate.

The effective video bitrate for the realistic adaptive modem with the three sets of switching thresholds is shown in Figure 1.10. The more conservative set of switching thresholds reduces the effective video bitrate but also reduces the transmission FER. The aggressive switching thresholds increase the effective video bitrate, but also increase the transmission FER. Therefore the optimal switching thresholds should be set such that the transmission FER is deemed acceptable in the range of channel SNRs considered. Let us now consider the performance improvements achievable, when employing powerful turbo codecs.

1.6.2 Turbo-coded AQAM videophone performance

Let us now demonstrate the additional performance gains that are achievable, when a somewhat more complex turbo codec [54] is used in comparison to similar-rate algebraically decoded binary BCH codecs [11]. The generic system parameters of the turbo-coded reconfigurable multi-mode video transceiver are the same as those used in

Features	Multi-rate System			
Mode	BPSK	4QAM	16QAM	64QAM
Bits/Symbol	1	2	4	6
FEC	Half-Rate Turbo coding with CRC			
Transmission bitrate (kbit/s)	140.4	280.8	561.6	842.5
Unprotected bitrate (kbit/s)	66.3	136.1	275.6	415.2
Effective Video-rate (kbit/s)	60.9	130.4	270.0	409.3
Video fr. rate (Hz)	30			

Table 1.5: Operational-mode specific turbo-coded transceiver parameters

the BCH-coded version summarised in Table 1.2. Turbo-coding schemes are known to perform best in conjunction with square-shaped turbo interleaver arrays and their performance is improved upon extending the associated interleaving depth, since then the two constituent encoders are fed with more independent data. This ensures that the turbo decoder can rely on two quasi-independent data streams in its efforts to make as reliable bit decisions, as possible. A turbo interleaver size of 18×18 bits was chosen, requiring 324 bits for filling the interleaver. The required so-called recursive systematic convolutional (RSC) component codes had a coding rate of 1/2 and a contraint length of $K = 3$. After channel coding the transmission burst length became 648 bits, which facilitated the decoding of all AQAM transmission bursts independently. The operational-mode specific turbo transceiver parameter are shown in Table 1.5, which should be compared to the corresponding BCH-coded parameters of Table 1.3. The turbo-coded parameters result in a 10% lower effective throughput bitrate compared to the similar-rate BCH-codecs under error-free conditions. However, Figure 1.11 demonstrates that the PSNR video quality versus channel SNR performance of the turbo-coded AQAM modem becomes better than that of the BCH-coded scenario, when the channel quality degrades. Having highlighted the operation of wideband single-carrier burst-by-burst AQAM modems, let us now consider briefly in the next two sections, how the above burst-by-burst adaptive principles can be extended to CDMA and Orthogonal Frequency Division Multiplex (OFDM) systems [13, 63].

1.7 Burst-by-burst Adaptive Joint-detection CDMA Video Transceiver

1.7.1 Multi-user Detection for CDMA

The effects of multi-user interference (MAI) are similar to those of the Intersymbol Interference (ISI) inflicted by the multipath propagation channel. More specifically, each user in a K-user system will suffer from MAI due to the other $(K-1)$ users. This MAI can also be viewed as a single user's signal contaminated by the ISI due to $(K-1)$

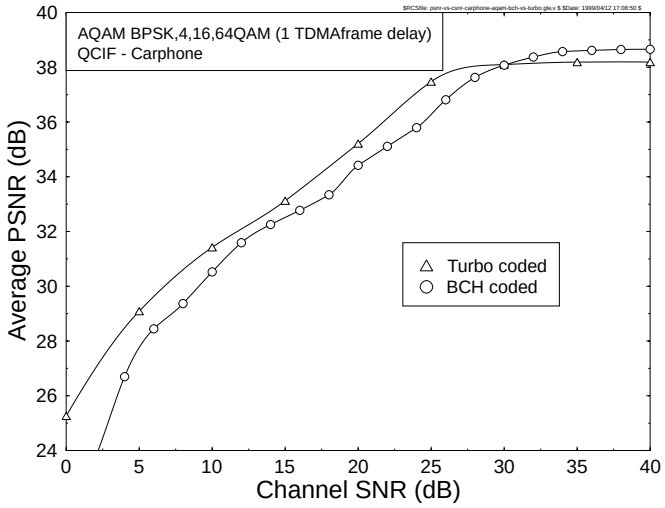

Figure 1.11: Decoded video quality (PSNR) versus transmission FER (or packet loss ratio) comparison of the realistic adaptive burst-by-burst modems (AQAM) using either BCH or turbo coding. The channel parameters were defined in Table 1.1 [62] Cherriman, Wong, Hanzo, 2000 ©IEEE.

propagation paths in a multipath channel. Therefore, conventional equalization techniques used to mitigate the effects of ISI can be modified for employment in multiuser detection assisted CDMA systems. The so-called joint detection (JD) receivers constitute a category of multiuser detectors developed for synchronous burst-based CDMA transmissions and they utilize these techniques.

Figure 1.12 depicts the block diagram of a synchronous joint-detection assisted CDMA system model for up-link transmissions. There are a total of K users in the system, where the information is transmitted in bursts. Each user transmits N data symbols per burst and the data vector for user k is represented as $\mathbf{d^{(k)}}$. Each data symbol is spread with a user-specific spreading sequence, $\mathbf{c^{(k)}}$, which has a length of Q chips. In the uplink, the signal of each user passes through a different mobile channel characterized by its time-varying complex impulse response, $\mathbf{h^{(k)}}$. By sampling at the chip rate of $1/T_c$, the impulse response can be represented by W complex samples. Following the approach of Klein *et al.* [64], the received burst can be represented as $\mathbf{y} = \mathbf{Ad} + \mathbf{n}$, where $\mathbf{y}$ is the received vector and consists of the synchronous sum of the transmitted signals of all the K users, corrupted by a noise sequence, $\mathbf{n}$. The matrix $\mathbf{A}$ is referred to as the system matrix and it defines the system's response, representing the effects of MAI and the mobile channels. Each column in the matrix represents the combined impulse response obtained by convolving the spreading sequence of a user with its channel impulse response, $\mathbf{b^{(k)}} = \mathbf{c^{(k)}} * \mathbf{h^{(k)}}$. This is the impulse response experienced by a transmitted data symbol. Upon neglecting the effects of the noise the joint detection formulation is simply based on inverting the system matrix $\mathbf{A}$, in order

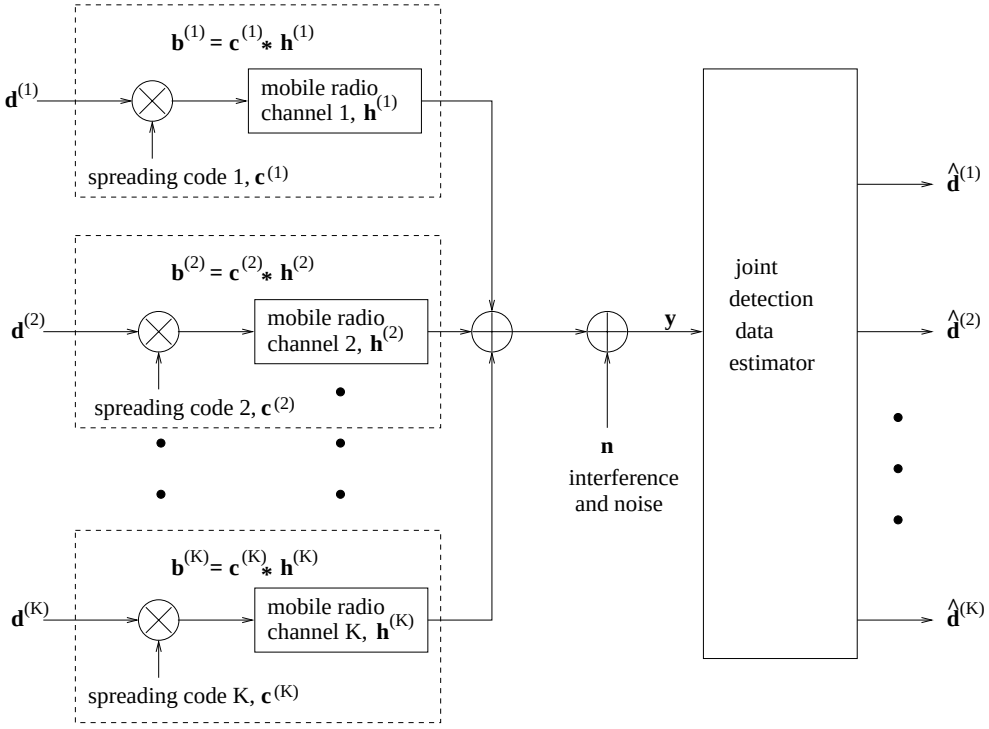

Figure 1.12: System model of a synchronous CDMA system on the up-link using joint detection.

to recover the data vector constituted by the superimposed transmitted information of all the K CDMA users.

1.7.2 JD-ACDMA Modem Mode Adaptation and Signalling

In mobile communications systems typically power control techniques are used to mitigate the effects of path loss and slow fading. However, in order to counteract the problem of fast fading and co-channel interference, agile and tight-specification power control algorithms are required [65]. Another technique that can be used to overcome the problems due to fading is adaptive-rate transmission, [35, 66] where the information rate is varied according to the quality of the channel.

Different methods of multi-rate transmission have been proposed by Ottosson and Svensson [67]. According to the multi-code method, multiple codes are assigned to a user requiring a higher bit rate [67]. Multiple data rates can also be provided by a multiple processing-gain scheme, where the chip rate is kept constant but the data rates are varied by changing the processing gain of the spreading codes assigned to the users. Performance comparisons for both of these schemes have been carried out by Ottosson *et al.* [67] and Ramakrishna *et al.* [68], demonstrating that both schemes achieved similar performance. Saquib *et al.* [69] and Johansson *et al.* [70] have also

investigated the employment of the so-called decorrelating detector and the successive interference cancellation receiver for multi-rate CDMA systems.

Adaptive rate transmission schemes, where the transmission rate is adapted according to the channel quality have also been proposed. Abeta *et al.* [71] have conducted investigations into an adaptive CDMA scheme, where the transmission rate is modified by varying the channel code rate and the processing gain of the CDMA user, employing the carrier to interference and noise ratio (CINR) as the switching metric. In their investigations, the overall packet rate was kept constant by transmitting in shorter bursts, when the transmission bit rate was high and lengthening the burst, when the bit rate was low. This resulted in a decrease in interference power, which translated to an increase in system capacity. Hashimoto *et al.* [72] extended this work to show that the proposed system was capable of achieving a higher capacity with a smaller hand-off margin and lower average transmitter power. In these schemes, the conventional RAKE receiver was used for the detection of the data symbols. Kim [66] analyzed the performance of two different methods of combatting the mobile channel's variations, which were the adaptation of the transmitter power to compensate for channel variations or the switching of the information rate to suit the channel conditions. Using a RAKE receiver, it was demonstrated that rate adaptation provided a higher average information rate, than power adaptation for a given average transmit power and a given BER.

In our design example here we also propose to vary the information rate in accordance with the channel quality. However, in comparison to conventional power control techniques - which may disadvantage other users by increasing their transmitted powers in an effort to maintain the quality of their own links - the JD-AQAM scheme employed does not disadvantage other users. This is achieved by 'non-destructively' adjusting the modulation mode of the user supported accoding to the near-instantaneous channel quality experienced. Additionally, burst-by-burst adaptive transceivers are capable of increasing the network capacity, as we will demonstrate it in the book. This is, because conventional transceivers would drop a call, when the interference levels become excessive. By contrast, adaptive transceivers reconfigure themselves in a more robust coding/modulation mode.

In this section we will quantify the expected video performance of a range of intelligent multi-mode CDMA transceivers, employing joint detection (JD) multi-user reception CDMA techniques at the BS, which are optional in the 3G system proposals due to their high implementational complexity and hence are likely to be employed only in future implementations of the 3G standards. As a potential further future enhancement, we will also invoke the powerful principle of burst-by-burst adaptive JD-CDMA (JD-ACDMA) transmissions, which was discussed in some depth in Section 1.7. Burst-by-burst adaptive transmissions can be readily accommodated by JD-CDMA receivers, as it will be augmented in more detail below. The duplex JD-ACDMA video transceiver used in our system design example operates on the basis of the following philosopy:

- The channel quality estimation is based on evaluating the Mean Squared Error (MSE) at the output of the JD-CDMA multi-user equaliser at the receiver, as suggested for wideband single-carrier Kalman-filtered DFE-based modems by Liew, Wong *et al.* in [73].

- The decision concerning the modem mode to be used by the local transmitter for the forthcoming CDMA transmission burst is based on the prediction of the expected channel quality.

- Specifically, if the channel quality can be considered predictable, then the channel quality estimate for the uplink can be extracted from the received signal and *the receiver instructs the local transmitter as to what modem mode to use in its next transmission burst. We refer to this regime as open–loop adaptation.* In this case, the transmitter has to explicitly signal the modem modes to the receiver.

- By contrast, if the channel cannot be considered reciprocal, then the channel quality estimation is still performed at the receiver, but *the receiver has to instruct the remote transmitter as to what modem modes have to be used at the transmitter, in order to meet the target integrity requirements of the receiver. We refer to this mode as closed–loop adaptation.*

1.7.3 The JD-ACDMA Video Transceiver

In this JD-CDMA system performance study we transmitted 176x144 pixel Quarter Common Intermediate Format (QCIF) and 128x96 pixel Sub-QCIF (SQCIF) video sequences at 10 frames/s using a reconfigurable Time Division Multiple Access / Code Division Multiple Access (TDMA / CDMA) transceiver, which can be configured as a 1, 2 or 4 bit/symbol scheme. The H.263 video codec [74] extensively employs variable-length compression techniques and hence achieves a high compression ratio. However, as all entropy- and variable-length coded bit streams, its bits are extremely sensitive to transmission errors.

This error sensitivity was counteracted in our system by invoking the adaptive video packetisation and video packet dropping regime of [75], when the channel codec protecting the video stream became incapable of removing all channel errors. Specifically, we refrained from decoding the corrupted video packets in order to prevent error propagation through the reconstructed video frame buffer [74, 75]. Hence - similarly to our AQAM / TDD -based system design example - these corrupted video packets were dropped at both the transmitter and receiver and the reconstructed video frame buffer was not updated, until the next video packet replenishing the specific video frame area was received. This required a low-delay, strongly protected video packet acknowledgement flag, which was superimposed on the transmitted payload packets [75]. As in the system design example of the previous section, the associated video performance degradation was found perceptually unobjectionable for transmission burst error rates below about 5%.

The associated JD-ACDMA video system parameters are summarised in Table 1.6, which will be addressed in more depth during our further discourse. Employing a low spreading factor of 16 allowed us to improve the system's multi-user performance with the aid of joint-detection techniques [76], whilst imposing a realistic implementational complexity. This is because the JD operation is based on inverting the system matrix, which is constructed from the convolution of the channel's impulse response (CIR) and the spreading codes. Hence maintaining a low spreading factor (SF) is

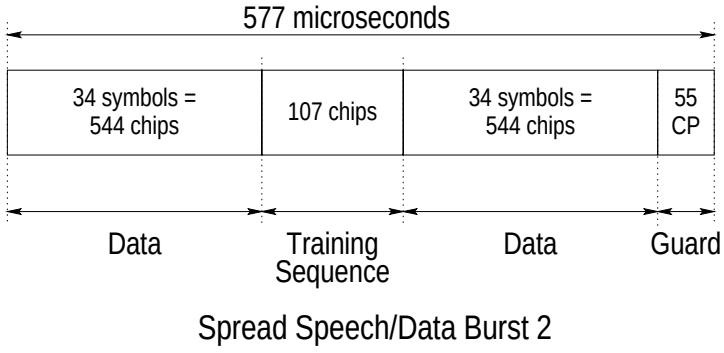

Figure 1.13: Transmission burst structure of the FMA1 spread speech/data mode 2 of the FRAMES proposal [61]

critical as to the implementational complexity. We note furthermore that the implementation of the joint detection receivers is independent of the number of bits per symbol associated with the modulation mode used, since the receiver simply inverts the associated system matrix and invokes a decision concerning the received symbol, irrespective of how many bits per symbol were used. *Therefore, joint detection receivers are amenable to amalgamation with the above 1, 2 and 4 bit/symbol CDMA modem, since they do not have to be reconfigured each time the modulation mode is switched.*

In this performance study we used the Pan-European FRAMES proposal [61] as the basis for our CDMA system. The associated transmission burst structure is shown in Figure 1.13, while a range of generic system parameters are summarised in Table 1.6. In our performance studies we used the COST207 [60] seven-path bad urban (BU) channel model, whose impulse response is portrayed in Figure 1.14.

Again, the remaining generic system parameters are defined in Table 1.6. In our JD-ACDMA design example we investigated the performance of a multi-mode convolutionally coded video system employing joint detection, while supporting two users. The associated convolutional codec parameters are summarised in Table 1.7 along with the operational-mode specific transceiver parameters of the multi-mode JD-ACDMA system. As seen in Table 1.7, when the channel is benign, the unprotected video bit rate will be approximately 26.9kbit/s in the 16QAM/JD-CDMA mode. However, as the channel quality degrades, the modem will switch to the BPSK mode of operation, where the video bit rate drops to 5kbit/s and for maintaining a reasonable video quality, the video resolution has to be reduced to SQCIF (128x96 pels).

1.7.4 JD-ACDMA video transceiver performance

The burst-by-burst adaptive JD-ACDMA scheme of our design example maximizes the system's throughput expressed in terms of the number of bits per transmitted non-binary symbol by allocating the highest possible number of bits to a symbol based on the receiver's perception concerning the instantaneous channel quality. When the

Table 1.6: Generic system parameters using the FRAMES spread speech/data mode 2 proposal [61]

Parameter	
Multiple access	TDMA/CDMA
Channel type	C0ST 207 Bad Urban
Number of paths in channel	7
Normalised Doppler frequency	3.7×10^{-5}
CDMA spreading factor	16
Spreading sequence	Random
Tx. Frame duration	4.615 ms
Tx. Slot duration	577 μs
Joint detection CDMA receiver	Whitening matched filter (WMF) or Minimum mean square error block decision feedback equalizer (MMSE-BDFE)
No. of Slots/Frame	8
TDMA slots/Video packet	3
Chip Periods/TDMA slot	1250
Data Symbols/TDMA slot	68
User Data Symbol Rate (kBd)	14.7
System Data Symbol Rate (kBd)	117.9

instantaneous channel conditions degrade, the number of bits per symbol (BPS) is reduced, in order to maintain the required target transmission burst error rate. Figure 1.15 provides a snap-shot of the JD-ACDMA system's mode switching dynamics, which is based on the fluctuating channel conditions determined by all factors influencing the channel's quality, such as path loss, fast-fading, slow-fading, dispersion, co-channel interference, etc. The adaptive modem uses the SINR estimate at the output of the joint-detector, in order to estimate the instantaneous channel quality, and hence to set the modulation mode. The probability density function (PDF) of the JD-ACDMA scheme using each modulation mode for a particular average channel SNR is portrayed in Figure 1.16. It can be seen at high channel SNRs that the modem predominantly uses the 16QAM/JD-ACDMA modulation mode, while at low channel SNRs the BPSK mode is most prevalent. However, the PDF is widely spread, indicating that often the channel quality is misjudged by the receiver due to unpredictable channel quality fluctuations caused by a high doppler frequency or co-channel interference, etc. Hence in certain cases BPSK is used under high channel quality conditions or 16QAM is employed under hostile channel conditions.

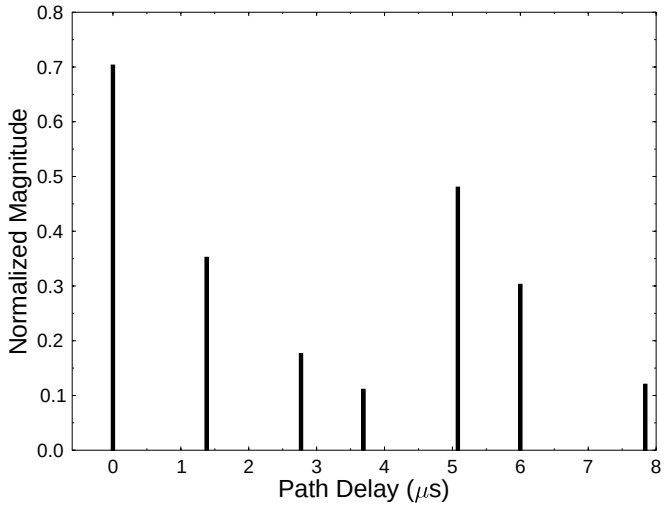

Figure 1.14: Normalized channel impulse response for the COST 207 [60] seven-path Bad Urban channel.

Table 1.7: Operational-mode specific JD-ACDMA video transceiver parameters used in our design example

Features	Multi-rate System		
Mode	BPSK	4QAM	16QAM
Bits/Symbol	1	2	4
FEC	Convolutional Coding		
Octal Gen. Pol.	561; 753		
Coding-rate	$R = 1/2$		
Constraint-length	$K = 9$		
Transmitted bits/packet	204	408	816
Total bit rate (kbit/s)	14.7	29.5	58.9
FEC-coded bits/packet	102	204	408
Assigned to FEC-coding (kbit/s)	7.4	14.7	29.5
Error detection per packet	16 bit CRC		
Feedback bits / packet	9		
Video packet size	77	179	383
Packet header bits	8	9	10
Video bits/packet	69	170	373
Unprotected video-rate (kbit/s)	5.0	12.3	26.9
Video framerate (Hz)	10		

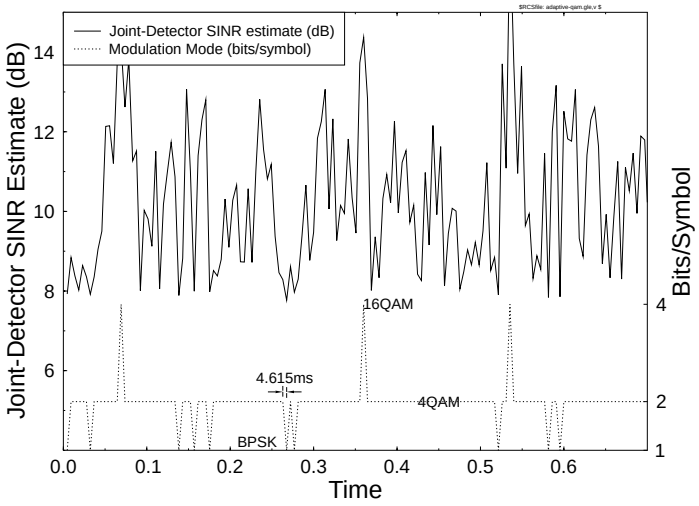

Figure 1.15: Example of modem mode switching in a dynamically reconfigured burst-by-burst modem in operation, where the modulation mode switching is based upon the SINR estimate at the output of the joint-detector over the channel model of Figure 1.14

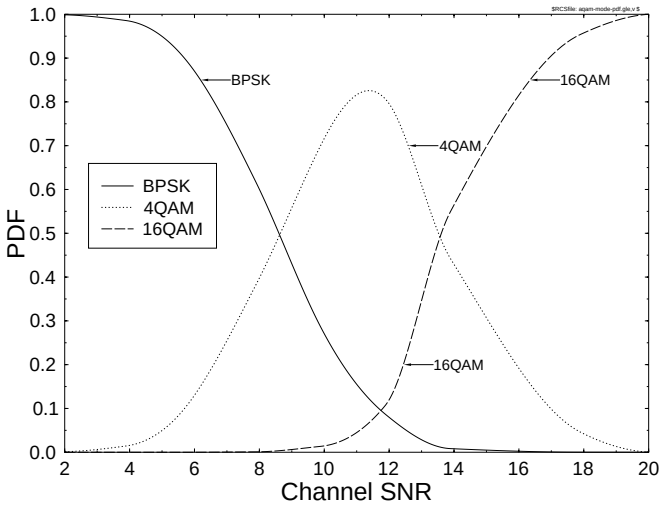

Figure 1.16: PDF of the various adaptive modem modes versus channel SNR over the channel model of Figure 1.14

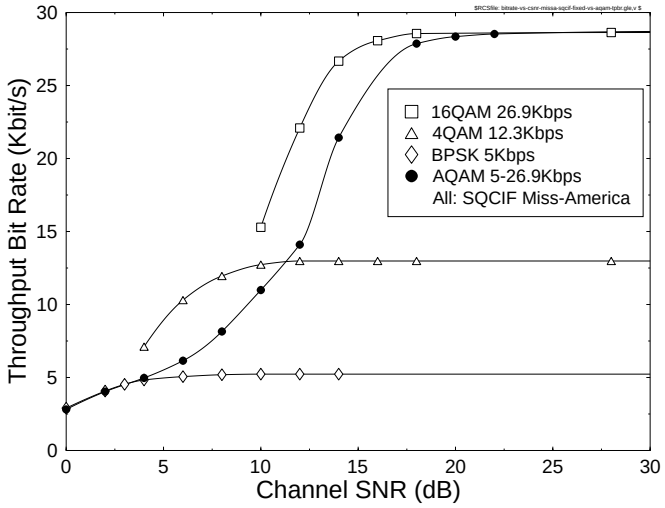

Figure 1.17: Throughput bit rate versus channel SNR comparision of the three fixed modulation modes (BPSK, 4QAM, 16QAM) and the adaptive burst-by-burst modem (AQAM), both supporting 2 users with the aid of joint detection over the channel model of Figure 1.14

The advantage of the dynamically reconfigured burst-by-adaptive JD-ACDMA modem over a statically reconfigured system, which would be incapable of near-instantaneous channel quality estimation and modem mode switching is that the video quality is smoothly - rather than abruptly - degraded, as the channel conditions deteriorate and vice versa. By contrast, a less 'agile' statically switched or reconfigured multi-mode system results in more visible reductions in video quality, when the modem switches to a more robust modulation mode, as it is demonstrated in Figure 1.17. Explicitly, Figure 1.17 shows the throughput bit rate of the dynamically reconfigured burst-by-burst adaptive modem, compared to the three modes of a less agile, statically switched multi-mode system. The reduction of the fixed modem modes' effective throughput at low SNRs is due to the fact that under such channel conditions an increased fraction of the transmitted packets have to be dropped, reducing the effective throughtput, since dropped packets do not contribute towards the system's effective throughput. The figure shows the smooth reduction of the throughput bit rate, as the channel quality deteriorates. The burst-by-burst modem matches the BPSK mode's bit rate at low channel SNRs, and the 16QAM mode's bit rate at high SNRs. In this example the dynamically reconfigured burst-by-burst adaptive modem characterised in the figure perfectly estimates the prevalent channel conditions although in practice the estimate of channel quality is not perfect and it is inherently delayed. Hence our results constitute the best-case performance.

The smoothly varying effective throughput bit rate of the burst-by-burst adaptive modem translates into a smoothly varying video quality, as the channel conditions

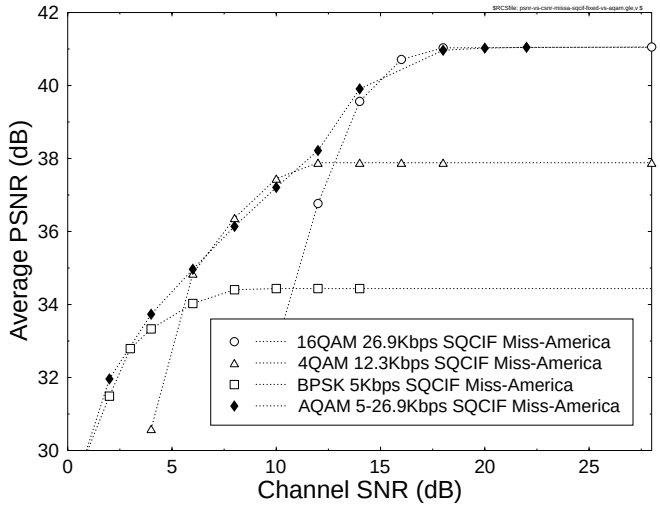

Figure 1.18: Average decoded video quality (PSNR) versus channel SNR comparision of the fixed modulation modes of BPSK, 4QAM and 16QAM, and the burst-by-burst adaptive modem. Both supporting 2-users with the aid of joint detection. These results were recorded for the Miss-America video sequence at SQCIF resolution (128x96 pels) over the channel model of Figure 1.14

change. The video quality measured in terms of the average PSNR is shown versus the channel SNR in Figure 1.18 in contrast to that of the individual modem modes. The figure demonstrates that the burst-by-burst adaptive modem provides equal or better video quality over a large proportion of the SNR range shown, than the individual modes. However, even at channel SNRs, where the adaptive modem has a slightly reduced PSNR, the perceived video quality of the adaptive modem is better, since the video packet loss rate is far lower, than that of the fixed modem modes.

1.8 Subband-Adaptive OFDM Video Transceivers

In order to demonstrate the benefits of the proposed near-instantaneously adaptive video transceivers also in the context of OFDM schemes [13, 63], in this section we compare the performance of a subband-adaptive OFDM video scheme [29] to that of a fixed modulation mode transceiver under identical propagation conditions, while having the same transmission bitrate. The subband-adaptive modem is capable of achieving a lower BER, since it can disable transmissions over low quality sub-carriers and compensate for the lost throughput by invoking a higher-order modulation mode, than that of the fixed-mode transceiver over the high-quality sub-carriers.

Table 1.8 shows the system parameters for the fixed-mode BPSK and QPSK transceivers, as well as for the corresponding AOFDM transceivers. The system

	BPSK mode	QPSK mode
Packet rate	4687.5 Packets/s	
FFT length	512	
OFDM symbols/packet	3	
OFDM symbol duration	2.6667μs	
OFDM time frame	80 Timeslots = 213μs	
Normalised Doppler frequency, f'_d	1.235×10^{-4}	
OFDM symbol normalised Doppler frequency, F_D	7.41×10^{-2}	
FEC coded bits/packet	1536	3072
FEC-coded video bitrate	7.2Mbps	14.4Mbps
Unprotected Bits/Packet	766	1534
Unprotected bitrate	3.6Mbps	7.2Mbps
Error detection CRC (bits)	16	16
Feedback error flag bits	9	9
Packet header bits/packet	11	12
Effective video bits/packet	730	1497
Effective video bitrate	3.4Mbps	7.0Mbps

Table 1.8: System parameters for the fixed QPSK and BPSK transceivers, as well as for the corresponding subband-adaptive OFDM (AOFDM) transceivers for Wireless Local Area Networks (WLANs).

employs constraint length three, half-rate turbo coding, using octal generator polynomials of 5 and 7 as well as random turbo interleavers, where the channel- and turbo-interleaver depth was adjusted for each AOFDM transmission burst, in order to facilitate burst-by-burst or symbol-by-symbol based OFDM demodulation and turbo decoding. Therefore the unprotected bitrate is approximately half the channel coded bitrate. The protected to unprotected video bitrate ratio is not exactly half, since two tailing bits are required to reset the convolutional encoders' memory to their default state in each transmission burst. In both the BPSK and QPSK modes 16-bit Cyclic Redundancy Checking (CRC) is used for error detection and 9 bits are used to encode the reverse link feedback acknowledgement information by simple repetition coding. The packet acknowledgement flag decoding ensues using majority logic decisions. The packetisation [29] requires a small amount of header information added to each transmitted packet, which is 11 and 12 bits per packet for BPSK and QPSK, respectively. The effective or useful video bitrates for the fixed BPSK and QPSK modes are then 3.4 and 7.0 Mbps.

The fixed-mode BPSK and QPSK transceivers are limited to one and two bits per symbol, respectively. By contrast, the proposed AOFDM transceivers operate at the same bitrate, as their corresponding fixed modem mode counterparts, although they

can vary their modulation mode on a subband by subband basis between 0, 1, 2 and 4 bits per symbol. Zero bits per symbol implies that transmissions are disabled for the subband concerned.

The "micro-adaptive" nature of the subband-adaptive modem is characterised by Figure 1.19, portraying at the top a contour plot of the channel Signal-to-Noise Ratio (SNR) for each subcarrier versus time. This channel SNR fluctuation was recorded here for the short indoor WLAN channel impulse response of Figure 1.20 having a maximum dispersion of about 60ns, which was referred to as the short Wireless Asynchronous Transfer Mode (WATM) channel in [13].

At the centre and bottom of the figure the modulation mode chosen for each 32-subcarrier subband is shown versus time for the 3.4 and 7.0 Mbps target-rate subband-adaptive modems, respectively. Again, this was recorded for the short WATM channel impulse response of Figure 1.20. It can be seen that when the channel is of high quality – like for example at about frame 1080 – the subband-adaptive modem used the same modulation mode, as the equivalent fixed rate modem in all subcarriers. When the channel is hostile – like around frame 1060 – the subband-adaptive modem used a lower-order modulation mode in some subbands, than the equivalent fixed mode scheme, or in extreme cases disabled transmission for that subband. In order to compensate for the loss of throughput in this subband a higher-order modulation mode was used in the highest quality subbands.

One video packet is transmitted per OFDM symbol, therefore the video packet loss ratio is the same, as the OFDM symbol error ratio. The video packet loss ratio is plotted versus the channel SNR in Figure 1.21. It is shown in the graph that the subband-adaptive transceivers – or synonymously termed as microscopic-adaptive (μAOFDM), in contrast to OFDM symbol-by-symbol adaptive transceivers – have a lower packet loss ratio (PLR) at the same SNR compared to the fixed modulation mode transceiver. Note in Figure 1.21 that the subband-adaptive transceivers can operate at lower channel SNRs, than the fixed modem mode transceivers, while maintaining the same required video packet loss ratio. Again, the figure labels the subband-adaptive OFDM transceivers as μAOFDM, implying that the adaptation is not noticeable from the upper layers of the system. A macro-adaption could be applied in addition to the microscopic adaption by switching between different target bitrates on an OFDM symbol-by-symbol basis, as the longer-term channel quality improves and degrades. This issue was further investigated in [29].

The figure shows that when the channel quality is high, the throughput bitrate of the fixed and adaptive transceivers is identical. However, as the channel degrades, the loss of packets due to channel impairments results in a lower throughput bitrate. The lower packet loss ratio of the subband-adaptive transceiver results in a higher throughput bitrate, than that of the fixed modulation mode transceiver. Finally, these improved throughput bitrate results translate to the enhanced decoded video quality performance results evaluated in terms of Peak Signal-to-Noise Ratio (PSNR) in Figure 1.22. Again, for high channel SNRs the performance of the fixed and adaptive OFDM transceivers is identical. However, as the channel quality degrades, the video quality of the subband-adaptive transceiver degrades less dramatically, than that of the corresponding fixed modulation mode transceiver.

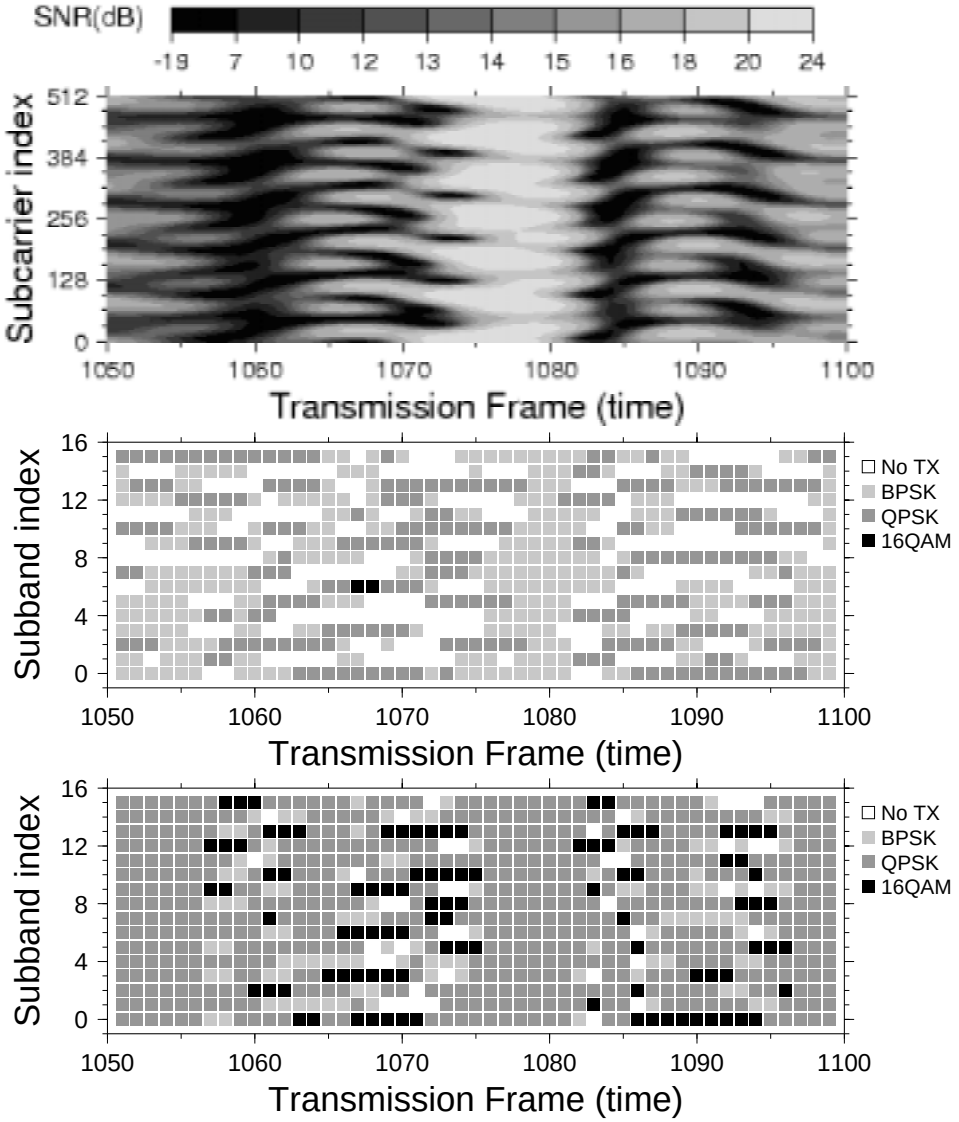

Figure 1.19: The 'micro-adaptive' nature of the subband-adaptive OFDM modem. The top graph is a contour plot of the channel SNR for all 512 subcarriers versus time. The bottom two graphs show the modulation modes chosen for all 16 32-subcarrier subbands for the same period of time. The middle graph shows the performance of the 3.4Mbps subband-adaptive modem, which operates at the same bitrate as a fixed BPSK modem. The bottom graph represents the 7.0Mbps subband-adaptive modem, which operated at the same bitrate as a fixed QPSK modem. The average channel SNR was 16dB. ©IEEE, 2001, Hanzo, Cherriman, Streit [29]

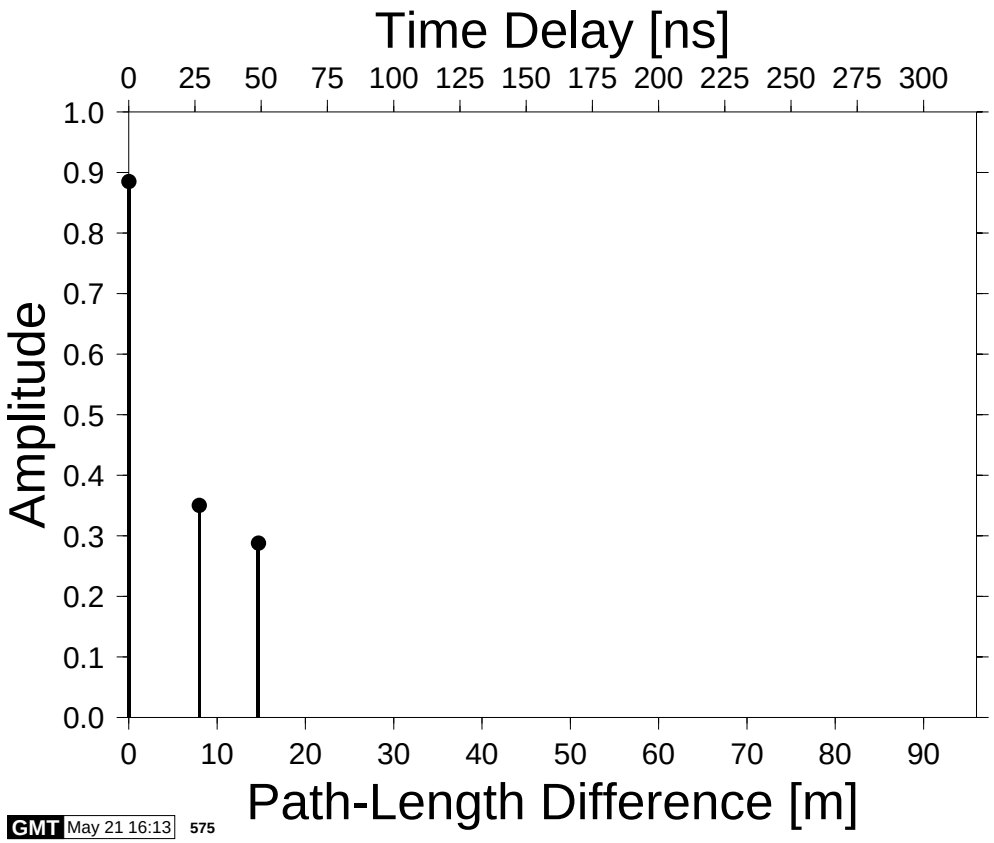

Figure 1.20: Indoor three-path WATM channel impulse response. ©IEEE, 2001, Hanzo, Webb, Keller [13]

1.9 Summary and Conclusions

In contrast to the statically reconfigured narrow-band multimode video transceivers [29] in this chapter we have advocated BbB-AQAM based wireless transceivers. We justified their service-related benefits in terms of the video quality improvements perceived by the users of such systems. As an example, the channel quality perceived by the channel equaliser or the multi-user equaliser was used for controlling the AQAM modes. When an adaptive packetiser is used in conjunction with the AQAM modem, it continually adjusts the video codec's target bitrate, in order to match the instantaneous throughput provided by the adaptive modem.

We have also shown that the delay between the instants of channel estimation and AQAM mode switching has an effect on the performance of the proposed AQAM video transceiver. This performance penalty can be mitigated by reducing the modem mode signalling delay. It was also demonstrated that the system can be tuned to the required FER performance using appropriate AQAM switching thresholds. In harmony with

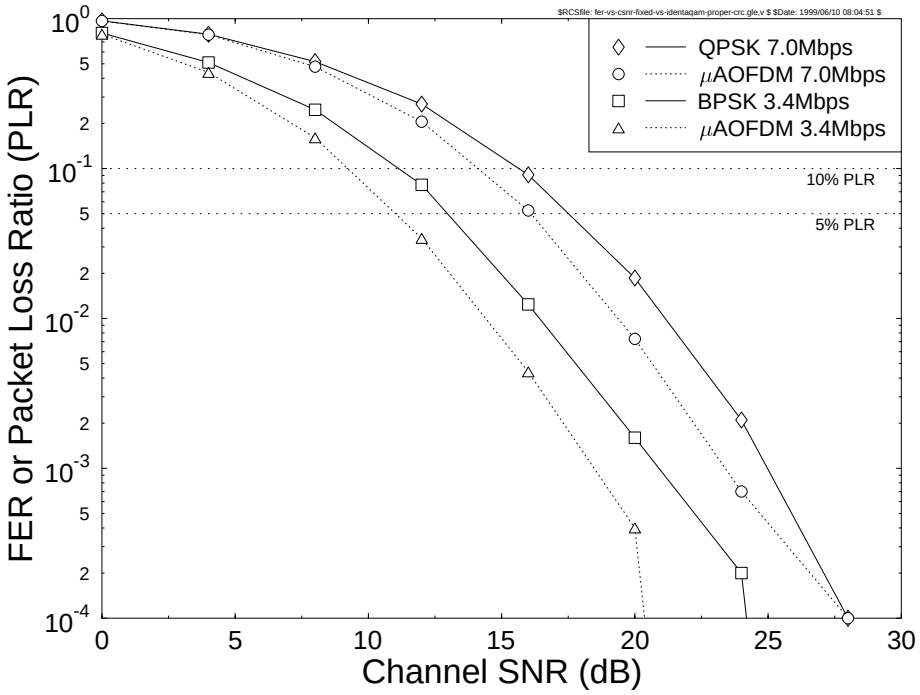

Figure 1.21: Frame Error Rate (FER) or video packet loss ratio (PLR) versus channel SNR for the BPSK and QPSK fixed modulation mode OFDM transceivers and for the corresponding subband-adaptive μAOFDM transceiver, operating at identical effective video bitrates, namely at 3.4 and 7.0 Mbps, over the channel model of Figure 1.20 at a normalised Doppler frequency of $F_D = 7.41 \times 10^{-2}$. ©IEEE, 2001, Hanzo, Cherriman, Streit [29]

our expectations, we found that the more complex turbo channel codecs were more robust against channel effects than the lower-complexity binary BCH codecs. Lastly, the AQAM principles were extended to joint-detection assisted AQAM/CDMA and adaptive OFDM systems, where similar findings were confirmed to those found in the context of unspread AQAM.

It is a natural thought to combine these adaptive transceivers with diversity aided Multiple Input, Multiple Output (MIMO) systems and space-time coding [77–80] in a further effort towards mitigating the effects of fading and rendering the channel more Gaussian-like. **A vital question in this context is, whether adaptive transceivers retain their performance advantages in conjunction with MIMOs?** As expected, no significant joint benefits accrue, since both of these regimes aim at mitigating the effects of fading and once the fading is mitigated sufficiently for it to become near-Gaussian, no further fading counter-measures are necessary. It is worth noting, however that MIMOs have been predominantly studied in the con-

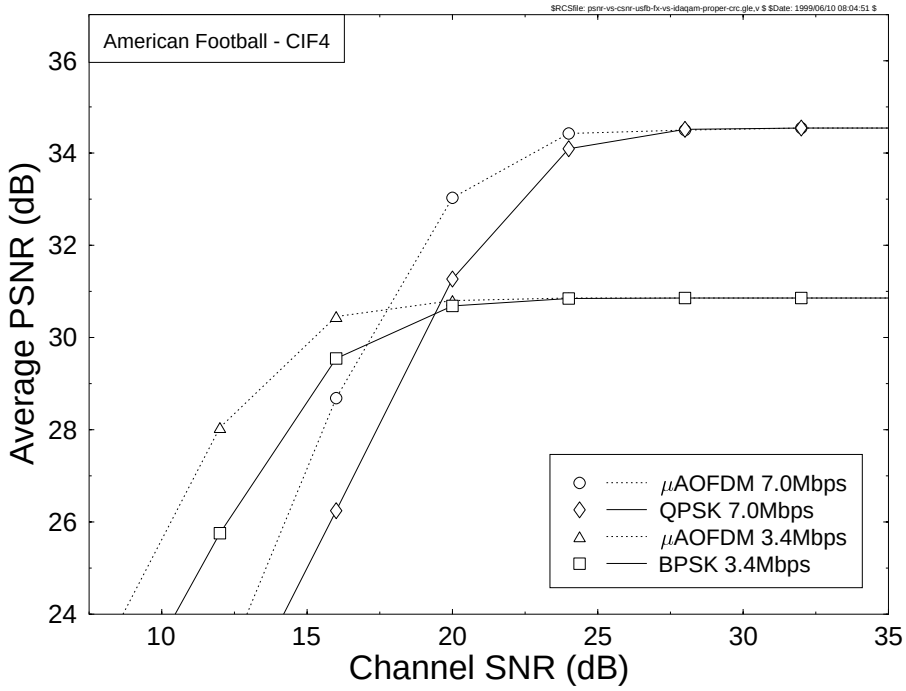

Figure 1.22: Average video quality expressed in PSNR versus channel SNR for the BPSK and QPSK fixed modulation mode OFDM transceivers and for the corresponding μAOFDM transceiver operating at identical channel SNRs over the channel model of Figure 1.20 at a normalised Doppler frequency of $F_D = 7.41 \times 10^{-2}$. ©IEEE, 2001, Hanzo, Cherriman, Streit [29]

text of narrowband or non-dispersive fading channels or in conjunction with OFDM - a scheme that decomposes a high-rate bit stream into a high number of low-rate bit streams - thereby rendering the dispersive channel non-dispersive for each of the low-rate composite streams.

A further problem, when invoking high-order receiver diversity in an effort to mitigate the effects of fading and hence rendering the wireless channel Gaussian-like is that the receiver complexity increases. It is a more attractive proposition to employ complex, transmit diversity assisted base stations, which allows us to aim for low-complexity terminals. In this context in recent years space-time codecs have found favour and have also been proposed for the IMT2000 system and for multi-user HIPERLAN 2 type systems.

Chapter 2

UTRA Network Performance Using Adaptive Arrays and Adaptive Modulation

2.1 Introduction

In January 1998, the European standardisation body for third generation mobile radio systems, the European Telecommunications Standards Institute - Special Mobile Group (ETSI SMG), agreed upon a radio access scheme for third generation mobile radio systems, referred to as the Universal Mobile Telecommunication System (UMTS) [11, 81]. The UMTS Terrestrial Radio Access (UTRA) consists of two modes, a Frequency Division Duplex (FDD) mode, where the uplink and downlink are transmitted on different frequencies, and a Time Division Duplex (TDD) mode, where the uplink and the downlink are transmitted on the same carrier frequency, but multiplexed in time. The agreement recommends the employment of Wideband Code Division Multiple Access (W-CDMA) for UTRA FDD and Time Division - Code Division Multiple Access (TD-CDMA) for UTRA TDD. TD-CDMA is based on a combination of Time Division Multiple Access (TDMA) and CDMA, whereas W-CDMA is a pure CDMA-based system. The UTRA scheme can be used for operation within a minimum spectrum of 2 x 5 MHz for UTRA FDD and 5 MHz for UTRA TDD. Both duplex or paired and simplex or unpaired frequency bands have been identified in the region of 2 GHz to be used for the UTRA third generation mobile radio system. Both modes of UTRA have been harmonised with respect to the basic system parameters, such as carrier spacing, chip rate and frame length. Thereby, FDD/TDD dual mode operation is facilitated, which provides a basis for the development of low cost terminals. Furthermore, the interworking of UTRA with GSM [11] is ensured.

In UTRA, the different service needs are supported in a spectrally efficient way

by a combination of FDD and TDD. The FDD mode is intended for applications in both macro- and micro-cellular environments, supporting data rates of up to 384kbps and high mobility. The TDD mode, on the other hand, is more suited to micro and pico-cellular environments, as well as for licensed and unlicensed cordless and wireless local loop applications. It makes efficient use of the unpaired spectrum - for example in wireless Internet applications, where much of the teletraffic is in the downlink - and supports data rates of up to 2 Mbps. Therefore, the TDD mode is particularly well suited for environments generating a high traffic density (e.g. in city centres, business areas, airports etc.) and for indoor coverage, where the applications require high data rates and tend to have highly asymmetric traffic again, as in Internet access.

In parallel to the European activities, extensive work has been carried out also in Japan and the USA on third generation mobile radio systems. The Japanese standardisation body known as the Association of Radio Industry and Business (ARIB) also opted for using W-CDMA, and the Japanese as well as European proposals for FDD bear strong similarities. Similar concepts have also been developed by the North-American T1 standardisation body for the pan-American third generation (3G) system known as cdma2000 [11].

In order to work towards a truly global third generation mobile radio standard, the Third Generation Partnership Project (3GPP) was formed in December 1998. 3GPP consists of members of the standardisation bodies in Europe (ETSI), the US (T1), Japan (ARIB), Korea (TTA - Telecommunications Technologies Association), and China (CWTS - China Wireless Telecommunications Standard). 3GPP merged the already well harmonised proposals by the regional standardisation bodies and now works towards a single common third generation mobile radio standard under the terminology UTRA, retaining its two modes, and aiming to operate on the basis of the evolved GSM core network. The Third Generation Partnership Project 2 (3GPP2), on the other hand, works towards a third generation mobile radio standard, which is based on an evolved IS-95 type system which was originally referred to as cdma2000 [11]. In June 1999, major international operators in the Operator Harmonisation Group (OHG) proposed a harmonised G3G (Global Third Generation) concept, which has been accepted by 3GPP and 3GPP2. The harmonised G3G concept is a single standard with the following three modes of operation:

- CDMA direct spread (CDMA-DS), based on UTRA FDD as specified by 3GPP.
- CDMA multi-carrier (CDMA-MC), based on cdma2000 using FDD as specified by 3GPP2.
- TDD (CDMA TDD) based on UTRA TDD as specified by 3GPP.

2.2 Direct Sequence Code Division Multiple Access

Traditional ways of separating signals in time using TDMA and in frequency ensure that the signals are transmitted orthogonal in either time or frequency and hence they are non-interfering. In CDMA different users are separated employing a set of waveforms exhibiting good correlation properties, which are known as spreading codes.

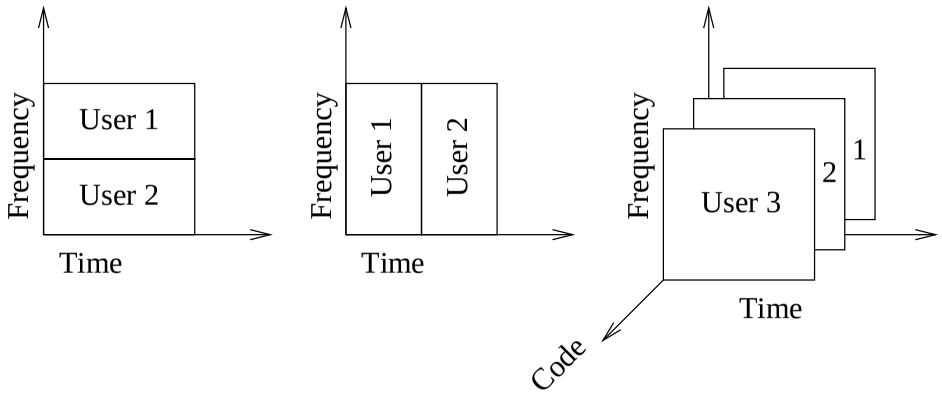

Figure 2.1: Multiple access schemes : FDMA (left), TDMA (middle) and CDMA (right)

Figure 2.1 illustrates the principles of FDMA, TDMA and CDMA. More explicitly, FDMA uses a fraction of the total FDMA frequency band for each communications link for the whole duration of a conversation, while TDMA uses the entire bandwidth of a TDMA channel for a fraction of the TDMA frame, namely for the duration of a time slot. Finally, CDMA uses the entire available frequency band all the time and separates the users with the aid of unique, orthogonal user signature sequences.

In a CDMA digital communications system, such as that shown in Figure 2.2, the data stream is multiplied by the spreading code, which replaces each data bit with a sequence of code chips. A chip is defined as the basic element of the spreading code, which typically assumes binary values. Hence, the spreading process consists of replacing each bit in the original user's data sequence with the complete spreading code. The chip rate is significantly higher than the data rate, hence causing the bandwidth of the user's data to be spread, as shown in Figure 2.2.

At the receiver, the composite signal containing the spread data of multiple users is multiplied by a synchronised version of the spreading code of the wanted user. The specific auto-correlation properties of the codes allow the receiver to identify and recover each delayed, attenuated and phase-rotated replica of the transmitted signal, provided that the signals are separated by more than one chip period and the receiver has the capability of tracking each significant path. This is achieved using a Rake receiver [5] that can process multiple delayed received signals. Coherent combination of these transmitted signal replicas allows the original signal to be recovered. The unwanted signals of the other simultaneous users remain wideband, having a bandwidth equal to that of the noise, and appear as additional noise with respect to the wanted signal. Since the bandwidth of the despread wanted signal is reduced relative to this noise, the signal-to-noise ratio of the wanted signal is enhanced by the despreading process in proportion to the ratio of the spread and despread bandwidths, since the noise power outside the useful despread signal's bandwidth can be removed by a low-pass filter. This bandwidth ratio is equal to the ratio of the chip rate to the data rate, which is known as the Processing Gain (PG). For this process to work efficiently, the

A/SF

Duplex scheme	FDD	TDD
Multiple access scheme	W-CDMA	TD-CDMA
Chip rate	3.84 Mchip/s	3.84 Mchip/s
Spreading factor range	4-512	1-16
Frequency bands	1920-1980 MHz (UL)	1900-1920 MHz
	2110-2170 MHz (DL)	2010-2025 MHz
Modulation mode	4-QAM/QPSK	4-QAM/QPSK
Bandwidth	5 MHz	5 MHz
Nyquist pulse shaping	0.22	0.22
Frame length	10 ms	10 ms
Number of timeslots per frame	15	15

Table 2.1: Key UTRA Parameters

2.3.1 Spreading and Modulation

As usual, the uplink is defined as the transmission path from the mobile station to the base station, which receives the unsynchronised channel impaired signals from the network's mobiles. The base station has the task of extracting the wanted signal from the received signal contaminated by both intra- and inter-cell interference. However, as described in Section 2.2, some degree of isolation between interfering users is achieved due to employing unique orthogonal spreading codes, although their orthogonality is destroyed by the hostile mobile channel.

The spreading process consists of two operations. The first one is the channelisation operation, which transforms every data symbol into a number of chips, thus increasing the bandwidth of the signal, as seen in Figure 2.2 of Section 2.2. The channelisation codes in UTRA are Orthogonal Variable Spreading Factor (OVSF) codes [11] that preserve the orthogonality between a given user's different physical channels, which are also capable of supporting multirate operation. These codes will be further discussed in the context of Figure 2.4. The second operation related to the spreading, namely the "scrambling" process then multiplies the resultant signals separately on the I- and Q-branches by a complex-valued scrambling code, as shown in Figure 2.3. The scrambling codes may be one of either 2^{24} different "long" codes or 2^{24} "short" uplink scrambling codes.

The Dedicated Physical Control CHannel (DPCCH) [11, 82] is spread to the chip rate by the channelisation code C_c, while the n^{th} Dedicated Physical Data CHannel (DPDCH), namely DPDCH$_n$, is spread to the chip rate by the channelisation code $C_{d,n}$. One DPCCH and up to six parallel DPDCHs can be transmitted simultaneously, i.e. $1 \leq n \leq 6$ as seen in Figure 2.3). However, it is beneficial to transmit with the aid of a single DPDCH, if the required bit-rate can be provided by a single DPDCH for reasons of terminal amplifier efficiency. This is because multi-code transmissions increase the peak-to-average ratio of the transmission, which reduces the efficiency of the terminal's power amplifier [81]. The maximum user data rate achievable with the aid of a single code is derived from the maximum channel bit rate, which is 960 kbps using a spreading factor of four without channel coding in the 1999 version of

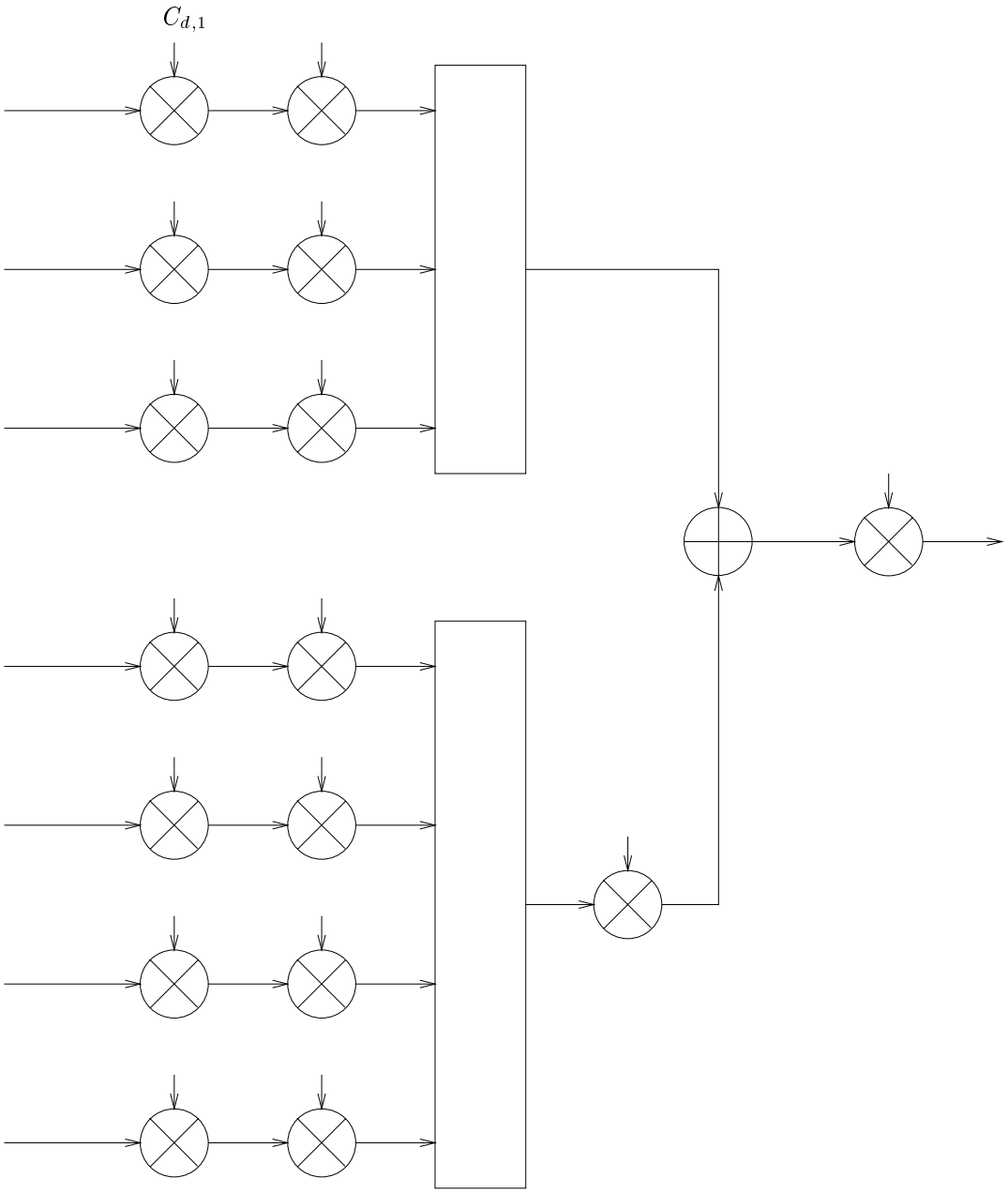
$C_{d,1}$

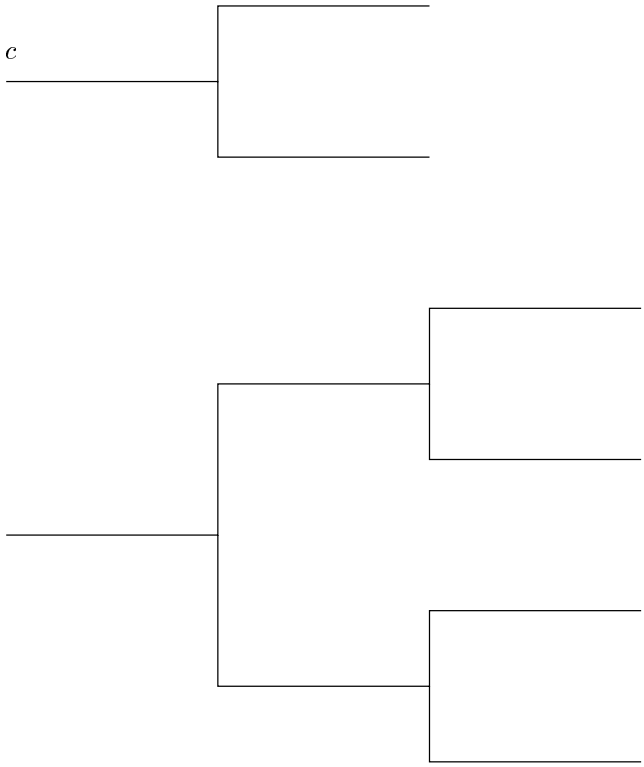
c

factor is equal to the spreading factor itself. All the codes of the same level in the code tree constitute a set and they are orthogonal to each other. Any two codes of different levels are also orthogonal to each other, as long as one of them is not the mother of the other code. For example, the codes $c_{15}(2)$, $c_7(1)$ and $c_3(1)$ are all the mother codes of $c_{31}(3)$ and hence are not orthogonal to $c_{31}(3)$, where the number in the round bracket indicates the code index. Thus not all the codes within the code tree can be used simultaneously by a mobile station. Specifically, a code can be used by an MS if and only if no other code on the path from the specific code to the root of the tree, or in the sub-tree below the specific node is used by the same MS.

For the DPCCH and DPDCHs the following applies :

- The PDCCH is always spread by code $C_c = C_{ch,256,0}$.
- When only one DPDCH is to be transmitted, DPDCH_1 is spread by the code $C_{d,1} = C_{ch,SF,k}$, where SF is the spreading factor of DPDCH_1 and $k = SF/4$.
- When more than one DPDCHs have to be transmitted, all DPDCHs have spreading factors equal to four. Furthermore, DPDCH_n is spread by the code $C_{d,n} = C_{ch,4,k}$, where $k = 1$ if $n \subset \{1, 2\}$, $k = 3$ if $n \subset \{3, 4\}$, and $k = 2$ if $n \subset \{5, 6\}$.

A fundamental difference between the uplink and the downlink is that in the downlink synchronisation is common to all users and channels of a given cell. This enables us to exploit the cross-correlation properties of the OVSF codes, which were originally proposed in [83]. These codes offer perfect cross-correlation in an ideal channel, but there is only a limited number of these codes available. The employment of OVSF codes allows the spreading factor to be changed and orthogonality between the spreading codes of different lengths to be maintained. The codes are selected from the code tree, which is illustrated in Figure 2.4. As illustrated above, there are certain restrictions as to which of the channelisation codes can be used for transmission from a single source. Another physical channel may invoke a certain code from the tree, if no other physical channel to be transmitted employing the same code tree is using a code on an underlying branch, since this would be equivalent to using a higher spreading factor code generated from the spreading code to be used, which are not orthogonal to each other on the same branch of the code tree. Neither can a smaller spreading factor code on the path to the root of the tree be used. Hence, the number of available codes depends on the required transmission rate and spreading factor of each physical channel.

In the UTRA downlink a part of the multi-user interference can be orthogonal - apart from the channel effects. The users within the same cell share the same scrambling code, but use different channelisation/OVSF codes. In a non-dispersive downlink channel, all intra-cell users are synchronised and therefore they are perfectly orthogonal. Unfortunately, in most cases the channel will be dispersive, implying that non-synchronised interference will be suppressed only by a factor corresponding to the processing gain, and thus they will interfere with the desired signal. The interference from other cells which is referred to as inter-cell interference, is non-orthogonal, due to employing different scrambling but possibly the same channelisation codes. Therefore

inter-cell interference is also suppressed by a factor corresponding to the processing gain.

The channelisation code used for the the Primary Common PIlot CHannel (CPICH) is fixed to $C_{ch,256,0}$, while the channelisation code for the Primary Common Control Physical CHannel (CCPCH) is fixed to $C_{ch,256,1}$ [82]. The channelisation codes for all other physical channels are assigned by the UTRAN [82].

A total of $2^{18}-1 = 262143$ scrambling codes, numbered as $0 \ldots 262142$ can be generated. However, not all of the scrambling codes are used. The scrambling codes are divided into 512 sets, each consisting of a primary scrambling code and 15 secondary scrambling codes [82].

More specifically, the primary scrambling codes consist of scrambling codes $n = 16 * i$, where $i = 0 \ldots 511$. The i^{th} set of secondary scrambling codes consists of scrambling codes $16 * i + k$ where $k = 1 \ldots 15$. There is a one-to-one mapping between each primary scrambling code and the associated 15 secondary scrambling codes in a set, such that the i^{th} primary scrambling code uniquely identifies the i^{th} set of secondary scrambling codes. Hence, according to the above statement, scrambling codes $k = 0 \ldots 8191$ are used. Each of these codes is associated with a left alternative scrambling code and a right alternative scrambling code, that may be used for the so-called compressed frames. Specifically, compressed frames are shortened duration frames transmitted right before a handover, in order to create an inactive period during which no useful data is transmitted. This allows the transceivers to carry out operations necessary for the handover to be successful. The left alternative scrambling code associated with scrambling code k is the scrambling code $k + 8192$, while the corresponding right alternative scrambling code is scrambling code $k + 16384$. In compressed frames, the left alternative scrambling code is used, if $n < SF/2$ and the right alternative scrambling code is used, if $n \geq SF/2$, where $C_{ch,SF,n}$ is the channelisation code used for non-compressed frames.

The set of 512 primary scrambling codes is further divided into 64 scrambling code groups, each consisting of 8 primary scrambling codes. The j^{th} scrambling code group consists of primary scrambling codes $16 * 8 * j + 16 * k$, where $j = 0 \ldots 63$ and $k = 0 \ldots 7$.

Each cell is allocated one and only one primary scrambling code. The primary CCPCH and primary CPICH are always transmitted using this primary scrambling code. The other downlink physical channels can be spread and transmitted with the aid of either the primary scrambling code or a secondary scrambling code from the set associated with the primary scrambling code of the cell.

2.3.2 Common Pilot Channel

The Common PIlot CHannel (CPICH) is an unmodulated downlink code channel, which is scrambled with the aid of the cell-specific primary scrambling code. The function of the downlink CPICH is to aid the Channel Impulse Response (CIR) estimation necessary for the detection of the dedicated channel at the mobile station and to provide the CIR estimation reference for the demodulation of the common channels, which are not associated with the dedicated channels.

UTRA has two types of common pilot channels, namely the primary and secondary

CPICHs. Their difference is that the primary CPICH is always spread by the primary scrambling code defined in Section 2.3.1. More explicitly, the primary CPICH is associated with a fixed channelisation code allocation and there is only one such channel and channelisation code for a cell or sector. The secondary CPICH may use any channelisation code of length 256 and may use a secondary scrambling code as well. A typical application of secondary CPICHs usage would be in conjunction with narrow antenna beams intended for service provision at specific teletraffic "hot spots" or places exhibiting a high traffic density [81].

An important application of the primary common pilot channel is during the collection of channel quality measurements for assisting during the handover and cell selection process. The measured CPICH reception level at the terminal can be used for handover decisions. Furthermore, by adjusting the CPICH power level the cell load can be balanced between different cells, since reducing the CPICH power level encourages some of the terminals to handover to other cells, while increasing it invites more terminals to handover to the cell, as well as to make their initial access to the network in that cell.

2.3.3 Power Control

Agile and accurate power control is perhaps the most important aspect in W-CDMA, in particular on the uplink, since a single high-powered rogue mobile can cause serious performance degradation to other users in the cell. The problem is referred to as the "near-far effect" and occurs when, for example, one mobile is near the cell edge, and another is near the cell centre. In this situation, the mobile at the cell edge is exposed to a significantly higher pathloss, say 70 dB higher, than that of the mobile near the cell centre. If there were no power control mechanisms in place, the mobile near the base station could easily "overpower" the mobile at the cell edge, and thus may block a large part of the cell. The optimum strategy in the sense of maximising the system's capacity is to equalise the received power per bit of all mobile stations at all times.

A so-called open-loop power control mechanism [81] attempts to make a rough estimate of the expected pathloss by means of a downlink beacon signal, but this method can be highly inaccurate. The prime reason for this is that the fast fading is essentially uncorrelated between the uplink and downlink, due to the large frequency separation of the uplink and downlink band of the W-CDMA FDD mode. Open-loop power control is however, used in W-CDMA, but only to provide a coarse initial power setting of the mobile station at the beginning of a connection.

A better solution is to employ fast closed-loop power control [81]. In closed-loop power control in the uplink, the base station performs frequent estimates of the received SIR and compares it to the target SIR. If the measured SIR is higher than the target SIR, the base station commands the mobile station to reduce the power, while if it is too low it will instruct the MS to increase its power. Since each 10 ms UTRA frame consists of 15 time slots, each corresponding to one power control power adjustment period, this procedure takes place at a rate of 1500 Hz. This is far faster than any significant change of pathloss, including street corner effects, and indeed faster than the speed of Rayleigh fading for low to moderate mobile speeds. The stree corner effect occurs, when a mobile turns the street corner and hence the

received signal power drops markedly. Therefore the mobile responds by rapidly incresing its transmit power, which may inflict sever interference upon other closely located base stations. In response, the mobiles using these base stations increase their transmit powers in an effort to maintain their communications quality. This is undesirable, since it results in a high level of co-channel interference, leading to excessive transmission powers and to a reductions of the battery recharge period.

The same closed-loop power control technique is used on the downlink, although the rationale is different. More specifically, there is no near-far problem due to the one-to-many distributive scenario, i.e. all the signals originate from the single base station to all mobiles. It is, however, desirable to provide a marginal amount of additional power to mobile stations near the cell edge, since they suffer from increased inter-cell interference. Hence, the closed loop power control in CDMA systems ensures that each mobile transmits just sufficient power to satisfy the outer-loop power control scheme's SIR target. The SIR target is controlled by an outer-loop power control process that adjusts the required SIR in order to meet the Bit Error Ratio (BER) requirements of a particular service. At higher mobile speeds typically a higher SIR is necessary for attaining a given BER/FER.

2.3.3.1 Uplink Power Control

The uplink's inner-loop power control adjusts the mobile's transmit power in order to maintain the received uplink SIR at the given SIR target, namely at SIR_{target}. The base stations that are communicating with the mobile generate Transit Power Control (TPC) commands and transmit them, once per slot, to the mobile. The mobile then derives from the TPC commands of the various base stations, a single TPC command, TPC_cmd, for each slot, combining multiple received TPC commands if necessary. In [84] two algorithms were defined for the processing of TPC commands and hence for deriving TPC_cmd.

Algorithm 1 : [84]

When not in soft-handover, i.e. when the mobile communicates with a single base station, only one TPC command will be received in each slot. Hence, for each slot, if the TPC command is equal to 0 ($SIR > SIR_{target}$) then $TPC\_cmd = -1$, otherwise, if the TPC command is 1 ($SIR < SIR_{target}$) then $TPC\_cmd = 1$, which implies powering down or up, respectively.

When in soft handover, multiple TPC commands are received in each slot from the different base stations in the active base station set. If all of the base station's TPC commands are identical, then they are combined to form a single TPC command, namely TPC_cmd. However, if the TPC commands of the different base stations differ, then a soft decision W_i is generated for each of the TPC commands, TPC_i, where $i = 1, 2, \ldots, N$, and N is the number of TPC commands. These N soft decisions are then used to form a combined TPC command TPC_cmd according to :

$$TPC\_cmd = \gamma(W_1, W_2, \ldots, W_N) \tag{2.1}$$

where TPC_cmd is either -1 or +1 and $\gamma()$ is the decision function combining the soft values, $W_1, \ldots, W_N$.

If the N TPC commands appear to be uncorrelated, and have a similar probability of being 0 or 1, then function $\gamma()$ should be defined such that the probability that the output of the function $\gamma()$ is equal to 1, is greater than or equal to $1/2^N$, and the probability that the output of $\gamma()$ is equal to -1, shall be greater than or equal to 0.5 [84]. Alternatively, the function $\gamma()$ should be defined such that $P(\gamma() = 1) \geq 1/2^N$ and $P(\gamma() = -1) \geq 0.5$.

Algorithm 2 : [84]

When not in soft handover, only one TPC command will be received in each slot, and the mobile will process the maximum 15 TPC commands in a five-slot cycle, where the sets of five slots are aligned with the frame boundaries and the sets do not overlap. Therefore, when not in soft handover, for the first four slots of a five-slot set $TPC\_cmd = 0$ is used for indicating that no power control adjustments are made. For the fifth slot of a set the mobile performs hard decisions on all five of the received TPC commands. If all five hard decisions result in a binary 1, then we set $TPC\_cmd = 1$. In contrast, if all five hard decisions yield a binary 0, then $TPC\_cmd = -1$ is set, else $TPC\_cmd = 0$.

When the mobile is in soft handover, multiple TPC commands will be received in each slot from each of the base stations in the set of active base stations. When the TPC commands of the active base stations are identical, then they can be combined into a single TPC command. However, when the received TPC commands are different, the mobile makes a hard decision concerning the value of each TPC command for three consecutive slots, resulting in N hard decisions for each of the three slots, where N is the number of base stations within the active set. The sets of three slots are aligned to the frame boundaries and do not overlap. Then $TPC\_cmd = 0$ is set for the first two slots of the three-slot set, and then TPC_cmd is determined for the third slot as follows.

The temporary command TPC_temp_i is determined for each of the N sets of three TPC commands of the consecutive slots by setting $TPC\_temp_i = 1$ if all three TPC hard decisions are binary 1. In contrast, if all three TPC hard decisions are binary 0, $TPC\_temp_i = -1$ is set, otherwise we set $TPC\_temp_i = 0$. These temporary TPC commands are then used to determine the combined TPC command for the third slot invoking the decision function $\gamma(TPC\_temp_1, TPC\_temp_2, \ldots, TPC\_temp_N)$ defined as:

$$\begin{aligned} TPC\_cmd = 1 \quad & \text{if } \frac{1}{N}\sum_{i=1}^{N} TPC\_temp_i > 0.5 \\ TPC\_cmd = -1 \quad & \text{if } \frac{1}{N}\sum_{i=1}^{N} TPC\_temp_i < -0.5 \\ TPC\_cmd = 0 \quad & \text{otherwise.} \end{aligned} \tag{2.2}$$

2.3.3.2 Downlink Power Control

The downlink transmit power control procedure simultaneously controls the power of a DPCCH and its corresponding DPDCHs, both of which are adjusted by the same amount, and hence the relative power difference between the DPCCH and DPDCHs

remains constant.

The mobile generates TPC commands for controlling the base station's transmit power and sends them in the TPC field of the uplink DPCCH. When the mobile is not in soft handover, the TPC command generated is transmitted in the first available TPC field using the uplink DPCCH. In contrast, when the mobile is in soft handover, it checks the downlink power control mode (DPC_MODE) before generating the TPC command. If $DPC\_MODE = 0$, the mobile sends a unique TPC command in the first available TPC field in the uplink DPCCH. If however, $DPC\_MODE = 1$, the mobile repeats the same TPC command over three consecutive slots of the same frame and the new TPC command is transmitted to the base station in an effort the control its power at the beginning of the next frame. The minimum required transmit power step size is 1dB, with a smaller step size of 0.5dB being optional. The power control step size can be increased from 1dB to 2dB, thus allowing a 30dB correction range during the 15 slots of a 10ms frame. The maximum transmit powers are +21dBm and +24dBm, although it is likely that in the first phase of network deployment most terminals will belong to the 21dBm power class [81].

2.3.4 Soft Handover

Theoretically, the ability of CDMA to despread the interfering signals, and thus adequately operate at low signal-to-noise ratios, allows a CDMA network to have a frequency reuse factor of one [81]. Traditionally, non-CDMA based networks have required adjacent cells to have different carrier frequencies, in order to reduce the co-channel interference to acceptable levels. Therefore, when a mobile hands over from one cell to another, it has to re-tune its synthesizer to the new carrier frequency, i.e. it performs an inter-frequency handover. This process is a "break-before-make" procedure, known as a hard handover, and hence call disruption or interruption is possible. However, in a CDMA based network, having a frequency reuse factor of one so-called soft handovers may be performed, which is a "make-before-break" process, potentially allowing for a smoother handover between cells. During a soft handover a mobile is connected to two or more base stations simultaneously, thus utilising more network resources and transmitting more signals, which interfere with other users. Therefore, it is in the network operator's interests to minimise the number of users in soft handover, whilst maintaining a satisfactory quality of service. In soft handover, each connected base station receives and demodulates the user's data, and selection diversity is performed between the base stations, i.e. the best version of the uplink frame is selected. In the downlink, the mobile station performs maximal ratio combining [5] of the signal received from the multiple base stations. This diversity combining improves the coverage in regions of previously low-quality service provision, but at the expense of increased backhaul connections.

The set of base stations engaged in soft handover is known as the *active set*. The mobile station continuously monitors the received power level of the PIlot CHannels (PICHs) transmitted by its neighbouring base stations. The received pilot power levels of these base stations are then compared to two thresholds, the acceptance threshold, T_{acc} and the dropping threshold T_{drop}. Therefore, as a mobile moves away from base station 1, and towards base station 2, the pilot signal strength received from

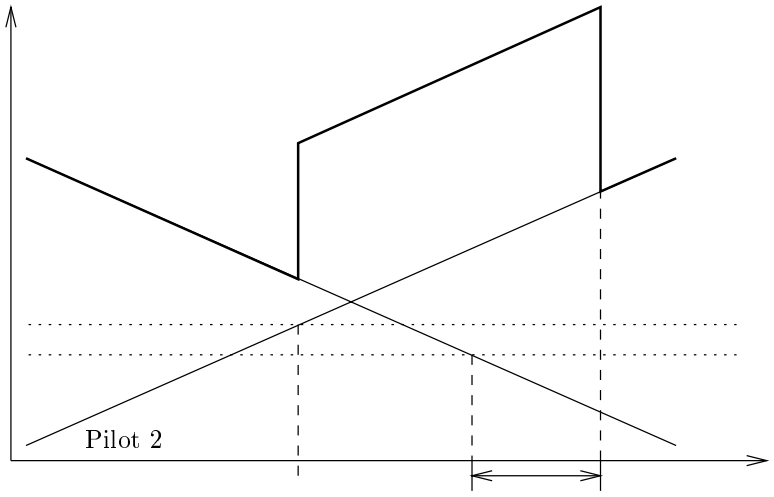
Pilot 2

spreading factor, SF, yielding

$$SINR_{DL} = \frac{SF \cdot S}{(1-\alpha)I_{Intra} + I_{Inter} + N_0}, \tag{2.3}$$

where $\alpha = 1$ corresponds to the ideal case of perfectly orthogonal intra-cell interference, and $\alpha = 0$ is for completely asynchronous intra-cell interference. Furthermore, N_0 is the thermal noise's power spectral density, S is the received signal power, I_{Intra} is the intra-cell interference and I_{Inter} is the inter-cell interference. Again, the interference plus noise power is scaled by the spreading factor, SF, since after the low-pass filtering the noise bandwidth is reduced by a factor of SF during the despreading process.

When in soft handover, the maximum ratio combining is performed on the N received signals of the N active base stations. Therefore, provided that the active base stations' received signals are independent, the SINR in this situation is :

$$SINR_{DL} = SINR_{DL_1} + SINR_{DL_2} + \ldots + SINR_{DL_N}. \tag{2.4}$$

2.3.5.2 Uplink

The uplink differs from the downlink in that the multiple access interference is asynchronous in the uplink due to the un-coordinated transmissions of the mobile stations, whereas it may remain quasi-synchronous in the downlink. Therefore, the intra-cell uplink interference is not orthogonal. A possible solution for mitigating this problem is employing Multi-User Detectors (MUDs) [85] at the base stations.

Thus, we define β as the MUD's efficiency, which effectively gives the percentage of the intra-cell interference that is removed by the MUD. Setting $\beta = 0.0$ implies 0% efficiency, when the intra-cell interference is not reduced by the MUD, whereas $\beta = 1.0$ results in the perfect suppression of all the intra-cell interference. Therefore, the expression for the uplink SINR is :

$$SINR_{UL} = \frac{SF \cdot S}{(1-\beta)I_{Intra} + I_{Inter} + N_0}. \tag{2.5}$$

When in soft handover, selection diversity is performed on the N received signals at each of the active base stations. Therefore, the SINR in this situation becomes :

$$SINR_{UL} = \max(SINR_{UL_1}, SINR_{UL_2}, \ldots, SINR_{UL_N}). \tag{2.6}$$

2.3.6 Multi-User Detection

Multiple access communications using DS-CDMA is interference limited due to the Multiple Access Interference (MAI) generated by the users transmitting simultaneously within the same bandwidth. The signals received from the users are separated with the aid of the despreader using spreading sequences that are unique to each user. Again, these spreading sequences are usually non-orthogonal. Even if they are orthogonal, the asynchronous uplink transmissions of the users or the time-varying nature of the mobile radio channel may partially destroy this orthogonality. The

non-orthogonal nature of the codes results in residual MAI, which degrades the performance of the system. The frequency selective mobile radio channel also gives rise to Inter-Symbol Interference (ISI) due to dispersive multipath propagation. This is exacerbated by the fact that the mobile radio channel is time-varying.

Conventional CDMA detectors - such as the matched filter [5,86] and the RAKE combiner [87] - are optimised for detecting the signal of a single desired user. RAKE combiners exploit the inherent multi-path diversity in CDMA, since they essentially consist of matched filters combining each resolvable path of the multipath channel. The outputs of these matched filters are then coherently combined according to a diversity combining technique, such as maximal ratio combining [88], equal gain combining or selective diversity combining . These conventional single-user detectors are inefficient, because the interference is treated as noise, and our knowledge concerning the CIR of the mobile channel, or that of the spreading sequences of the interferers is not exploited. The efficiency of these detectors is dependent on the cross-correlation (CCL) between the spreading codes of all the users. The higher the cross-correlation, the higher the MAI. This CCL-induced MAI is exacerbated by the effects of the dispersive multi-path channel and asynchronous transmissions. The utilisation of these conventional receivers results in an interference-limited system. Another weakness of the above-mentioned conventional CDMA detectors is the phenomenon known as the "near-far effect" [89,90]. For conventional detectors to operate efficiently, the signals received from all the users have to arrive at the receiver with approximately the same power. A signal that has a significantly weaker signal strength compared to the other signals will be "swamped" by the relatively higher powers of the other signals and the quality of the weaker signal at the output of the conventional receiver will be severely degraded. Therefore, stringent power control algorithms are needed to ensure that the signals arrive at similar powers at the receiver, in order to achieve a similar quality of service for different users [90, 91]. Using conventional detectors to detect a signal corrupted by MAI, while encountering a hostile channel results in an irreducible BER, even if the E_s/N_0 ratio is increased. This is because at high E_s/N_0 values the probability of errors due to thermal noise is insignificant compared to the errors caused by the MAI and the channel. Therefore, detectors that can reduce or remove the effects of MAI and ISI are needed in order to achieve user capacity gains. These detectors also have to be "near-far resistant", in order to avoid the need for stringent power control requirements. In order to mitigate the problem of MAI, Verdú [85] proposed the optimum multi-user detector for asynchronous Gaussian multiple access channels. This optimum detector significantly outperforms the conventional detector and it is near-far resistant, but unfortunately its complexity increases exponentially according to the order of $O(2^{NK})$, where N is the number of overlapping asynchronous bits considered in the detector's window, and K is the number of interfering users. In order to reduce the complexity of the receiver and yet to provide an acceptable BER performance, significant research efforts have been invested in the field of sub-optimal CDMA multiuser receivers [85, 92].

In summary, multi-user detectors reduce the error floor due to MAI and this translates into user capacity gains for the system. These multi-user detectors are also near-far resistant to a certain extent and this results in less stringent power control requirements. However, multi-user detectors are more complex than conventional

detectors. Coherent detectors require the explicit knowledge of the channel impulse response estimates, which implies that a channel estimator is needed in the receiver, and hence training sequences have to be included in the transmission frames. Training sequences are specified in the TDD mode of the UTRA standard and enable the channel impulse response of each simultaneously communicating user to be derived, which is necessary for the multi-user detectors to be able to separate the signals received from each user. These multi-user detectors also exhibit an inherent latency, which results in delayed reception. Multi-user detection is more suitable for the uplink receiver since the base station has to detect all users' signals anyway and it can tolerate a higher complexity. In contrast, a hand-held mobile receiver is required to be compact and lightweight, imposing restrictions on the available processing power. Recent research into blind MUDs has shown that data detection is possible for the desired user without invoking the knowledge of the spreading sequences and channel estimates of other users. Hence using these detectors for downlink receivers is becoming feasible.

2.4 Simulation Results

This section presents simulation results obtained for an FDD mode UMTS type CDMA cellular network, investigating the applicability of various soft handover metrics when subjected to different propagation conditions. This is followed by performance curves obtained using adaptive antenna arrays, when subjected to both non-shadowed as well as shadowed propagation conditions. The performance of adaptive modulation techniques used in conjunction with adaptive antenna arrays in a shadow faded environment is then characterised.

2.4.1 Simulation Parameters

Simulations of an FDD mode UMTS type CDMA based cellular network were conducted for various scenarios and algorithms in order to study the interactions of the processes involved in such a network. As in the standard, the frame length was set to 10 ms, containing 15 power control timeslots. The power control target SINR was chosen to give a Bit Error Ratio (BER) of 1×10^{-3}, with a low quality outage occurring at a BER of 5×10^{-3} and an outage taking place at a BER of 1×10^{-2}. The received SINRs at both the mobile and the base stations were required for each of the power control timeslots, and hence the outage and low quality outage statistics were gathered. If the received SINR was found to be below the outage SINR for 75 consecutive power control timeslots, corresponding to 5 consecutive transmission frames or 50 ms, the call was dropped. The post despreading SINRs necessary for obtaining the target BERs were determined with the aid of physical-layer simulations using a 4-QAM modulation scheme, in conjunction with 1/2 rate turbo coding and joint detection over a COST 207 seven-path Bad Urban channel [93]. For a spreading factor of 16, the post-de-spreading SINR required to give a BER of 1×10^{-3} was 8.0 dB, for a BER of 5×10^{-3} it was 7.0 dB, and for a BER of 1×10^{-2} was about 6.6 dB. These values can be seen along with the other system parameters in Table 2.2.

The-pre de-spreading SINR is related to E_b/N_o and to the spreading factor by :

$$SINR = (E_b/N_o)/SF, \tag{2.7}$$

where the spreading factor $SF = W/R$, with W being the chip rate and R the data rate. A receiver noise figure of 7 dB was assumed for both the mobile and the base stations [81]. Thus, in conjunction with a thermal noise density of -174 dBm/Hz and a noise bandwidth of 3.84 MHz, this resulted in a receiver noise power of -100 dBm. The power control algorithm used was relatively simple, and unrelated to the previously introduced schemes of Section 2.3.3. Furthermore, since it allowed a full transmission power change of 15 dB within a 15-slot UTRA data frame, the power control scheme advocated is unlikely to limit the network's capacity.

Specifically, for each of the 15 timeslots per transmitted frame, both the mobile and base station transmit powers were adjusted such that the received SINR was greater than the target SINR, but less than the target SINR plus 1 dB of hysteresis. When in soft handover, a mobile's transmission power was only increased, if all of the base stations in the Active Base station Set (ABS) requested a power increase, but was it decreased if any of the base stations in the ABS had an excessive received SINR. In the downlink, if the received SINR at the mobile was insufficiently high then all of the active base stations were commanded to increase their transmission powers. Similarly, if the received SINR was unnecessarily high, then the active base stations would reduce their transmit powers. The downlink intra-cell interference orthogonality factor, α, as described in Section 2.3.5, was set to 0.5 [94–96]. Due to the frequency reuse factor of one, with its associated low frequency reuse distance, it was necessary for both the mobiles and the base stations, when initiating a new call or entering soft handover, to increase their transmitted power gradually. This was required to prevent sudden increases in the level of interference, particularly on links using the same base station. Hence, by gradually increasing the transmit power to the desired level, the other users of the network were capable of compensating for the increased interference by increasing their transmit powers, without encountering undesirable outages. In an FDMA/TDMA network this effect is less noticeable due to the significantly higher frequency reuse distance.

Since a dropped call is less desirable from a user's viewpoint than a blocked call, two resource allocation queues were invoked, one for new calls and the other - higher priority - queue, for handovers. By forming a queue of the handover requests, which have a higher priority during contention for network resources than new calls, it is possible to reduce the number of dropped calls at the expense of an increased blocked call probability. A further advantage of the Handover Queueing System (HQS) is that during the time a handover is in the queue, previously allocated resources may become available, hence increasing the probability of a successful handover. However, in a CDMA based network the capacity is not hard-limited by the number of frequency/timeslot combinations available, like in a FDMA/TDMA based network, such as GSM. The main limiting factors are the number of available spreading and OVSF codes, where the number of the available OVSF codes is restricted to the spreading factor minus one, since an OVSF code is reserved for the pilot channel. This is, because although the pilot channel has a spreading factor of 256, it removes an entire branch of the OVSF code generation tree. Other limiting factors are the

Parameter	Value	Parameter	Value
Frame length	10 ms	Timeslots per frame	15
Target E_b/N_o	8.0 dB	Outage E_b/N_o	6.6 dB
Low Quality (LQ) Outage E_b/N_o	7.0 dB	BS Pilot Power	-5 dBm
BS/MS Minimum TX Power	-44 dBm	BS Antenna Gain	11 dBi
BS/MS Maximum TX Power	+21 dBm	MS Antenna Gain	0 dBi
Attenuation at 1 m reference point	39 dB	Pathloss exponent	-3.5
Power control SINR hysteresis	1 dB	Cell radius	150 m
Downlink scrambling codes per BS	1	Modulation scheme	4-QAM
Downlink OVSF codes per BS	Variable	Max new-call queue-time	5 s
Uplink scrambling codes per BS	Variable	Average inter-call time	300 s
Uplink OVSF codes per BS	Variable	Average call length	60 s
Spreading factor	Variable	Data/voice bit rate	Variable
Remove BS from ABS threshold	Variable	Add BS to ABS threshold	Variable
User speed	1.34 m/s (3 mph)	Noisefloor	-100 dBm
		Size of ABS	2

Table 2.2: Simulation parameters of the UTRA-type CDMA based cellular network.

interference levels in conjunction with the restricted maximum transmit power, resulting in excessive call dropping rates. New call allocation requests were queued for up to 5s, if they could not be immediately satisfied, and were blocked if the request had not been completed successfully within the 5s.

Similarly to our TDMA-based investigations portrayed in Chapter **??**, several network performance metrics were used in order to quantify the quality of service provided by the cellular network, namely the :

- New Call Blocking probability, P_B,
- Call Dropping or Forced Termination probability, P_{FT},
- Probability of low quality connection, P_{low},
- Probability of Outage, P_{out},
- Grade Of Service, GOS.

The new call blocking probability, P_B, is defined as the probability that a new call is denied access to the network. In an FDMA/TDMA based network, such as GSM, this may occur because there are no available physical channels at the desired base station or the available channels are subject to excessive interference. However, in a CDMA based network this does not occur, provided that no interference level based admission control is performed and hence the new call blocking probability is typically low.

The call dropping probability, P_{FT}, is the probability that a call is forced to terminate prematurely. In a GSM type network, an insufficiently high SINR, which inevitably leads to dropped calls, may be remedied by an intra- or inter-cell handover. However, in CDMA either the transmit power must be increased, or a soft handover must be performed in order to exploit the available diversity gain.

Again, the probability of a low quality connection is defined as :

$$\begin{aligned} P_{low} &= P\{SINR_{uplink} < SINR_{req} \text{ or } SINR_{downlink} < SINR_{req}\} \\ &= P\{min(SINR_{uplink}, SINR_{downlink}) < SINR_{req}\}. \end{aligned} \quad (2.8)$$

The GOS was defined in [97] as :

$$\begin{aligned} GOS &= P\{\text{unsuccessful or low-quality call access}\} \\ &= P\{\text{call is blocked}\} + P\{\text{call is admitted}\} \times \\ &\quad P\{\text{low signal quality and call is admitted}\} \\ &= P_B + (1 - P_B)P_{low}, \end{aligned} \quad (2.9)$$

and is interpreted as the probability of unsuccessful network access (blocking), or low quality access, when a call is admitted to the system.

In our forthcoming investigations, in order to compare the network capacities of different networks, similarly to our TDMA-based investigations in Chapter **??**, it was decided to use two scenarios defined as :

- A *conservative scenario*, where the maximum acceptable value for the new call blocking probability, P_B, is 3%, the maximum call dropping probability, P_{FT}, is 1%, and P_{low} is 1%.
- A *lenient scenario*, where the maximum acceptable value for the new call blocking probability, P_B, is 5%, the maximum call dropping probability, P_{FT}, is 1%, and P_{low} is 2%.

In the next section we consider the network's performance considering both fixed and normalised soft handover thresholds using both received pilot power and received pilot power versus interference threshold metrics. A spreading factor of 16 was used, corresponding to a channel data rate of 3.84Mbps/16 = 240 kbps with no channel coding, or 120 kbps when using 1/2 rate channel coding. It must be noted at this stage that the results presented in the following sections are network capacities obtained using a spreading factor of 16. The network capacity results presented in the previous chapter, which were obtained for an FDMA/TDMA GSM-like system, were achieved for speech-rate users. Here we assumed that the channel coded speech-rate was 15 kbps, which is the lowest possible Dedicated Physical Data CHannel (DPDCH) rate. Speech users having a channel coded rate of 15 kbps may be supported by invoking a spreading factor of 256. Hence, subjecting the channel data rate of 15 kbps to 1/2 rate channel coding gives a speech-rate of 7.5 kbps, or if protected by a 2/3 rate code the speech-rate becomes 10 kbps, which are sufficiently high for employing the so-called Advanced MultiRate (AMR) speech codec [98–100] capable of operating at rates between 4.7 kbps and 12.2 kbps. Therefore, by multiplying the resultant network capacities according to a factor of 256/16=16, it is possible to estimate the number of speech users supported by a speech-rate network. However, with the aid of our exploratory simulations, conducted using a spreading factor of 256, which are not presented here, we achieved network capacities higher than 30 times the network capacity supported in conjunction with a spreading factor of 16. Therefore, it would

appear that the system is likely to support more than 16 times the number of 240 kbps data users, when communicating at the approximately 16 times lower speech-rate, employing a high spreading factor of 256. Hence, using the above-mentioned scaling factor of 16 we arrive at the lower bound of network capacity. A mobile speed of 3 mph was used in conjunction with a cell size of 150m radius, which was necessarily small in order to be able to support the previously assumed 240 kbps high target data rate. The performance advantages of using both adaptive beamforming and adaptive modulation assisted networks are also investigated.

2.4.2 The Effect of Pilot Power on Soft Handover Results

In this section we consider the settings of the soft handover thresholds, for an IS-95 type handover algorithm [101], where the handover decisions are based on downlink pilot power measurements. Selecting inappropriate values for the soft handover thresholds, namely for the *acceptance threshold* and the *drop threshold*, may result in an excessive number of blocked and dropped calls in certain parts of the simulation area. For example, if the *acceptance threshold* that has to be exceeded by the signal level for a base station to be added to the active set is too high (Threshold B in Figure 2.6), then a user may be located within a cell, but it would be unable to add any base stations to its active base station set. Hence this user is unable to initiate a call. Figure 2.6 illustrates this phenomenon and shows that the *acceptance thresholds* must be set sufficiently low for ensuring that at least one base station covers every part of the network.

Another consequence of setting the *acceptance threshold* to an excessively high value, is that soft handovers may not be completed. This may occur when a user leaving the coverage area of a cell, since the pilot signal from that cell drops below the *drop threshold*, before the signal from the adjacent cell becomes sufficiently strong for it to be added to the active base station set. However, if the *acceptance threshold*, in conjunction with the *drop threshold*, is set correctly, then new calls and soft handovers should take place as required, so long as the availability of network resources allows it. Care must be taken however, not to set the soft handover threshold too low, otherwise the mobiles occupy additional network resources and create extra interference, due to initiating unnecessary soft-handovers.

2.4.2.1 Fixed Received Pilot Power Thresholds without Shadowing

Figure 2.7 shows the new call blocking probability of a network using a spreading factor of 16, in conjunction with fixed received pilot signal strength based soft handover thresholds without imposing any shadowing effects. The figure illustrates that reducing both the acceptance and the dropping soft handover thresholds results in an improved new call blocking performance. Reducing the threshold at which further base stations may be added to the Active Base station Set (ABS) increases the probability that base stations exist within the ABS, when a new call request is made. Hence, as expected, the new call blocking probability is reduced, when the acceptance threshold is reduced. Similarly, dropping the threshold at which base stations are removed from the ABS also results in an improved new call blocking probability, since

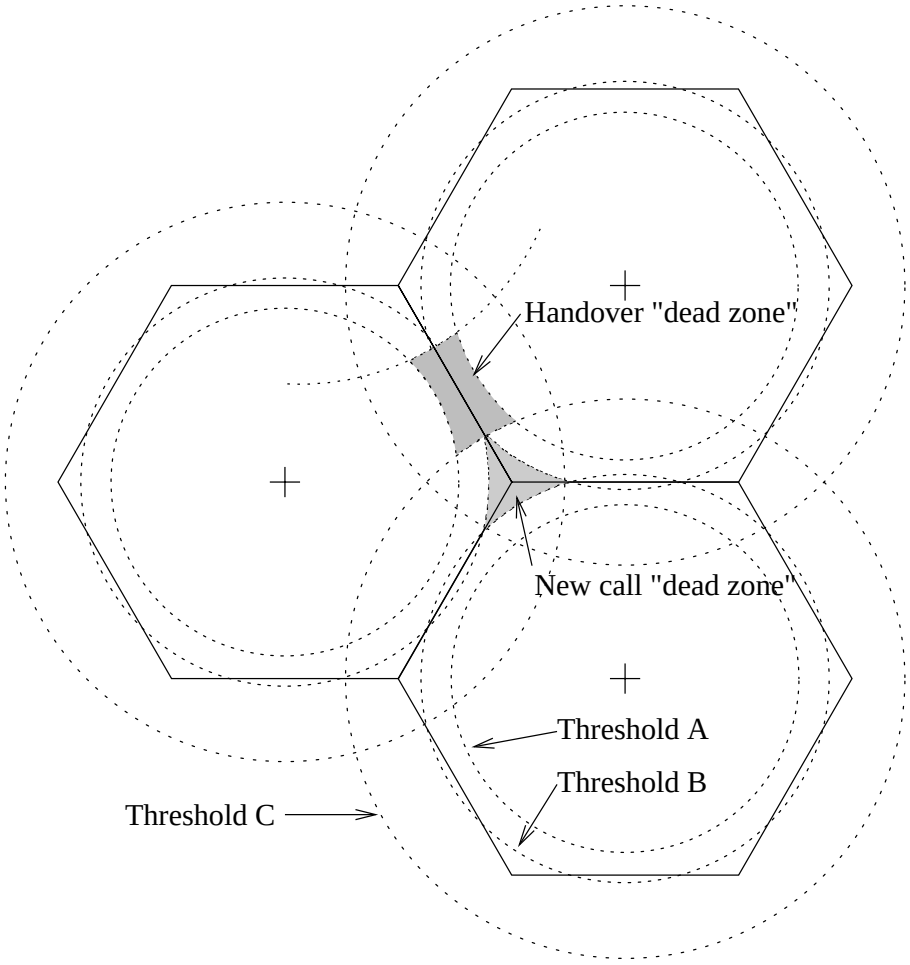

Figure 2.6: This figure indicates that using inappropriate soft handover thresholds may lead to blocked and dropped calls due to insufficient pilot coverage of the simulation area. Threshold A is the drop threshold, which when combined with the acceptance threshold C can fail to cover the simulation area sufficiently well, thus leading to soft handover failure. When combining threshold A with the acceptance threshold B, users located in the "new call dead zone" may become unable to initiate calls.

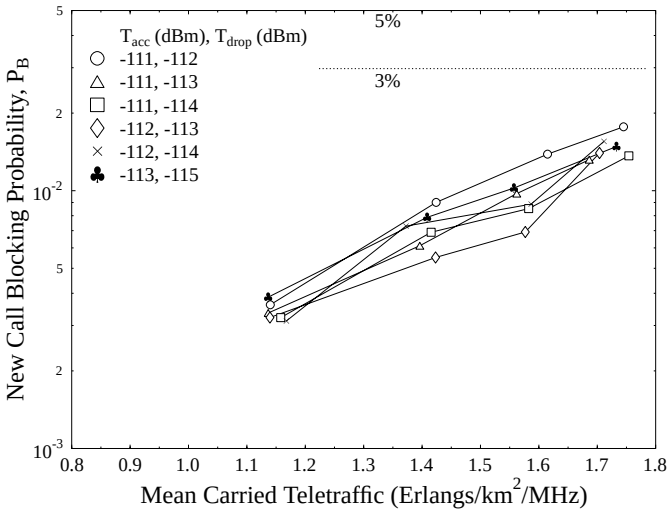

Figure 2.7: New call blocking probability versus mean carried traffic of a CDMA based cellular network using **fixed received pilot power** based soft handover thresholds **without shadowing** for SF=16.

a base station is more likely to be retained in the ABS as a mobile moves away from it. Therefore, should a mobile attempt to initiate a call in this situation, there is a greater chance that the ABS will contain a suitable base station.

The associated call dropping probability is depicted in Figure 2.8, indicating that reducing the soft handover thresholds, and thus increasing the time spent in soft handover, improved the performance up to a certain point. However, above this point the additional interference inflicted by the soft handover process led to a degraded performance. For example, in this figure the performance associated with T_{acc}=-111 dBm improved, when T_{drop} was decreased from -112 dBm to -113 dBm. However, at high traffic levels the performance degraded when T_{drop} was decreased further, to -114 dBm. The call dropping probability obtained using T_{acc}=-113 dBm and T_{drop}=-115 dBm was markedly lower for the lesser levels of traffic carried due to the extra diversity gain provided by the soft handover process. However, since these soft handover thresholds resulted in a greater proportion of time spent in soft handover, the levels of interference were increased, and thus at the higher traffic levels the performance degraded rapidly, as can be seen in Figure 2.8. Hence, the call dropping performance is based on a trade-off between the diversity gain provided by the soft handover process and the associated additional interference.

The probability of low quality access (not explicitly shown) was similar in terms of its character to the call dropping probability, since reducing T_{drop} improved the performance to a certain point, after which it degraded.

The mean number of base stations in the ABS is shown in Figure 2.9, illustrating that reducing the soft handover thresholds leads, on average, to a higher number of

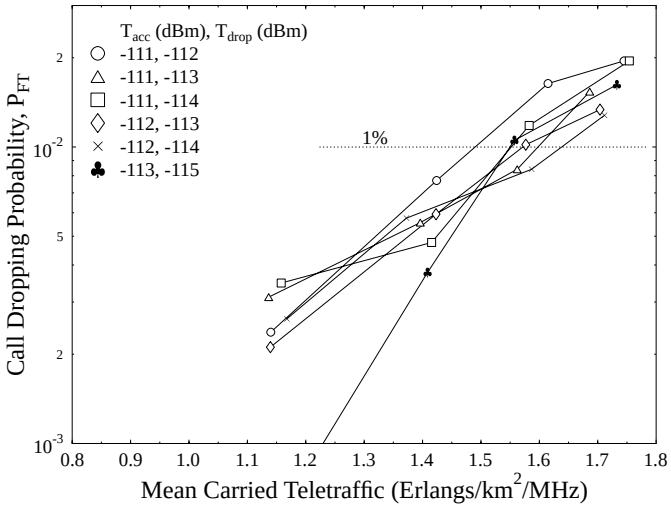

Figure 2.8: Call dropping probability versus mean carried traffic of a CDMA based cellular network using **fixed received pilot power** based soft handover thresholds **without shadowing** for SF=16.

base stations in the ABS. Therefore, a greater proportion of call time is spent in soft handover. The associated diversity gain improves the link quality of the reference user but additional co-channel interference is generated by the diversity links, thus ultimately reducing the call quality, as shown in Figure 2.8. Additionally, this extra co-channel interference required more transmission power for maintaining the target SINR as depicted in Figure 2.10. This figure shows that when lower soft handover thresholds are used, and thus a greater proportion of time is spent in soft handover, greater levels of co-channel interference are present, and thus the required mean transmission powers became higher. It is interesting to note that for the highest soft handover thresholds employed in Figure 2.10, the downlink transmission power required for maintaining the target SINR is lower than the uplink transmission power, whereas, for the lower soft handover thresholds, the required mean uplink transmission power is lower than the downlink transmission power. The required downlink transmission power was, in general, lower than the uplink transmission power due to the mobile stations' ability to perform maximal ratio combining when in soft handover. This was observed despite the absence of the pilot interference in the uplink, and despite the base stations' ability to perform selective diversity which offers less diversity gain when compared to maximal ratio combining. However, reducing the soft handover thresholds to the lowest levels shown in Figure 2.10, led to increased co-channel interference on the downlink, thus requiring higher base station transmission powers, as clearly seen in the figure.

In summary, as seen by comparing Figures 2.7-2.10 the maximum capacity of the network using fixed received pilot power based soft handover thresholds was limited

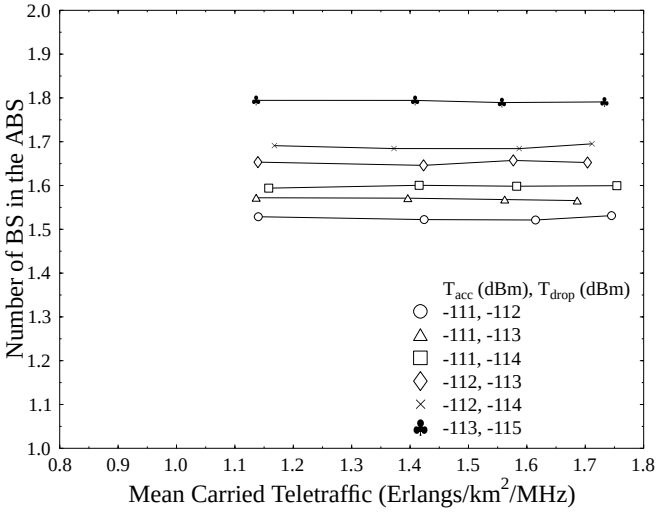

Figure 2.9: Mean number of base stations in the active base station set versus mean carried traffic of a CDMA based cellular network using **fixed received pilot power** based soft handover thresholds **without shadowing** for SF=16.

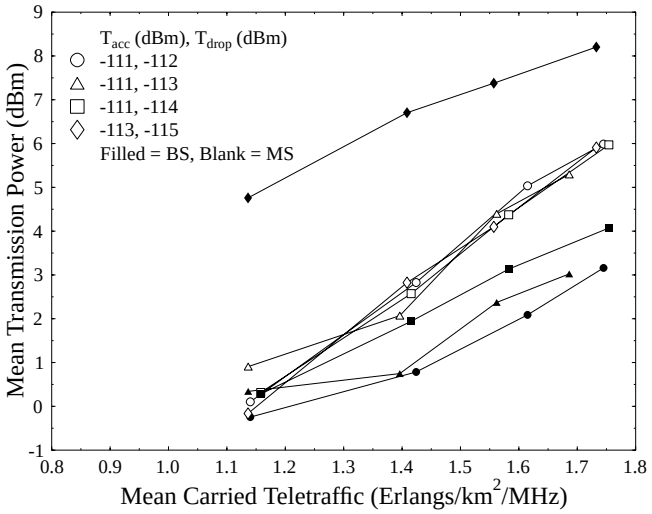

Figure 2.10: Mean transmission power versus mean carried traffic of a CDMA based cellular network using **fixed received pilot power** based soft handover thresholds **without shadowing** for SF=16.

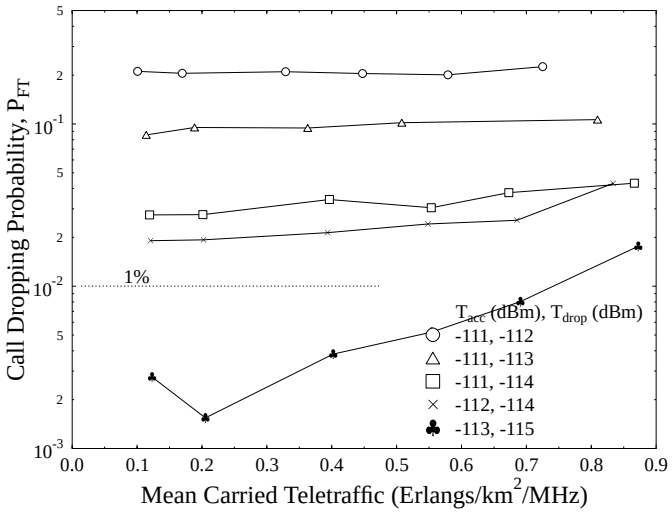

Figure 2.11: Call dropping probability versus mean carried traffic of a CDMA based cellular network using **fixed received pilot power** based soft handover thresholds in conjunction **with 0.5 Hz shadowing having a standard deviation of 3 dB** for SF=16.

by the call dropping probability. The new call blocking probability remained below the 3% limit, thanks to the appropriate choice of thresholds used, whilst the probability of low quality access was constantly below the 1% mark. Therefore, the maximum normalised teletraffic load was 1.64 Erlangs/km^2/MHz, corresponding to a total network capacity of 290 users, while satisfying both quality of service constraints, was achieved with the aid of an acceptance threshold of -112 dBm and a dropping threshold of -114 dBm. A mean ABS size of 1.7 base stations was registered at this traffic level, and both the mobile and base stations exhibited a mean transmission power of 5.1 dBm.

2.4.2.2 Fixed Received Pilot Power Thresholds with 0.5 Hz Shadowing

In this section we examine the achievable performance, upon using fixed received pilot power based soft handover thresholds when subjected to log-normal shadow fading having a standard deviation of 3 dB and a maximum frequency of 0.5 Hz.

The call dropping results of Figure 2.11 suggested that the network's performance was poor when using fixed received pilot power soft handover thresholds in the above mentioned shadow fading environment. The root cause of the problem is that the fixed thresholds must be set such that the received pilot signals, even when subjected to shadow fading, are retained in the active set. Therefore, setting the thresholds too high results in the base stations being removed from the active set, thus leading to an excessive number of dropped calls. However, if the thresholds are set too low, in order

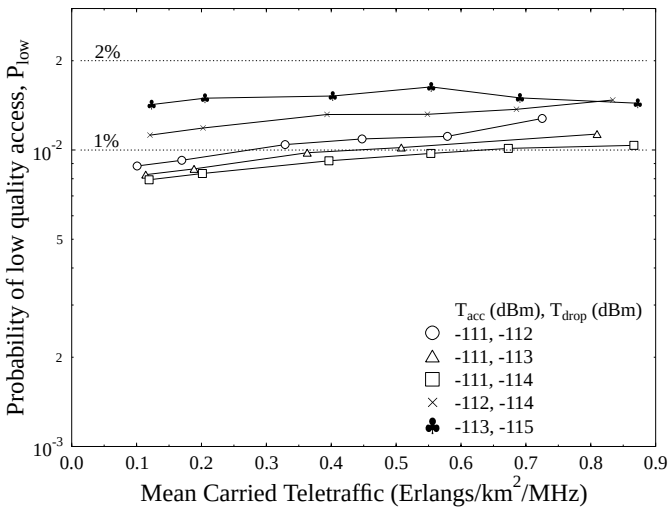

Figure 2.12: Probability of low quality access versus mean carried traffic of a CDMA based cellular network using **fixed received pilot power** based soft handover thresholds in conjunction **with 0.5 Hz shadowing having a standard deviation of 3 dB** for SF=16.

to counteract this phenomenon, then the base stations can be in soft handover for too high a proportion of time, and thus an unacceptable level of low quality accesses is generated due to the additional co-channel interference inflicted by the high number of active base stations. Figure 2.11 shows that reducing the soft handover thresholds improved the network's call dropping probability, but Figure 2.12 illustrates that reducing the soft handover thresholds engendered an increase in the probability of a low quality access.

The network cannot satisfy the quality requirements of the conservative scenario, namely that of maintaining a call dropping probability of 1% combined with a maximum probability of low quality access below 1%. However, the entire network supported 127 users, whilst meeting the lenient scenario's set of criteria, which consists of a maximum call dropping probability of 1% and a probability of low quality access of below 2%, using the thresholds of T_{acc}=-113 dBm and T_{drop}=-115 dBm.

2.4.2.3 Fixed Received Pilot Power Thresholds with 1.0 Hz Shadowing

This section presents results obtained using fixed receiver pilot power based soft handover thresholds in conjunction with log-normal shadow fading having a standard deviation of 3 dB and a maximum fading frequency of 1.0 Hz.

The corresponding call dropping probability is depicted in Figure 2.13, showing that using fixed thresholds in a propagation environment exposed to shadow fading resulted in a very poor performance. This was due to the shadow fading induced fluc-

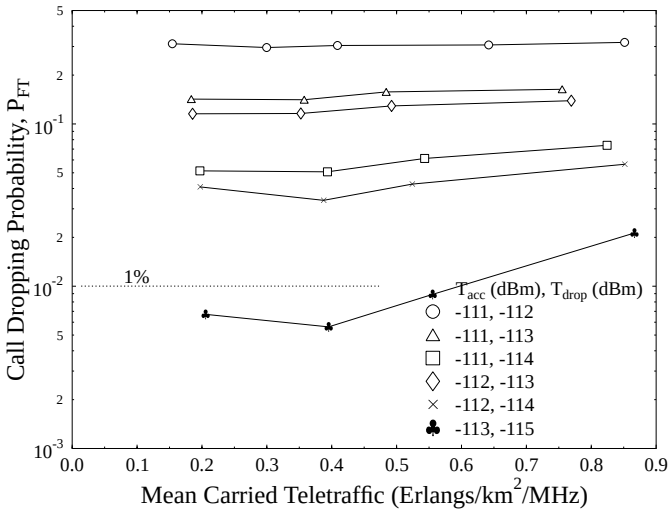

Figure 2.13: Call dropping probability versus mean carried traffic of a CDMA based cellular network using **fixed received pilot power** based soft handover thresholds in conjunction **with 1 Hz shadowing having a standard deviation of 3 dB** for SF=16.

tuations of the received pilot signal power, which resulted in removing base stations from the ABS mid-call, which ultimately engendered dropped calls. Hence, lowering the fixed thresholds significantly reduced the call dropping probability. However, this led to a deterioration of the low quality access probability, as shown in Figure 2.14. The probability of low quality access was also very poor due to the rapidly fluctuating interference-limited environment. This was shown particularly explicitly in conjunction with T_{acc}=-113 dBm and T_{drop}=-115 dBm, where reducing the number of users resulted in a degradation of the low quality access performance due to the higher deviation of the reduced number of combined sources of interference. In contrast, adding more users led to a near-constant level of interference that varied less dramatically.

It was found that the network was unable to support any users at the required service quality, since using the thresholds that allowed the maximum 1% call dropping probability restriction to be met, led to a greater than 2% probability of a low quality outage occurring.

2.4.2.4 Summary

In summary of our findings in the context of Figure 2.7-2.14, a disadvantage of using fixed soft handover thresholds is that in some locations all pilot signals may be weak, whereas in other locations, all of the pilot signals may be strong due to the localised propagation environment or terrain. Hence, using relative or normalised soft handover thresholds is expected to be advantageous in terms of overcoming this

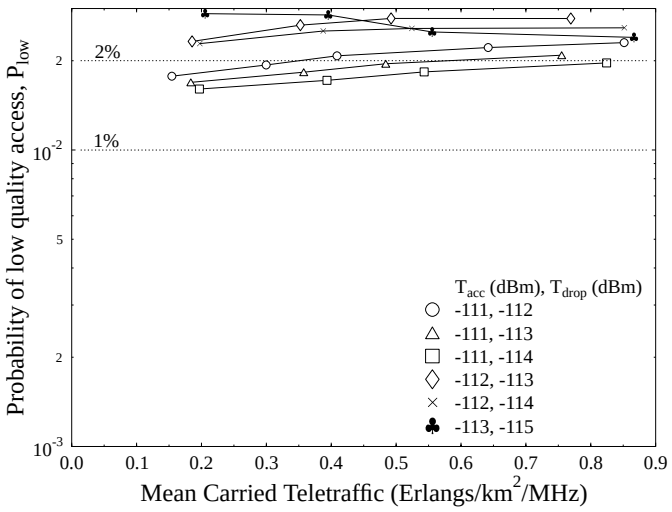

Figure 2.14: Probability of low quality access versus mean carried traffic of a CDMA based cellular network using **fixed received pilot power** based soft handover thresholds in conjunction **with 1 Hz shadowing having a standard deviation of 3 dB** for SF=16.

limitation. An additional benefit of using dynamic thresholds is confirmed within a fading environment, where the received pilot power may drop momentarily below a fixed threshold, thus causing unnecessary removals and additions to/from the ABS. However, these base stations may have been the only base stations in the ABS, thus ultimately resulting in a dropped call. When using dynamically controlled thresholds this scenario would not have occurred. Hence, in the next section we considered the performance of using relative received pilot power based soft handover thresholds under both non-shadowing and shadowing impaired propagation conditions.

To summarise, using fixed received pilot power thresholds in a non-shadowing environment resulted in a total network capacity of 290 users for both quality of service scenarios, namely for both the conservative and lenient scenarios considered. However, this performance was severely degraded in a shadow fading impaired propagation environment, where a total network capacity of 127 users was supported in conjunction with a maximum shadow fading frequency of 0.5 Hz. Unfortunately, the network capacity could not be evaluated when using a maximum shadow fading frequency of 1.0 Hz due to the contrasting characteristics of the dropped call and low quality access probability results.

2.4.2.5 Relative Received Pilot Power Thresholds without Shadowing

Employing relative received pilot power thresholds is important in realistic propagation environments exposed to shadow fading. More explicitly, in contrast to the

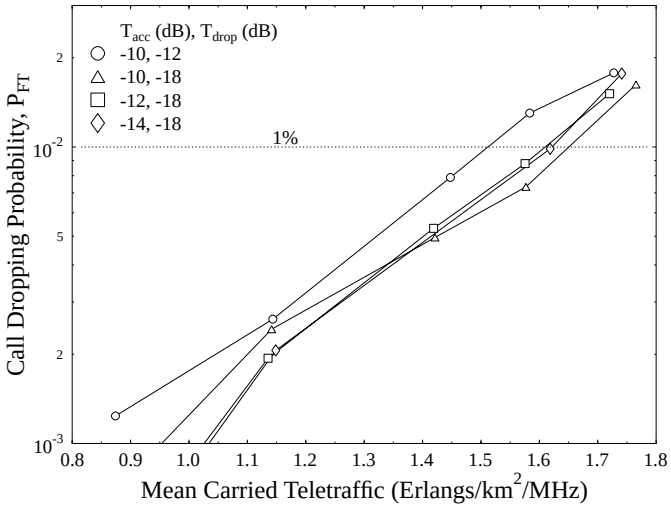

Figure 2.15: Call dropping probability versus mean carried traffic of a CDMA based cellular network using **relative received pilot power** based soft handover thresholds **without shadowing** for SF=16.

previously used thresholds, which were expressed in terms of dBm, i.e. with respect to 1 mW, in this section the thresholds T_{acc} and T_{drop} are expressed in terms of dB relative to the received pilot strength of the base stations in the ABS. Their employment also caters for situations, where the absolute pilot power may be too low for use in conjunction with fixed thresholds, but nonetheless sufficiently high for reliable communications. Hence, in this section we examine the performance of relative received pilot power based soft handover thresholds in a non-shadow faded environment.

The call dropping performance is depicted in Figure 2.15, which shows that reducing the soft handover thresholds, and thus increasing the time spent in soft handover, improved the call dropping performance. It was also found in the cases considered here, that simultaneously the probability of a low quality access decreased, as illustrated by Figure 2.16. However, it was also evident in both figures, that reducing the soft handover thresholds past a certain point resulted in degraded performance due to the extra interference incurred during the soft handover process.

Since the probability of low quality access was under the 1% threshold, the network capacity for both the lenient and conservative scenarios were the same, namely 1.65 Erlangs/km^2/ MHz or a total of 288 users over the entire simulation area of 2.86 km^2. The mean ABS size was 1.7 base stations, with a mean mobile transmission power of 4.1 dBm and an average base station transmit power of 4.7 dBm.

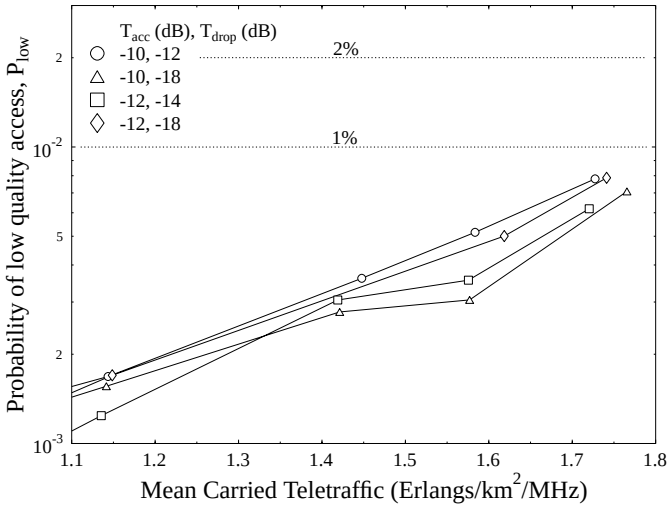

Figure 2.16: Probability of low quality access versus mean carried traffic of a CDMA based cellular network using **relative received pilot power** based soft handover thresholds **without shadowing** for SF=16.

2.4.2.6 Relative Received Pilot Power Thresholds with 0.5 Hz Shadowing

In this section we present results obtained using relative received pilot power based soft handover thresholds in a shadowing-impaired propagation environment. The maximum shadow fading frequency was 0.5 Hz and the standard deviation of the log-normal shadowing was 3 dB.

Figure 2.17 depicts the call dropping probability for several relative thresholds and shows that by reducing both the thresholds, the call dropping performance is improved. This enables the mobile to add base stations to its ABS earlier on during the soft handover process, and to relinquish them at a much later stage than in the case of using higher handover thresholds. Therefore, using lower relative soft handover thresholds results in longer period of time spent in soft handover, as can be seen in Figure 2.18, which shows the mean number of base stations in the ABS.

The probability of low quality access is shown in Figure 2.19, illustrating that, in general, as the relative soft handover thresholds were reduced, the probability of low quality access increased. This demonstrated that spending more time in soft handover generated more co-channel interference and thus degraded the network's performance. However, the difference between the two thresholds must also be considered. For example, the probability of low quality access is higher in conjunction with T_{acc}=-16 dB and T_{drop}=-18 dB, than using T_{acc}=-16 dB and T_{drop}=-20 dB, since the latter scenario has a higher mean number of base stations in its ABS. Therefore, there is a point at which the soft handover gain experienced by the desired user outweighs the detrimental effects of the extra interference generated by base stations' transmissions

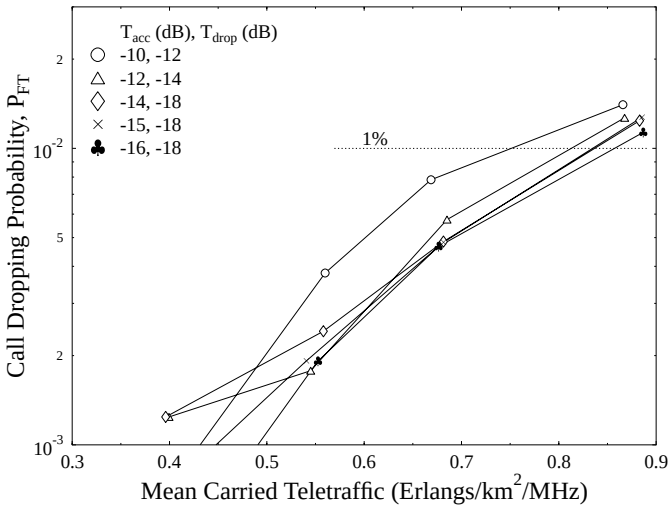

Figure 2.17: Call dropping probability versus mean carried traffic of a CDMA based cellular network using **relative received pilot power** based soft handover thresholds in conjunction **with 0.5 Hz shadowing and a standard deviation of 3 dB** for SF=16.

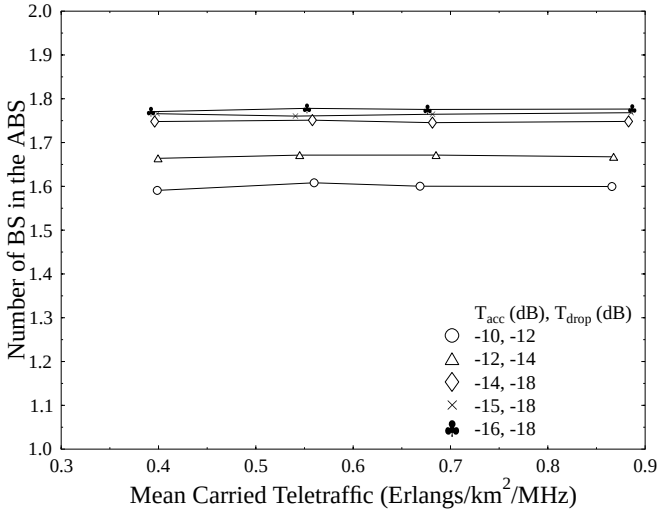

Figure 2.18: Mean number of base stations in the active base station set versus mean carried traffic of a CDMA based cellular network using **relative received pilot power** based soft handover thresholds in conjunction **with 0.5 Hz shadowing and a standard deviation of 3 dB** for SF=16.

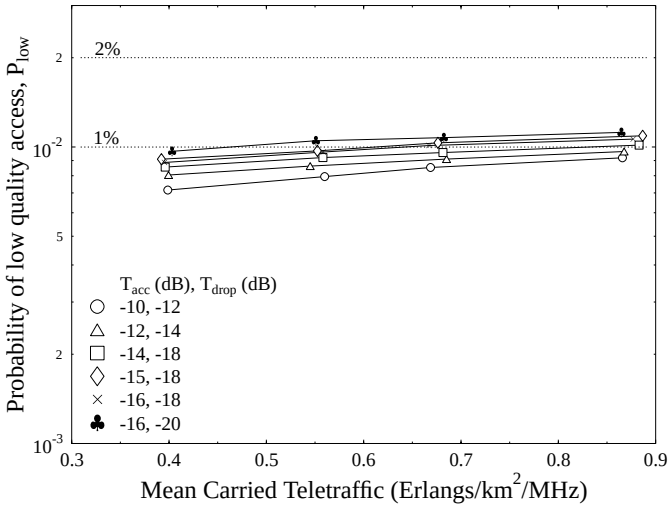

Figure 2.19: Probability of low quality access versus mean carried traffic of a CDMA based cellular network using **relative received pilot power** based soft handover thresholds in conjunction **with 0.5 Hz shadowing and a standard deviation of 3 dB** for SF=16.

to users engaged in the soft handover process.

Figure 2.20 shows the mean transmission powers of both the mobiles and the base stations. The mobiles are required to transmit at a lower power than the base stations, because the base stations are not subjected to downlink pilot power interference and to soft handover interference. Furthermore, the mobiles are not affected by the level of the soft handover thresholds, because only selective diversity is performed in the uplink, and hence the mobile transmits as if not in soft handover. As the soft handover thresholds were reduced, the time spent in soft handover increased and thus the mean base transmission power had to be increased in order to overcome the additional downlink interference.

The maximum network capacity of 0.835 Erlangs/km^2/MHz, or 144 users over the entire simulation area, was achieved using the soft handover thresholds of T_{acc}=-14 dB and T_{drop}=-18 dB for the conservative scenario. The mean ABS size was 1.77 base stations, while the mean mobile transmit power was -1.5 dBm and 0.6 dBm for the base stations. In the lenient scenario a maximum teletraffic load of 0.865 Erlangs/km^2/MHz, corresponding to a total network capacity of 146 users was maintained using soft handover thresholds of T_{acc}=-16 dB and T_{drop}=-18 dB. The mean number of base stations in the ABS was 1.78, with an average transmit power of -1.5 dBm for the mobile handset, and 1.3 dBm for the base station.

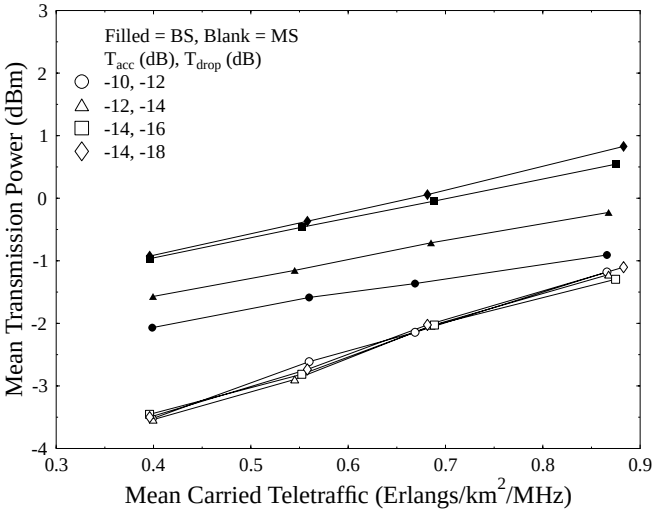

Figure 2.20: Mean transmission power versus mean carried traffic of a CDMA based cellular network using **relative received pilot power** based soft handover thresholds in conjunction **with 0.5 Hz shadowing and a standard deviation of 3 dB** for SF=16.

2.4.2.7 Relative Received Pilot Power Thresholds with 1.0 Hz Shadowing

In this section we present further performance results obtained using relative received pilot power based soft handover thresholds in a shadowing propagation environment. The maximum shadow fading frequency was 1.0 Hz and the standard deviation of the log-normal shadowing was 3 dB.

On comparing the call dropping probability curves seen in Figure 2.21 with the call dropping probability obtained for a maximum shadow fading frequency of 0.5 Hz in Figure 2.17 it was found that the performance of the 1.0 Hz frequency shadowing scenario was slightly worse. However, the greatest performance difference was observed in the probability of low quality access, as can be seen in Figure 2.22.

Using the soft handover thresholds which gave a good performance for a maximum shadow fading frequency of 0.5 Hz resulted in significantly poorer low quality access performance for a maximum shadowing frequency of 1.0 Hz. In order to obtain a probability of low quality access of below 1% it was necessary to use markedly different soft handover thresholds, which reduced the time spent in soft handover and hence also the size of the ABS, as illustrated in Figure 2.23.

For the conservative scenario, where the maximum probability of low quality access, P_{low}, was set to 1%, the maximum network capacity was found to be 0.69 Erlangs/km^2/MHz, equivalent to a total network capacity of 127 users, obtained using T_{drop}=-2 dB and T_{acc}=-16 dB. In contrast, in the lenient scenario, where the P_{low} limit was 2%, the maximum number of users supported was found to be 144, or

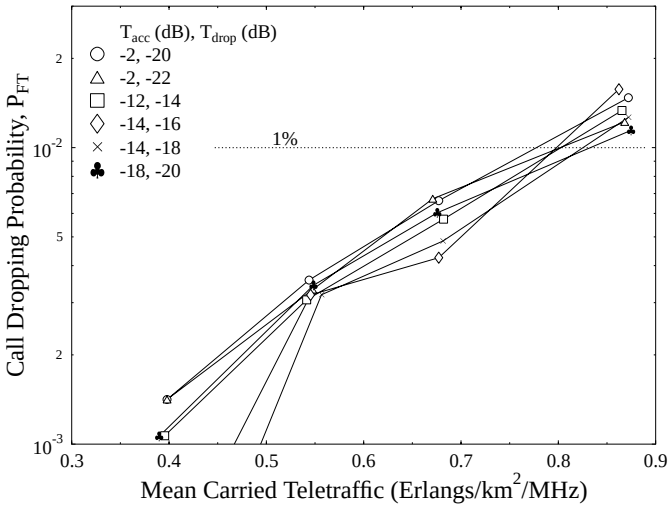

Figure 2.21: Call dropping probability versus mean carried traffic of a CDMA based cellular network using **relative received pilot power** based soft handover thresholds in conjunction **with 1 Hz shadowing and a standard deviation of 3 dB** for SF=16.

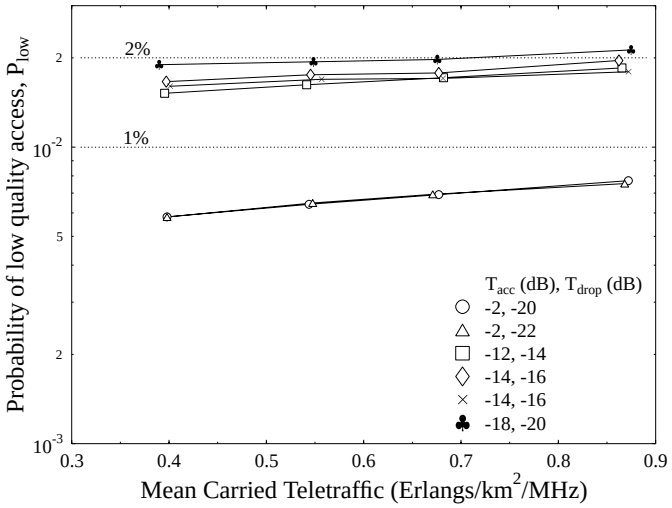

Figure 2.22: Probability of low quality access versus mean carried traffic of a CDMA based cellular network using **relative received pilot power** based soft handover thresholds in conjunction **with 1 Hz shadowing and a standard deviation of 3 dB** for SF=16.

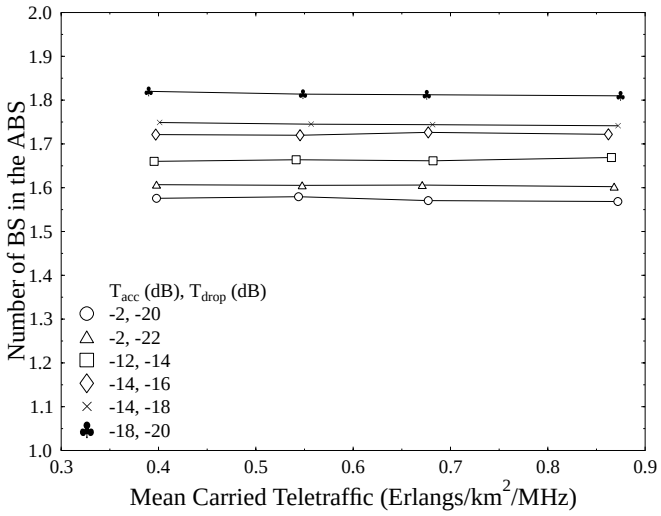

Figure 2.23: Mean number of base stations in the active base station set versus mean carried traffic of a CDMA based cellular network using **relative received pilot power** based soft handover thresholds in conjunction **with 1 Hz shadowing and a standard deviation of 3 dB** for SF=16.

0.825 Erlangs/km^2/MHz, in conjunction with T_{acc}=-14 dB and T_{drop}=-18 dB.

2.4.2.8 Summary

In summary, using relative received pilot power as a soft handover metric has resulted in a significantly improved performance in comparison to that of the fixed received pilot power based results in a shadow fading environment. In the non-shadowed environment the network capacity was approximately the same as when using the fixed threshold algorithm, albeit with a slightly improved mean transmission power. Due to the time varying nature of the received signals subjected to shadow fading, using relative thresholds has been found to be more amenable to employment in a realistic propagation environment, than using fixed thresholds. In conclusion, without shadow fading the network supported a total of 288 users, whilst with a maximum shadow fading frequency of 0.5 Hz, approximately 145 users were supported by the entire network, for both the conservative and lenient scenarios. However, different soft handover thresholds were required for each situation, for achieving these capacities. At a maximum shadowing frequency of 1.0 Hz, a total of 127 users were supported in the conservative scenario, and 144 in the lenient scenario. However, again, different soft handover thresholds were required in each scenario in order to maximise the network capacity.

2.4.3 E_c/I_o Power Based Soft Handover Results

An alternative soft handover metric used to determine "cell ownership" is the pilot to downlink interference ratio of a cell, which was proposed for employment in the 3rd generation systems [81]. The pilot to downlink interference ratio, or E_c/I_o, may be calculated thus as [102]:

$$\frac{E_c}{I_o} = \frac{P_{pilot}}{P_{pilot} + N_0 + \sum_{k=1}^{N_{cells}} P_k T_k}, \tag{2.10}$$

where P_k is the total transmit power of cell k, T_k is the transmission gain, which includes the antenna gain and pathloss as well as shadowing, N_0 is the power spectral density of the thermal noise and N_{cells} is the number of cells in the network. The advantage of using such a scheme is that it is not an absolute measurement that is used, but the ratio of the pilot power to the interference power. Thus, if fixed thresholds were used a form of admission control may be employed for new calls if the interference level became too high. A further advantage is that it takes into account the time-varying nature of the interference level in a shadowed environment.

2.4.3.1 Fixed E_c/I_o Thresholds without Shadowing

The new call blocking probability obtained when using fixed E_c/I_o soft handover thresholds without any form of shadow fading is shown in Figure 2.24, which suggests that in general, lowering the soft handover thresholds reduced the probability of a new call attempt being blocked. However, it was found that in conjunction with T_{drop}=-40 dB, dropping the threshold T_{acc} from -20 dB to -24 dB actually increased the new call blocking probability. This was attributed to the fact that the lower threshold precipitated a higher level of co-channel interference, since there was a higher mean number of base stations in the ABS, as evidenced by Figure 2.25. Therefore, since the mean level of interference present in the network is higher, when using a lower threshold, and the threshold determines the value of the pilot to downlink interference ratio at which base stations may be added to the ABS, a more frequent blocking of calls occurs. Alternatively, a lower threshold resulted in a higher level of downlink interference due to the additional interference inflicted by supporting the mobiles in soft handover, which prevented base stations from being included in the ABS due to insufficient pilot to interference "head-room". This then ultimately led to blocked calls due to the lack of base stations in the ABS.

Again, the mean number of base stations in the ABS is given in Figure 2.25, which illustrates that as expected, reducing the soft handover thresholds increased the proportion of time spent in soft handover, and thus reduced the mean number of base stations in the ABS. The average size of the ABS was found to decrease, as the network's traffic load increased. This was a consequence of the increased interference levels associated with the higher traffic loads, which therefore effectively reduced the pilot to interference ratio at a given point, and hence base stations were less likely to be in soft handover and in the ABS.

Figure 2.26 depicts the mean transmission powers for both the uplink and the downlink, for a range of different soft handover thresholds. These results show similar

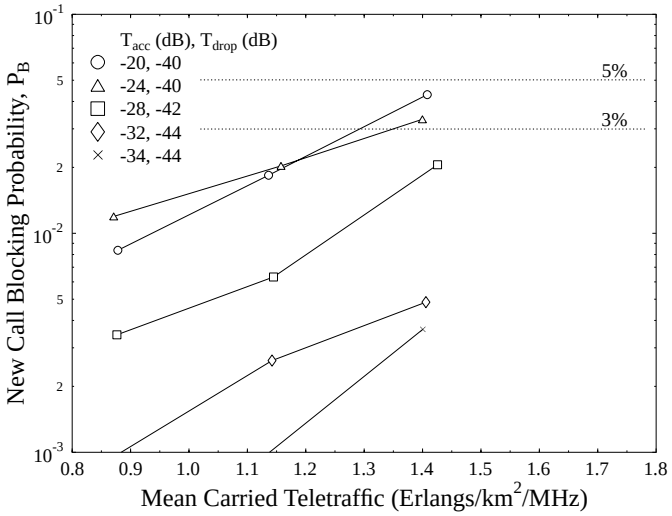

Figure 2.24: New call blocking probability versus mean carried traffic of a CDMA based cellular network using **fixed** E_c/I_o based soft handover thresholds **without shadowing** for SF=16.

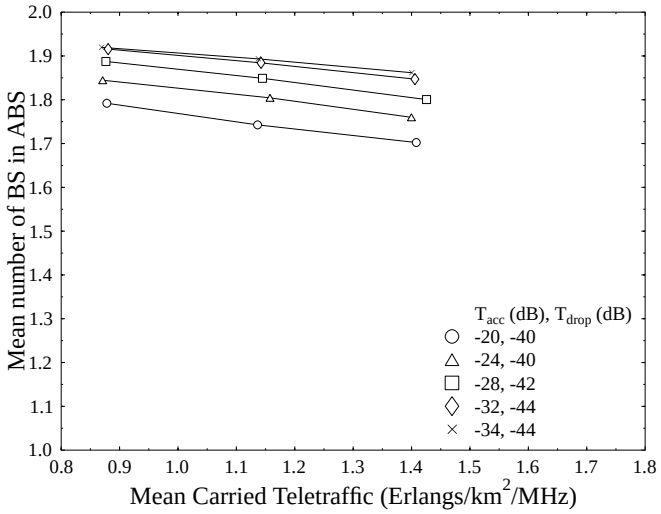

Figure 2.25: Mean number of base stations in the active base station set versus mean carried traffic of a CDMA based cellular network using **fixed** E_c/I_o based soft handover thresholds **without shadowing** for SF=16.

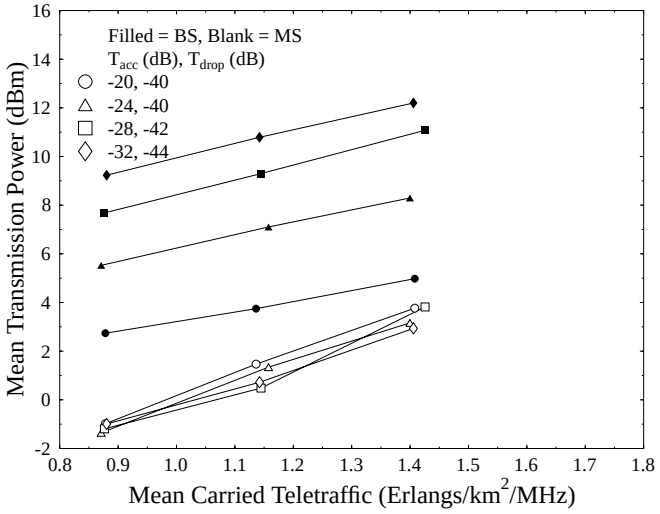

Figure 2.26: Mean transmission power versus mean carried traffic of a CDMA based cellular network using **fixed received** E_c/I_o based soft handover thresholds **without shadowing** for SF=16.

trends to the results presented in previous sections, with the required average downlink transmission power increasing, since a greater proportion of call time is spent in soft handover. Again, the mean uplink transmission power varied only slightly, since the selection diversity technique of the base stations only marginally affected the received interference power at the base stations.

Figure 2.27 shows the call dropping performance, indicating that lowering the soft handover thresholds generally improved the call dropping performance. However, reducing the soft handover thresholds too much resulted in a degradation of the call dropping probability due to the increased levels of co-channel interference inherent, when a higher proportion of the call time is spent in soft handover. This is explicitly illustrated by Figure 2.28, which indicates that reducing the soft handover thresholds caused a significant degradation in the probability of low quality access. This was a consequence of the additional co-channel interference associated with the soft handover process. The figure also shows that there is a point, where the diversity gain of the mobiles obtained with the advent of the soft handover procedure outweighs the extra interference that it generates.

On the whole, the capacity of the network when using fixed E_c/I_o soft handover thresholds was lower than when using fixed received pilot power based soft handover thresholds. This can be attributed to the fact that the E_c/I_o thresholds are related to the interference level of the network, which changes with the network load and propagation conditions. Hence using a fixed threshold is sub-optimal. In the conservative scenario, the network capacity was 1.275 Erlangs/km^2/MHz, corresponding to a total network capacity of 223 users. In the lenient scenario, this increased to 1.305

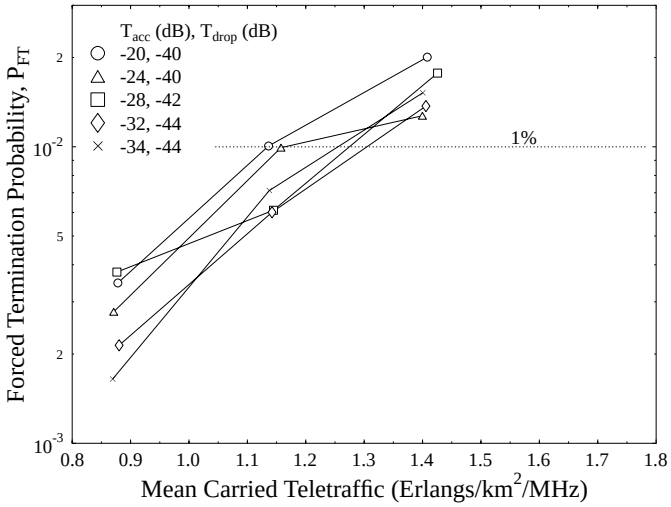

Figure 2.27: Call dropping probability versus mean carried traffic of a CDMA based cellular network using **fixed received** E_c/I_o based soft handover thresholds **without shadowing** for SF=16.

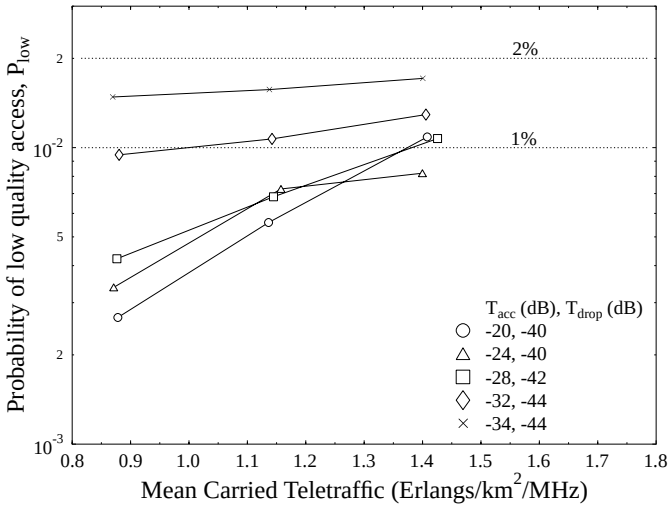

Figure 2.28: Probability of low quality access versus mean carried traffic of a CDMA based cellular network using **fixed received** E_c/I_o based soft handover thresholds **without shadowing** for SF=16.

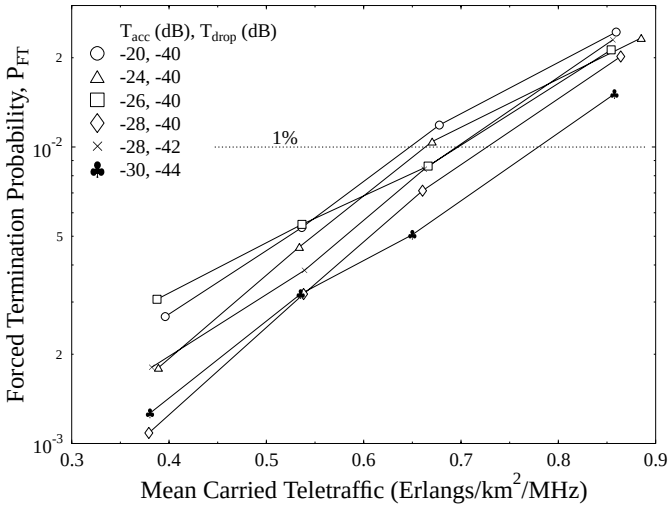

Figure 2.29: Call dropping probability versus mean carried traffic of a CDMA based cellular network using **fixed received** E_c/I_o based soft handover thresholds in conjunction **with 0.5 Hz shadowing and a standard deviation of 3 dB** for SF=16.

Erlangs/km^2/MHz, or 231 users. In contrast, when using fixed received pilot power thresholds the entire network supported 290 users.

2.4.3.2 Fixed E_c/I_o Thresholds with 0.5 Hz Shadowing

In this section we consider fixed pilot to downlink interference ratio based soft handover thresholds in a propagation environment exhibiting shadow fading in conjunction with a maximum fading frequency of 0.5 Hz and a standard deviation of 3 dB.

Examining Figure 2.29, which shows the call dropping probability, we see, again, that reducing the soft handover thresholds typically resulted in a lower probability of a dropped call. However, since the handover thresholds are dependent upon the interference level, there was some interaction between the handover thresholds and the call dropping rate. For example, it can be seen in the figure that when T_{drop}=-40 dB, the call dropping probability fell as T_{acc} was reduced from -20 dB to -24 dB. However, on lowering T_{acc} further, to -26 dB, the call dropping rate at low traffic loads became markedly higher. A similar phenomenon was observed in Figure 2.30, which shows the probability of low quality outage.

It is explicitly seen from Figures 2.29 and 2.30 that the performance of the fixed E_c/I_o soft handover threshold based scheme clearly exceeded that of the fixed received pilot power threshold based system in a shadow fading environment. The network supported a teletraffic load of 0.7 Erlangs/km^2/MHz or a total of 129 users in the conservative scenario, which rose to 0.78 Erlangs/km^2/MHz, or 140 users, in the

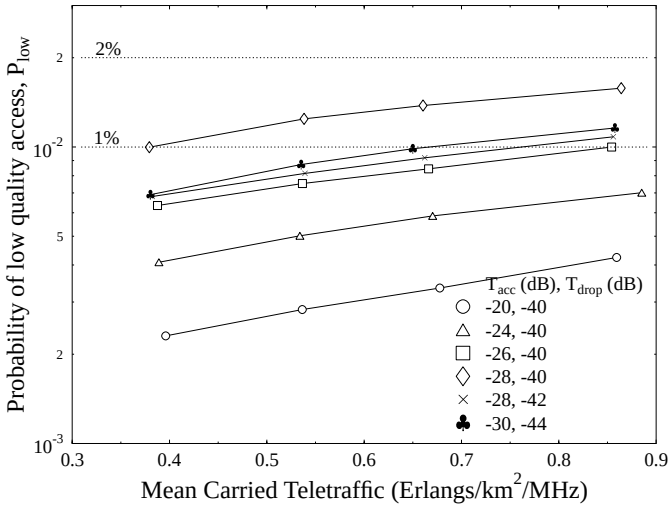

Figure 2.30: Probability of low quality access versus mean carried traffic of a CDMA based cellular network using **fixed received** E_c/I_o based soft handover thresholds in conjunction **with 0.5 Hz shadowing and a standard deviation of 3 dB** for SF=16.

lenient scenario. These network capacities were achieved with the aid of a mean number of active base stations in the ABS, which were 1.88 and 1.91, respectively. In order to achieve the total network capacity of 129 users in the conservative scenario, a mean mobile transmit power of -2.4 dBm was required, while the mean base station transmission power was 7 dBm. For the lenient scenario, these figures were -2.4 dBm and 8.7 dBm, respectively.

2.4.3.3 Fixed E_c/I_o Thresholds with 1.0 Hz Shadowing

Increasing the maximum shadow fading frequency from 0.5 Hz to 1.0 Hz resulted in an increased call dropping probability and a greater probability of low quality access, for a given level of carried teletraffic. This is clearly seen by comparing Figures 2.31 and 2.32 with Figures 2.29 and 2.30. Explicitly, Figure 2.31 and 2.32 show that reducing the soft handover threshold, T_{acc} from -20 dB to -24 dB led to both an increased call dropping probability and an increased probability of low quality access. This can be attributed to the extra co-channel interference generated by the greater proportion of call time being spent in soft handover. This is also confirmed by the increased probability of low quality access observed in Figure 2.32 for lower soft handover thresholds T_{acc} and T_{drop}.

The network capacity of the conservative scenario was 0.583 Erlangs/km^2/MHz, giving an entire network capacity of 107 users. In the lenient scenario the network supported a total of 128 users or a traffic load of 0.675 Erlangs/km^2/MHz was carried.

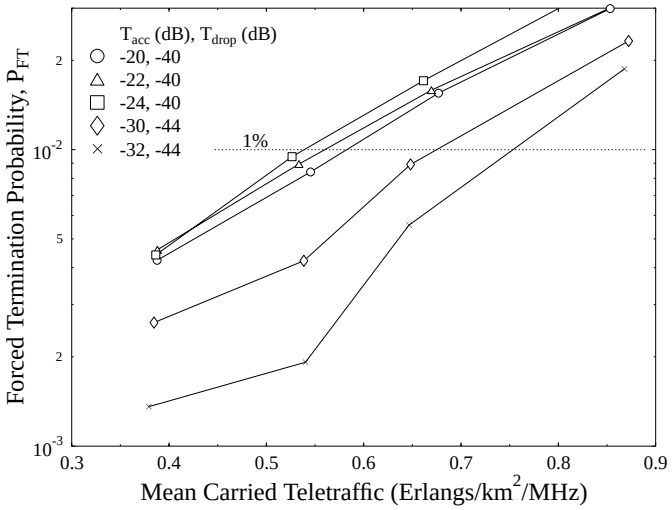

Figure 2.31: Call dropping probability versus mean carried traffic of a CDMA based cellular network using **fixed received** E_c/I_o based soft handover thresholds in conjunction **with 1.0 Hz shadowing and a standard deviation of 3 dB** for SF=16.

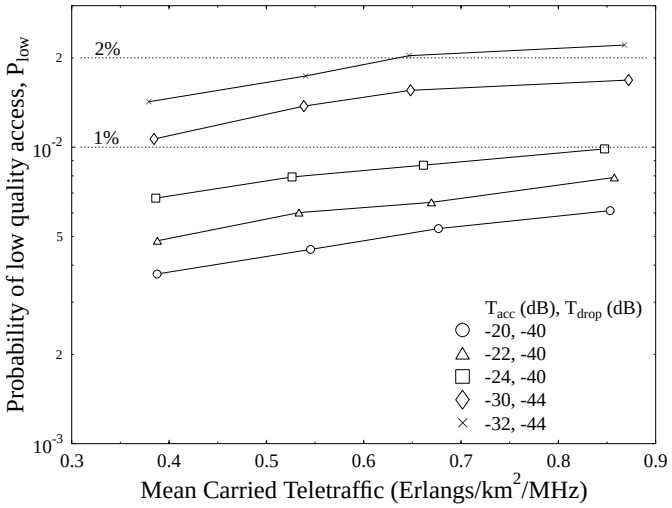

Figure 2.32: Probability of low quality access versus mean carried traffic of a CDMA based cellular network using **fixed received** E_c/I_o based soft handover thresholds in conjunction **with 1.0 Hz shadowing and a standard deviation of 3 dB** for SF=16.

The 107 users were serviced in conjunction with a mean ABS size of 1.86, a mean mobile transmit power of -3 dBm and a mean base station transmit power of 4.5 dBm. The 128 users supported in the lenient scenario necessitated an average mobile transmit power of -3 dBm and an average base station transmit power of 9.5 dBm. The mean number of base stations in the ABS was 1.91.

2.4.3.4 Summary

In summary, a maximum network capacity of 290 users was obtained when employing the fixed E_c/I_o soft handover thresholds. This capacity was equal to that when using fixed received pilot power thresholds in the lenient scenario without shadow fading. However, in the conservative scenario the network capacity was reduced from 290 to 231 users. Nevertheless, when a realistic shadowed propagation environment was considered, using the pilot power to interference ratio based soft handover metric improved the network capacity significantly. This was particularly evident in conjunction with the maximum shadow fading frequency of 1.0 Hz, when using the fixed received pilot power thresholds no users could be supported whilst maintaining the desired call quality. In contrast, using the fixed E_c/I_o soft handover thresholds led to a total network capacity of between 107 and 128 users, for the conservative and lenient scenarios, respectively. This capacity increase was the benefit of the more efficient soft handover mechanism, which was capable of taking into account the interference level experienced, leading to a more intelligent selection of base station supporting the call. At a maximum shadow fading frequency of 0.5 Hz the network had a maximum capacity of 129 and 140 users, for the conservative and lenient scenario, respectively, when using the fixed E_c/I_o soft handover thresholds.

2.4.3.5 Relative E_c/I_o Thresholds without Shadowing

In this section we combined the benefits of using the received E_c/I_o ratio and relative soft handover thresholds, thus ensuring that variations in both the received pilot signal strength and interference levels were monitored in the soft handover process.

The call dropping performance is shown in Figure 2.33, illustrating that reducing the soft handover thresholds improved the probability of dropped calls, in particular at higher traffic loads. This phenomenon is also evident in Figure 2.34, which shows the probability of a low quality outage. However, in some cases it was evident that excessive reduction of the thresholds led to increasing the co-channel interference, and hence to a greater probability of outage associated with low quality. Again, this was the consequence of supporting an excessive number of users in soft handover, which provided a beneficial diversity gain for the mobiles but also increased the amount of downlink interference inflicted by the base stations supporting the soft handovers.

The entire network supported a total of 256 users employing soft handover thresholds of T_{acc}=-12 dB and T_{drop}=-16 dB. The mean number of base stations in the active set was 1.68, and the mean mobile transmit power was 3.1 dBm. The average base station transmit power was 2.7 dBm.

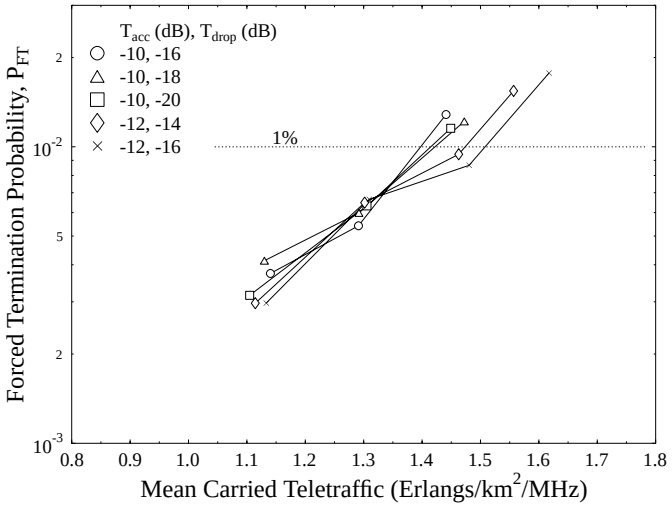

Figure 2.33: Call dropping probability versus mean carried traffic of a CDMA based cellular network using **relative received** E_c/I_o based soft handover thresholds **without shadowing** for SF=16.

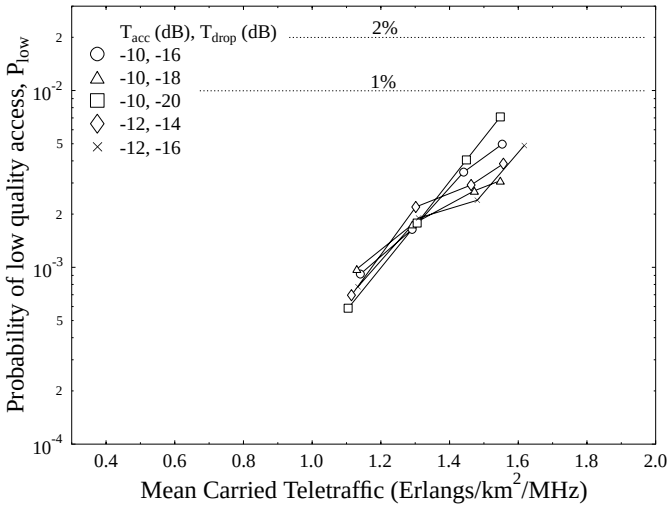

Figure 2.34: Probability of low quality access versus mean carried traffic of a CDMA based cellular network using **relative received** E_c/I_o based soft handover thresholds **without shadowing** for SF=16.

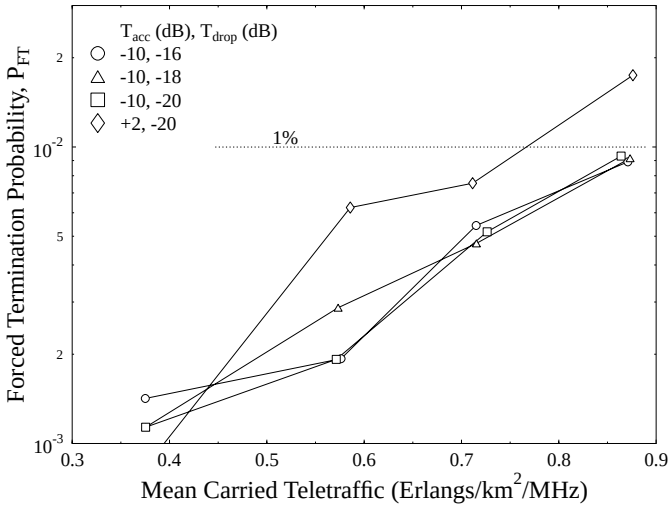

Figure 2.35: Call dropping probability versus mean carried traffic of a CDMA based cellular network using **relative received** E_c/I_o based soft handover thresholds in conjunction **with 0.5 Hz shadowing and a standard deviation of 3 dB** for SF=16.

2.4.3.6 Relative E_c/I_o Thresholds with 0.5 Hz Shadowing

Examining the call dropping probability graphs in Figure 2.35 shows that the probability of a dropped call was significantly lower than that of the other soft handover algorithms considered for the same propagation environment. This was because the handover algorithm was capable of taking the current interference levels into account, when deciding whether to initiate a handover, additionally, the employment of the relative thresholds minimised the chances of making an inappropriate soft handover decision concerning the most suitable base station to use. The superiority of this soft handover algorithm was further emphasised by the associated low probability of a low quality access, as illustrated in Figure 2.36, which was an order of magnitude lower than that achieved using the alternative soft handover algorithms.

When T_{acc} was set to -10 dB the ultimate capacity of the network was only marginally affected by changing T_{drop}, although some variation could be observed in the call dropping probability. Furthermore, the probability of low quality access increased for the lowest values of T_{drop}. This degradation of the probability of low quality access was due to the higher proportion of time spent in soft handover, as indicated by the correspondingly increased ABS size in Figure 2.37, which was a consequence of the associated increased co-channel interference levels.

The mean transmit power curves of Figure 2.38 exhibited a different characteristic in comparison to that observed for the other soft handover algorithms. Specifically, at low traffic loads the mean mobile transmit power was less than that of the base

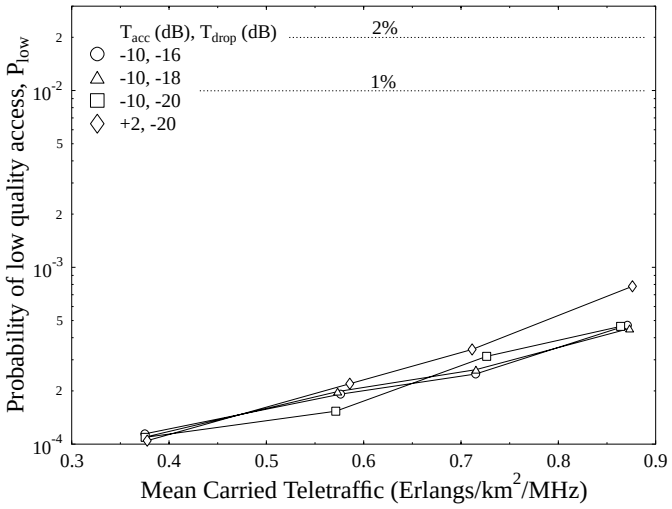

Figure 2.36: Probability of low quality access versus mean carried traffic of a CDMA based cellular network using **relative received** E_c/I_o based soft handover thresholds in conjunction **with 0.5 Hz shadowing and a standard deviation of 3 dB** for SF=16.

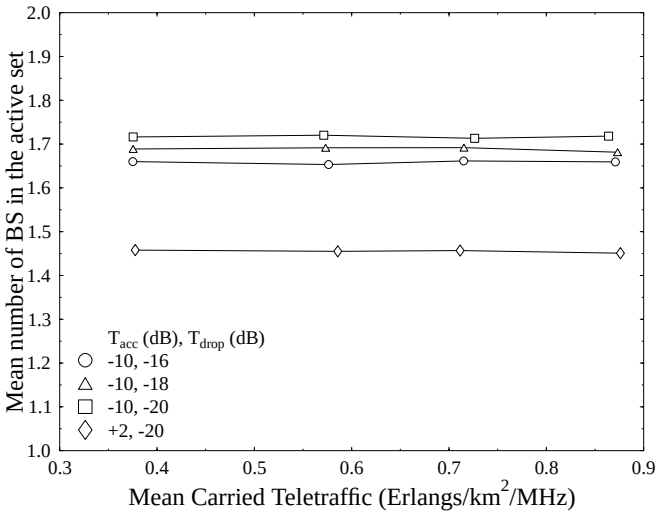

Figure 2.37: Mean number of base stations in the active base station set versus mean carried traffic of a CDMA based cellular network using **relative received** E_c/I_o based soft handover thresholds in conjunction **with 0.5 Hz shadowing and a standard deviation of 3 dB** for SF=16.

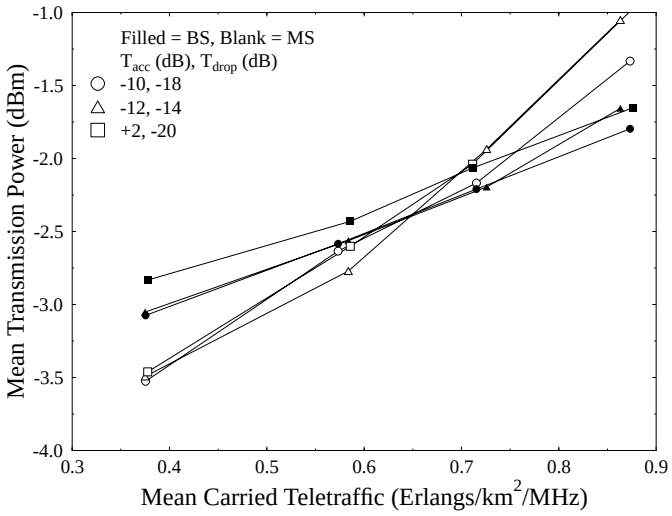

Figure 2.38: Mean transmission power versus mean carried traffic of a CDMA based cellular network using **relative received** E_c/I_o based soft handover thresholds in conjunction **with 0.5 Hz shadowing and a standard deviation of 3 dB** for SF=16.

stations, whereas at the higher traffic loads, the mobile transmit power was greater than that of the base stations. Although, comparing this graph with Figure 2.20 revealed that the spread and the rate of change of the mobile transmit power versus the traffic load was similar in both scenarios, the mean base station transmission power was lower in Figure 2.38. This reduced base station transmission power, again demonstrated the superiority of this soft handover algorithm, which manifested itself in its more efficient use of resources.

Since the probability of low quality access fell well below the 1% threshold, both the conservative and lenient scenarios exhibited the same total network capacity, which was slightly above 150 users for the entire network. This was achieved on average with the aid of 1.65 base stations, at a mean mobile transmit power of -1.2 dBm and at a mean base station transmit power of -1.7 dBm.

2.4.3.7 Relative E_c/I_o Thresholds with 1.0 Hz Shadowing

The call dropping probability shown in Figure 2.39 is slightly worse than that obtained in Figure 2.35 for a maximum shadow fading frequency of 0.5 Hz, with a greater performance difference achieved by altering T_{drop}. A similar performance degradation was observed for the probability of low quality access in Figure 2.40, with an associated relatively low impact due to varying the soft handover thresholds. Although not explicitly shown, we found that the mean transmission powers were similar to those required for a maximum shadow fading frequency of 0.5 Hz.

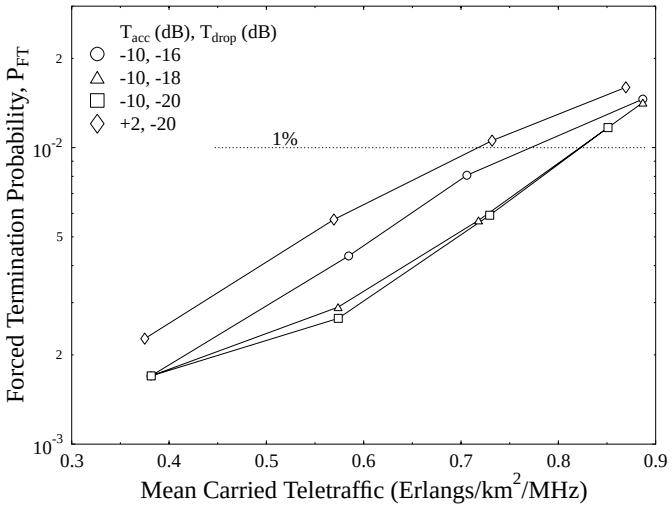

Figure 2.39: Call dropping probability versus mean carried traffic of a CDMA based cellular network using **relative received** E_c/I_o based soft handover thresholds in conjunction **with 1.0 Hz shadowing and a standard deviation of 3 dB** for SF=16.

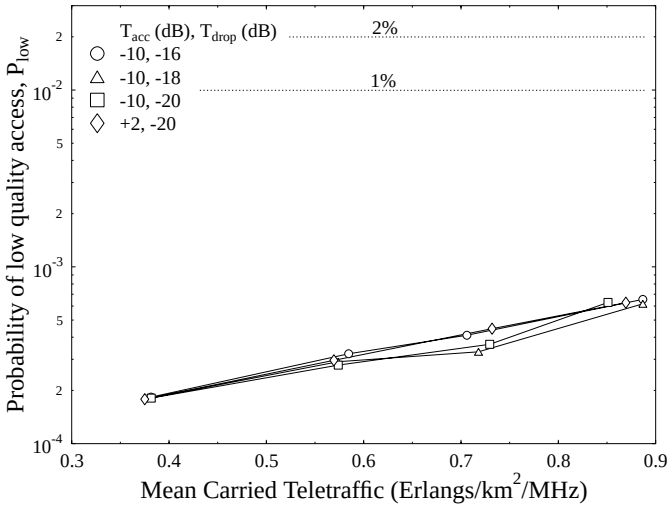

Figure 2.40: Probability of low quality access versus mean carried traffic of a CDMA based cellular network using **relative received** E_c/I_o based soft handover thresholds in conjunction **with 1.0 Hz shadowing and a standard deviation of 3 dB** for SF=16.

2.4.3.8 Summary

In summary, the employment of relative E_c/I_o soft handover thresholds resulted in a superior network performance and capacity under all the propagation conditions investigated. This was achieved whilst invoking the lowest average number of base stations and the minimum mean base station transmit power. A further advantage of this handover scheme is that the same soft handover thresholds excelled in all of the propagation environments studied, unlike the previously considered algorithms, which obtained their best results at different thresholds for different conditions. The entire network capacity was 256 users without shadow fading, with a mean ABS size of 1.68. At a maximum shadowing frequency of 0.5 Hz the network supported just over a total of 150 users, whilst 144 users were served by the entire network, when a maximum shadow fading frequency of 1.0 Hz was encountered.

2.4.4 Overview of Results

Soft handover algorithm	Shadowing	Conservative scenario P_{FT}=1%, P_{low}=1%		Power (dBm)		Lenient scenario P_{FT}=1%, P_{low}=2%		Power (dBm)	
		Users	ABS	MS	BS	Users	ABS	MS	BS
Fixed pilot pwr.	No	290	1.7	5.1	5.1	290	1.7	5.1	5.1
Fixed pilot pwr.	0.5 Hz, 3dB	-	-	-	-	127	1.83	-2.0	6.5
Fixed pilot pwr.	1.0 Hz, 3dB	-	-	-	-	-	-	-	-
Delta pilot pwr.	No	288	1.7	4.1	4.7	288	1.7	4.1	4.1
Delta pilot pwr.	0.5 Hz, 3dB	144	1.77	-1.5	0.6	146	1.78	-1.5	1.3
Delta pilot pwr.	1.0 Hz, 3dB	127	1.5	-2.4	-1.9	144	1.72	-1.5	0.8
Fixed E_c/I_o	No	223	1.83	2.0	10.0	231	1.86	2.0	10.3
Fixed E_c/I_o	0.5 Hz, 3dB	129	1.88	-2.4	7.0	140	1.91	-2.4	8.7
Fixed E_c/I_o	1.0 Hz, 3dB	107	1.86	-3.0	4.5	128	1.91	-3.0	9.5
Delta E_c/I_o	No	256	1.68	3.1	2.7	256	1.68	3.1	2.7
Delta E_c/I_o	0.5 Hz, 3dB	$\approx$150	1.65	-1.2	-1.7	$\approx$150	1.65	-1.2	-1.7
Delta E_c/I_o	1.0 Hz, 3dB	144	1.65	-1.1	-1.6	144	1.65	-1.1	-1.6

Table 2.3: Maximum number of mobile users that can be supported by the network, for different soft handover metrics/algorithms whilst meeting the preset quality constraints. The mean number of base stations in the Active Base station Set (ABS) is also presented, along with the mean mobile and mean base station transmit powers.

Table 2.3 summarises the results obtained for the various soft handover algorithms over the three different propagation environments considered. The fixed receiver pilot power based algorithm performed the least impressively overall, as expected due to its inherent inability to cope with shadow fading. However, it did offer a high network capacity in a non-shadowed environment. Using the relative received pilot power based soft handover algorithm improved the performance under shadow fading, but different fading rates required different thresholds to meet the conservative and lenient quality criteria. The performance of the fixed E_c/I_o based soft handover algorithm also varied significantly, when using the same thresholds for the two different fading rates considered. However, the maximum network capacity achieved under the different shadow

fading conditions was significantly higher, than that of the fixed received pilot power based algorithm. This benefit resulted from the inclusion of the interference levels in the handover process, which thus took into account the fading of both the signal and the co-channel interference. Combining the relative threshold based scheme with using E_c/I_o thresholds allowed us to support the highest number of users under the shadow fading conditions investigated. Whilst its performance was not the highest in the non-shadowed environment, this propagation environment is often unrealistic, and hence the relative received E_c/I_o based soft handover algorithm was chosen as the basis for our future investigations, while using the soft handover thresholds of T_{acc}=-10 dB and T_{drop}=-18 dB. The advantages of this handover algorithm were its reduced fraction of time spent in soft handover, and its ability to perform well under both shadow fading conditions evaluated, whilst utilising the same soft handover thresholds. Since the constraining factor of these network capacity results was the probability of a dropped call, P_{FT}, which was the same for both scenarios, further network capacity results were only shown for the conservative scenario.

2.4.5 Performance of Adaptive Antenna Arrays in a High Data Rate Pedestrian Environment

In our previous investigations we endeavoured to identify the soft handover algorithm, which supports the greatest number of users, at the best call quality, regardless of the propagation conditions. In the section we study the impact of adaptive antenna arrays on the network's performance. The investigations were conducted using the relative E_c/I_o based soft handover algorithm in conjunction with T_{acc}=-10 dB and T_{drop}=-18 dB, using a spreading factor of 16. Given that the chip rate of UTRA is 3.84 Mchips/sec, this spreading factor corresponds to a channel data rate of $3.84\times10^6/16$=240 kbps. Applying 1/2 rate error correction coding would result in an effective data throughput of 120 kbps, whereas utilising a 2/3 rate error correction code would provide a useful throughput of 160 kps. As in the previous simulations, a cell radius of 150 m was assumed and a pedestrian walking velocity of 3 mph was used. In our previous results investigations employing adaptive antenna arrays at the base station and using a FDMA/TDMA based network, as in Chapter **??**, we observed quite significant performance gains as a direct result of the interference rejection capabilities of the adaptive antenna arrays invoked. Since the CDMA based network considered here has a frequency reuse of 1, the levels of co-channel interference are significantly higher, and hence the adaptive antennas may be able to null the interference more effectively. However, the greater number of interference sources may limit the achievable interference rejection.

Network performance results were obtained using two and four element adaptive antenna arrays, both in the absence of shadow fading, and in the presence of 0.5 Hz and 1.0 Hz frequency shadow fading exhibiting a standard deviation of 3 dB. The adaptive beamforming algorithm used was the Sample Matrix Inversion (SMI) algorithm, as described in Chapter **??** and used in the FDMA/TDMA network simulations of Chapter **??**. The specific adaptive beamforming implementation used in the CDMA based network was identical to that used in the FDMA/TDMA network simulations. Briefly, one of the eight possible 8-bit BPSK reference signals was used to identify the

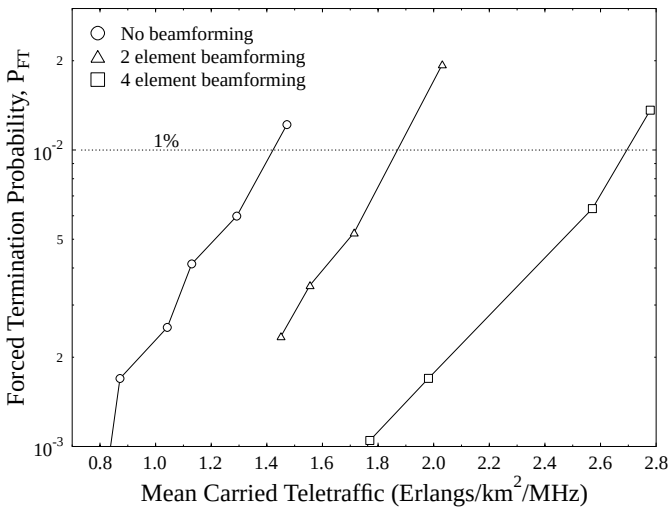

Figure 2.41: Call dropping probability versus mean carried traffic of a CDMA based cellular network using **relative received** E_c/I_o based soft handover thresholds **with and without beamforming and without shadowing** for SF=16.

desired user, and the remaining interfering users were assigned the other seven 8-bit reference signals. The received signal's autocorrelation matrix was then calculated, and from the knowledge of the desired user's reference signal, the receiver's optimal antenna array weights were determined with the aid of the SMI algorithm. The reader is referred to Section **??** for further details. Since this implementation of the algorithm only calculated the receiver's antenna array weights, i.e. the antenna arrays weights used by the base station in the uplink, these weights may not be suitable for use in the downlink, when independent up/downlink shadow fading is experienced. Hence, further investigations were conducted, where the uplink and downlink channels were identical, in order to determine the potential performance gain that may be achieved by separately calculating the antenna array weights to be used in the downlink. The antenna array weights were re-calculated for every power control step, i.e. 15 times per UTRA data frame, due to the potential significant changes in terms of the desired signal and interference powers that may occur during one UTRA frame as a result of the possible 15 dB change in power transmitted by each user.

Figure 2.41 shows the significant reduction in the probability of a dropped call, i.e. the probability of forced termination P_{FT}, achieved by employing adaptive antenna arrays in a non-shadowed propagation environment. The figure has demonstrated that, even with only two antenna elements, the adaptive antenna arrays have considerably reduced the levels of co-channel interference, leading to a reduced call dropping probability. This has been achieved in spite of the numerous sources of co-channel interference resulting from the frequency reuse factor of one, which was remarkable in the light of the limited number of degrees of freedom of the two element array.

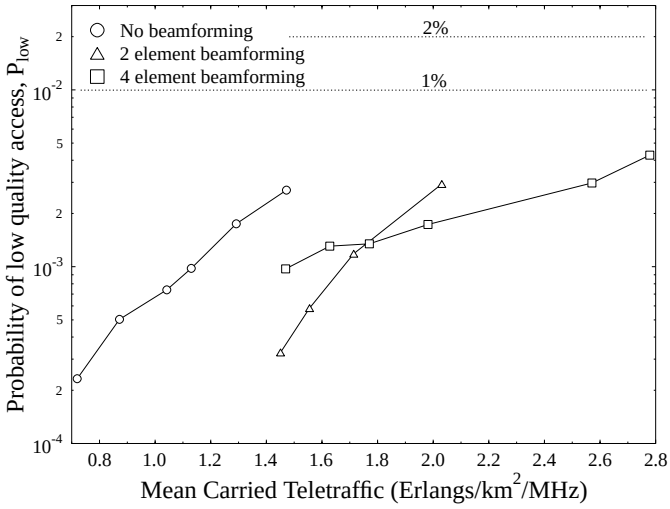

Figure 2.42: Probability of low quality access versus mean carried traffic of a CDMA based cellular network using **relative received** E_c/I_o based soft handover thresholds **with and without beamforming and without shadowing** for SF=16.

Without employing antenna arrays at the base stations the network capacity was limited to 256 users, or to a teletraffic load of approximately 1.4 Erlangs/km^2/MHz. However, with the advent of two element adaptive antenna arrays at the base stations the number of users supported by the network rose by 27% to 325 users, or almost 1.9 Erlangs/km^2/MHz. Replacing the two element adaptive antenna arrays with four element arrays led to a further rise of 48%, or 88% with respect to the capacity of the network using no antenna arrays. This is associated with a network capacity of 480 users, or 2.75 Erlangs/km^2/MHz. A summary of the network capacities achieved under different conditions is given in Table 2.4.

The probability of low quality outage, presented in Figure 2.42 also exhibited a substantial improvement with the advent of two element adaptive antenna arrays. However, the performance gains obtained when invoking four element adaptive antenna arrays were more involved. It can be seen from the figure that higher traffic loads were carried with at a sufficiently low probability of a low quality occurring, and at higher traffic loads the probability of a low quality access was lower than that achieved using a two element array. However, at lower traffic loads the performance was worse than that obtained when using two element arrays, and the gradient of the performance curve was significantly lower. Further in-depth analysis of the results suggested that the vast majority of the low quality outages were occurring when new calls started. When a user decided to commence communications with the base station, the current interference level was measured, and the target transmission power was determined in order to reach the target SINR necessary for reliable communica-

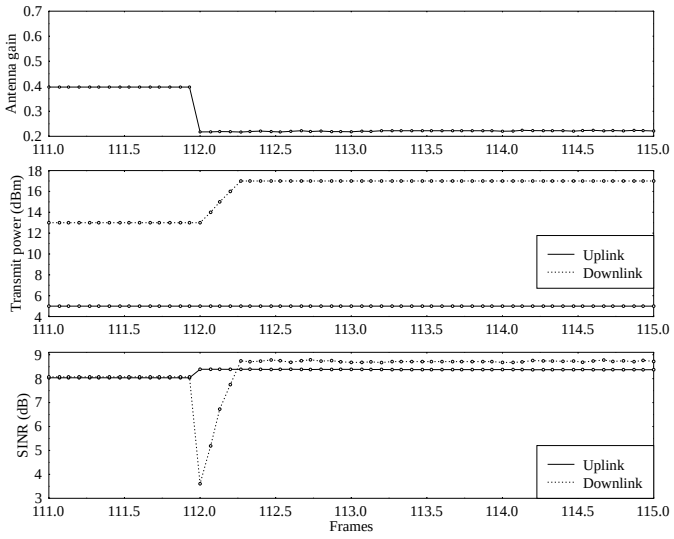

Figure 2.43: The changes in the antenna array gain, versus time, in the direction of the desired user, the up- and down-link transmission powers, and the up- and down-link received SINRs, when a new call starts using four element adaptive antenna arrays without shadowing in conjunction with the **original power ramping** algorithm and SF=16.

tions. However, in order to avoid disrupting existing calls the transmission power was ramped up slowly, until the target SINR was reached. A network using no adaptive antenna arrays, i.e. employing omnidirectional antennas, can be viewed as offering equal gain to all users of the network, which we assumed to be 1.0, or 0 dB. Thus, when a new call is initiated, the level of interference rises gradually, and the power control algorithm ensures that the existing users compensate for the increased level of co-channel interference by increasing their transmission power. In a network using adaptive antenna arrays, the adaptive antenna arrays are used to null the sources of interference, and in doing so the array may reduce the antenna gain in the direction of the desired user, in order to maximise the SINR. Hence a user starting a new call, even if it has low transmission power, can alter the antenna array's response, and thus the antenna gain experienced by the existing users. This phenomenon is more marked, when using four element arrays since their directivity, and thus sensitivity to interfering signals, is greater.

Figure 2.43 illustrates this phenomenon, where another user starts a new call at frame 112 suddenly reducing the antenna gain in the direction of the desired user from 0.4 to just above 0.2, a drop of 3 dB. As can be seen from the figure, the downlink SINR falls sharply below the low quality outage threshold of 7.0 dB, resulting in several consecutive outages, until the downlink transmission power is increased sufficiently. The impact of reducing the initial transmission power, in order to ensure that the power ramping takes place more gently, is depicted in Figure 2.44. In this figure it

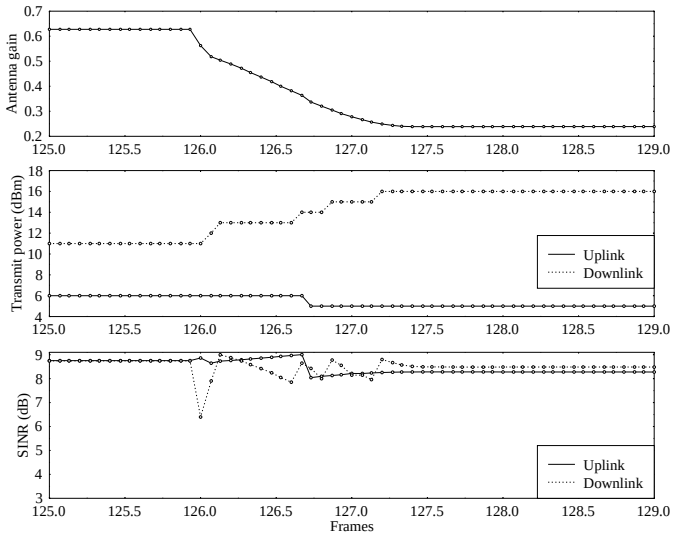

Figure 2.44: The changes in the antenna array gain, versus time, in the direction of the desired user, the up- and down-link transmission powers, and the up- and down-link received SINRs, when a new call starts using four element adaptive antenna arrays without shadowing in conjunction with a **slower power ramping** algorithm and SF=16.

can be seen that the antenna gain falls much more gently, over a prolonged period of time, thus reducing the number of low quality outages, as the downlink transmission power is increased in an effort to compensate for the lower antenna gain. It is of interest to note how the received SINR varies as the antenna gain and the power control algorithm interact, in order to maintain the target SINR.

Even though the employment of adaptive antenna arrays can result in the attenuation of the desired signal, this is performed in order to maximise the received SINR, and thus the levels of interference are attenuated more strongly, ultimately leading to the reduction of the mean transmission power, as emphasised by Figure 2.45. This figure clearly shows the lower levels of transmission power, required in order to maintain an acceptable performance, whilst using adaptive antenna arrays at the base stations. A reduction of 3 dB in the mean mobile transmission power was achieved by invoking two element antenna arrays, and a further reduction of 1.5 dB resulted from using four element arrays. These power budget savings were obtained in conjunction with reduced levels of co-channel interference, leading to superior call quality, as illustrated in Figures 2.41 and 2.42. A greater performance advantage was evident in the uplink scenario, suggesting that the selective base station diversity techniques employed in the uplink are amenable to amalgamation with adaptive antenna arrays. In contrast, the maximum ratio combining performed at the mobile inherently reduces the impact of co-channel interference, and hence benefits to a lesser extent from the employment of adaptive antenna arrays.

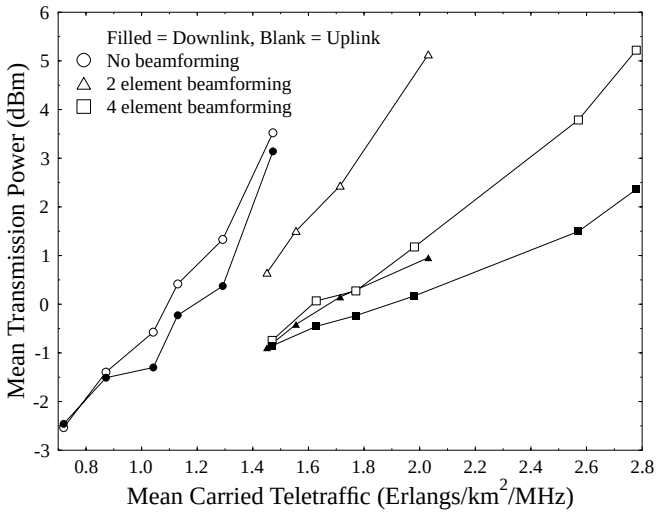

Figure 2.45: Mean transmission power versus mean carried traffic of a CDMA based cellular network using **relative received** E_c/I_o based soft handover thresholds **with and without beamforming and without shadowing** for SF=16.

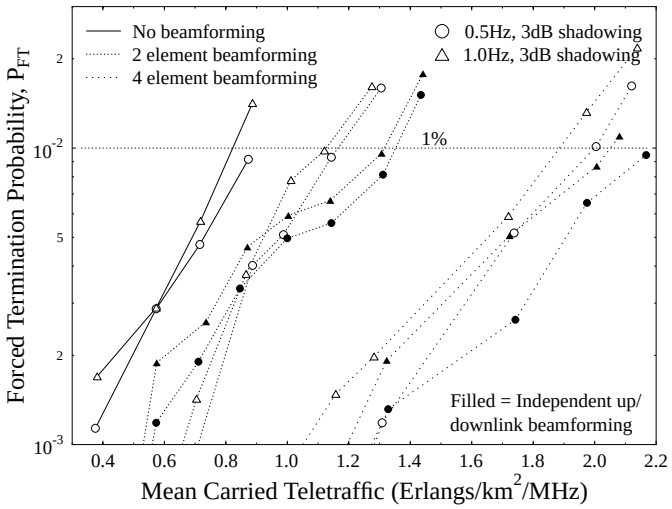

Figure 2.46: Call dropping probability versus mean carried traffic of a CDMA based cellular network using **relative received** E_c/I_o based soft handover thresholds **with and without beamforming and with shadowing having a standard deviation of 3 dB** for SF=16.

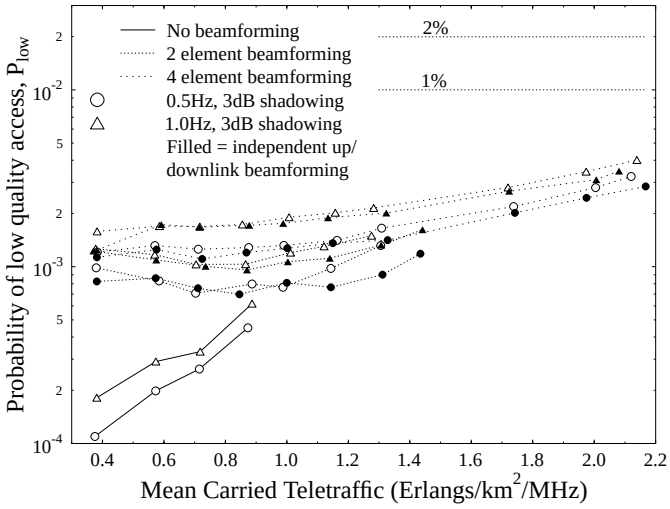

Figure 2.47: Probability of low quality access versus mean carried traffic of a CDMA based cellular network using **relative received** E_c/I_o based soft handover thresholds **with and without beamforming and with shadowing having a standard deviation of 3 dB** for SF=16.

The impact of adaptive antenna arrays in a propagation environment subjected to shadow fading was then investigated. The associated call dropping performance is shown in Figure 2.46. This figure illustrates the substantial network capacity gains achieved with the aid of both two and four element adaptive antenna arrays under shadow fading propagation conditions. Simulations were conducted in conjunction with log-normal shadow fading having a standard deviation of 3 dB, and maximum shadowing frequencies of both 0.5 Hz and 1.0 Hz. As expected the network capacity was reduced at the faster fading frequency. The effect of performing independent up- and down-link beamforming, as opposed to using the base station's receive antenna array weights in the downlink was also studied, and a small, but not insignificant call dropping probability reduction can be seen in the Figure 2.46. The network supported just over 150 users, and 144 users, when subjected to 0.5 Hz and 1.0 Hz frequency shadow fading, respectively. With the application of two element adaptive antenna arrays, re-using the base station's uplink receiver weights on the downlink, these capacities increased by 35% and 40%, to 203 users and 201 users. Performing independent up- and down-link beamforming resulted in a mean further increase of 13% in the network capacity. The implementation of four element adaptive antenna arrays led to a network capacity of 349 users at a 0.5 Hz shadowing frequency, and 333 users at a 1.0 Hz shadowing frequency. This corresponded to relative gains of 133% and 131% over the capacity provided without beamforming. Invoking independent up- and down-link beamforming gave another boost of 7% and 10% to network capacity for 0.5 Hz and 1.0 Hz frequency shadowing environments, respectively, giving final

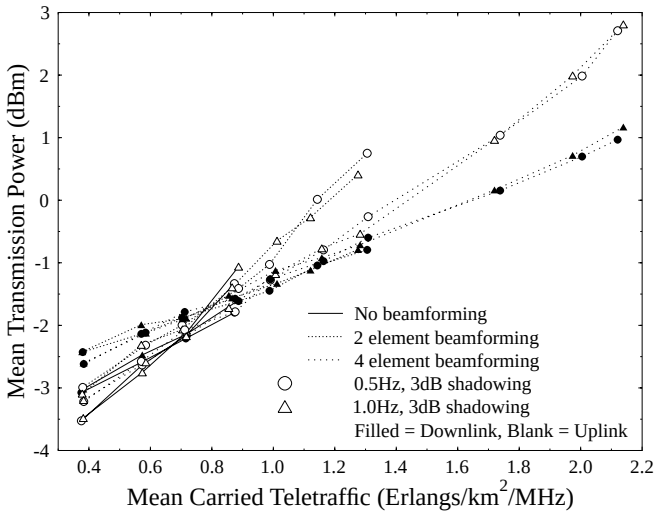

Figure 2.48: Mean transmission power versus mean carried traffic of a CDMA based cellular network using **relative received** E_c/I_o based soft handover thresholds **with and without beamforming and shadowing having a standard deviation of 3 dB** for SF=16.

network capacities of just over 375 users and 365 users.

Similar trends were observed regarding the probability of low quality outage to those found in the non-shadowing scenarios. However, the trend was much more prevalent under shadowing, due to greater variation of the received signal strengths, as a result of the shadow fading, as shown in Figure 2.47. The figure indicates that the trend is also evident, when using two element adaptive antenna arrays in conjunction with shadow fading. As expected, the performance deteriorated as the number of antenna elements increased, and when the maximum shadow fading frequency was increased from 0.5 Hz to 1.0 Hz. It should be noted, however that the probability of low quality access always remained below the 1% constraint of the conservative scenario, and the call dropping probability was considerably reduced by the adaptive antenna arrays.

The mean transmission power performance is depicted in Figure 2.48, suggesting that as for the non-shadowing scenario of Figure 2.45, the number of antenna elements had only a limited impact on the base stations' transmission power, although there was some reduction in the mobile stations' mean transmission power. The mean transmission powers required when using independent up- and down-link beamforming are not explicitly shown, but were slightly less than those presented here, with a mean reduction of about 0.4 dB.

A summary of the maximum network capacities of the networks considered in this section both with and without shadowing, employing beamforming using two and four element arrays is given in Table 2.4, along with the teletraffic carried and the mean

mobile and base station transmission powers required.

The lower bounds of the maximum network capacities obtained under identical scenarios in conjunction with a spreading factor of 256, are also presented in Table 2.5, leading to a bit rate of 15 kbps, which is suitable for use by speech-rate users. The network capacity calculations were performed by scaling the number of users supported, as presented in Table 2.4, by the ratio of their spreading factors, i.e. 256/16=16. Further interesting user capacity figures can be inferred for a variety of target bit rates by comparing Tables 2.4, 2.5, 2.7 and 2.8 and applying the appropriate spreading factor related scaling mentioned in the context of estimating the number of 15 kbps speech users supported.

Shadowing	Beamforming:	independent up/down-link	Conservative scenario, P_{FT}=1%, P_{low}=1% Users	Traffic (Erlangs /km^2/MHz)	Power (dBm) MS	BS
No	No	-	256	1.42	3.1	2.7
No	2 elements	-	325	1.87	3.75	0.55
No	4 elements	-	480	2.75	4.55	1.85
0.5 Hz, 3 dB	No	-	≈150	0.87	-1.2	-1.7
0.5 Hz, 3 dB	2 elements	No	203	1.16	0.1	-1.1
0.5 Hz, 3 dB	4 elements	No	349	2.0	2.0	0.65
0.5 Hz, 3 dB	2 elements	Yes	233	1.35	0.2	-0.8
0.5 Hz, 3 dB	4 elements	Yes	≈375	2.2	2.15	0.85
1.0 Hz, 3 dB	No	-	144	0.82	-1.1	-1.6
1.0 Hz, 3 dB	2 elements	No	201	1.12	-0.3	-1.1
1.0 Hz, 3 dB	4 elements	No	333	1.88	1.6	0.5
1.0 Hz, 3 dB	2 elements	Yes	225	1.31	0.1	-0.9
1.0 Hz, 3 dB	4 elements	Yes	365	2.05	1.65	0.6

Table 2.4: Maximum mean carried traffic and maximum number of mobile users that can be supported by the network, whilst meeting the conservative quality constraints. The carried traffic is expressed in terms of normalised Erlangs (Erlang/km^2/MHz) for the network described in Table 2.2 both **with and without beamforming (as well as with and without independent up/down-link beamforming), and also with and without shadow fading having a standard deviation of 3 dB** for SF=16.

2.4.6 Performance of Adaptive Antenna Arrays and Adaptive Modulation in a High Data Rate Pedestrian Environment

In this section we build upon the results presented in the previous section by applying Adaptive Quadrature Amplitude Modulation (AQAM) techniques. The various scenarios and channel conditions investigated were identical to those of the previous section, except for the application of AQAM. Since in the previous section an increased network capacity was achieved due to using independent up- and down-link beamforming, this procedure was invoked in these simulations. AQAM involves the selection of the appropriate modulation mode in order to maximise the achievable data throughput over a channel, whilst minimising the Bit Error Ratio (BER). More

Shadowing	Beamforming:	independent up/down-link	Users when SF=256	Traffic (Erlangs /km^2/MHz)
No	No	-	4096	22.7
No	2 elements	-	5200	29.9
No	4 elements	-	7680	44.0
0.5 Hz, 3 dB	No	-	2400	13.9
0.5 Hz, 3 dB	2 elements	No	3248	18.6
0.5 Hz, 3 dB	4 elements	No	5584	32.0
0.5 Hz, 3 dB	2 elements	Yes	3728	21.6
0.5 Hz, 3 dB	4 elements	Yes	6000	35.2
1.0 Hz, 3 dB	No	-	2304	13.1
1.0 Hz, 3 dB	2 elements	No	3216	17.9
1.0 Hz, 3 dB	4 elements	No	5328	30.1
1.0 Hz, 3 dB	2 elements	Yes	3600	21.0
1.0 Hz, 3 dB	4 elements	Yes	5840	32.8

Table 2.5: A lower bound estimate of the maximum mean traffic and the maximum number of mobile **speech-rate** users that can be supported by the network, whilst meeting the **conservative quality constraints**. The carried traffic is expressed in terms of normalised Erlangs (Erlang/km^2/MHz) for the network described in Table 2.2 both **with and without beamforming (as well as with and without independent up/down-link beamforming), and also with and without shadow fading having a standard deviation of 3 dB** for SF=256. The number of users supported in conjunction with a spreading factor of 256 was calculated by multiplying the capacities obtained in Table 2.4 by 256/16=16.

explicitly, the philosophy behind adaptive modulation is the most appropriate selection of a modulation mode according to the instantaneous radio channel quality experienced [12,13]. Therefore, if the SINR of the channel is high, then a high-order modulation mode may be employed, thus exploiting the temporal fluctuation of the radio channel's quality. Similarly, if the channel is of low quality, exhibiting a low SINR, a high-order modulation mode would result in an unacceptably high BER or FER, and hence a more robust, but lower throughput modulation mode would be employed. Therefore, adaptive modulation combats the effects of time-variant channel quality, while also attempting to maximise the achieved data throughput, and maintaining a given BER or FER. In the investigations conducted, the modulation modes of the up and downlink were determined independently, thus taking advantage of the lower levels of co-channel interference on the uplink, or of the potentially greater transmit power of the base stations.

The particular implementation of AQAM used in these investigations is illustrated in Figure 2.49. This figure describes the algorithm in the context of the downlink, but the same implementation was used also in the uplink. The first step in the process was to establish the current modulation mode. If the user was invoking 16-QAM and the SINR was found to be below the Low Quality (LQ) outage SINR threshold after the completion of the power control iterations, then the modulation mode for the next data frame was 4-QAM. Alternatively, if the SINR was above the LQ outage SINR threshold, but any of the base stations in the ABS were using a transmit power within 15 dB of the maximum transmit power - which is the maximum possible power

change range during a 15-slot UTRA frame - then the 4-QAM modulation mode was selected. This "headroom" was introduced in order to provide a measure of protection, since if the interference conditions degrade, then at least 15 dB of increased transmit power would be available in order to mitigate the consequences of the SINR reduction experienced.

A similar procedure was invoked, when switching to other legitimate AQAM modes from the 4-QAM mode. If the SINR was below the 4-QAM target SINR and any one of the base stations in the ABS was within 15 dB (the maximum possible power change during a 15-slot UTRA data frame) of the maximum transmit power, then the BPSK modulation mode was employed for the next data frame. However, if the SINR exceeded the 4-QAM target SINR and there would be 15 dB of headroom in the transmit power budget in excess of the extra transmit power required for switching from 4-QAM to 16-QAM, then the 16-QAM modulation mode was invoked.

And finally, when in the BPSK mode, the 4-QAM modulation mode was selected if the SINR exceeded the BPSK target SINR, and the transmit power of any of the base stations in the ABS was less than the power required to transmit reliably using 4-QAM, while being at least 15 dB below the maximum transmit power. The algorithm was activated at the end of each 15-slot UTRA data frame, after the power control algorithm had performed its 15 iterations per data frame, and thus the AQAM mode selection was performed on a UTRA transmission frame-by-frame basis. When changing from a lower-order modulation to a higher-order modulation mode, the lower-order mode was retained for an extra frame in order to ramp up the transmit power to the required level, as shown in Figure 2.50(a). Conversely, when changing from a higher-order modulation mode to a lower-order modulation mode, the lower-order modulation mode was employed whilst ramping the power down, in order to avoid excessive outages in the higher-order modulation mode due to the reduction of the transmit power, as illustrated in Figure 2.50(b).

Table 2.6 gives the BPSK, 4-QAM and 16-QAM SINR thresholds used in the simulations. The BPSK SINR thresholds were 4 dB lower than those necessary when using 4-QAM, while the 16-QAM SINR thresholds were 5.5 dB higher [93]. In other words, in moving from the BPSK modulation mode to the 4-QAM modulation mode, the target SINR, low quality outage SINR and outage SINR all increased by 4 dB. When switching to the 16-QAM mode from the 4-QAM mode, the SINR thresholds increased by 5.5 dB. However, setting the BPSK to 4-QAM and the 4-QAM to 16-QAM mode switching thresholds to a value 7 dB higher than the SINR required for maintaining the target BER/FER was necessary in order to prevent excessive outages due to sudden dramatic channel-induced variations in the SINR levels.

SINR Threshold	BPSK	4-QAM	16-QAM
Outage SINR	2.6 dB	6.6 dB	12.1 dB
Low Quality Outage SINR	3.0 dB	7.0 dB	12.5 dB
Target SINR	4.0 dB	8.0 dB	13.5 dB

Table 2.6: The target SINR, low quality outage SINR and outage SINR thresholds used for the BPSK, 4-QAM and 16-QAM modulation modes of the adaptive modem.

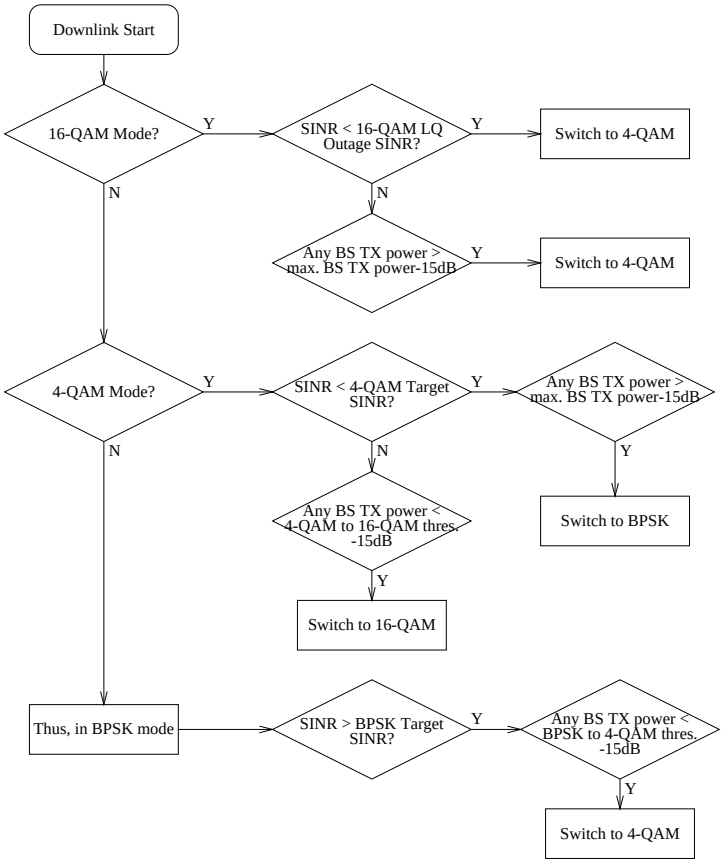

Figure 2.49: The AQAM mode switching algorithm used in the downlink of the CDMA based cellular network.

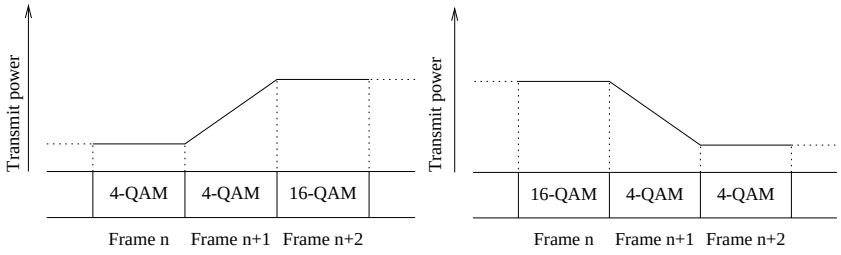

(a) Ramping up the transmit power whilst remaining in the lower order modulation mode.

(b) Ramping down the transmit power whilst switching to the lower order modulation mode.

Figure 2.50: Power rampimg requirements whilst switching modulation modes.

Performance results were obtained both with and without beamforming in a log-normal shadow fading environment, at maximum fading frequencies of 0.5 Hz and 1.0 Hz, and a standard deviation of 3 dB. A pedestrian velocity of 3 mph, a cell radius of 150 m and a spreading factor of 16 were used, as in our previous investigations.

Figure 2.51 shows the significant reduction in the probability of a dropped call, achieved by employing adaptive antenna arrays in conjunction with adaptive modulation in a log-normal shadow faded environment. The figure demonstrates that, even with the aid of a two element adaptive antenna array and its limited degrees of freedom, a substantial call dropping probability reduction was achieved. The performance benefit of increasing the array's degrees of freedom, achieved by increasing the number of antenna elements, becomes explicit from the figure, resulting in a further call dropping probability reduction. Simulations were conducted in conjunction with log-normal shadow fading having a standard deviation of 3 dB, and maximum shadowing frequencies of 0.5 Hz and 1.0 Hz. As expected, the call dropping probability was generally higher at the faster fading frequency, as demonstrated by Figure 2.51. The network was found to support 223 users, corresponding to a traffic load of 1.27 Erlang/km^2/MHz, when subjected to 0.5 Hz frequency shadow fading. The capacity of the network was reduced to 218 users, or 1.24 Erlang/km^2/MHz, upon increasing the maximum shadow fading frequency to 1.0 Hz. On employing two element adaptive antenna arrays, the network capacity increased by 64% to 366 users, or to an equivalent traffic load of 2.11 Erlang/km^2/MHz when subjected to 0.5 Hz frequency shadow fading. When the maximum shadow fading frequency was raised to 1.0 Hz, the number of users supported by the network was 341 users, or 1.98 Erlang/km^2/MHz, representing an increase of 56% in comparison to the network without adaptive antenna arrays. Increasing the number of antenna elements to four, whilst imposing shadow fading with a maximum frequency of 0.5 Hz, resulted in a network capacity of 2.68 Erlang/km^2/MHz or 476 users, corresponding to a gain of an extra 30% with respect to the network employing two element arrays, and of 113% in comparison to the network employing no adaptive antenna arrays. In conjunction with a maximum shadow fading frequency of 1.0 Hz the network capacity was 460 users or 2.59 Erlang/km^2/MHz, which represented an increase of 35% with respect to the network invoking two element antenna arrays, or 111% relative to the identical network without adaptive antenna arrays.

The probability of low quality outage, presented in Figure 2.52, did not benefit from the application of adaptive antenna arrays, or from the employment of adaptive modulation. Figure 2.47 depicts the probability of low quality outage without adaptive modulation, and upon comparing these results to those obtained in conjunction with adaptive modulation shown in Figure 2.52, the performance degradation due to adaptive modulation can be explicitly seen. However, the increase in the probability of low quality access can be attributed to the employment of less robust, but higher throughput, higher-order modulation modes invoked by the adaptive modulation scheme. Hence, under given propagation conditions and using the fixed 4-QAM modulation mode a low quality outage may not occur, yet when using adaptive modulation and a higher order modulation mode, the same propagation conditions may inflict a low quality outage. This phenomenon is further exacerbated by the adaptive antenna arrays, as described in Section 2.4.5, where the addition of a new source of

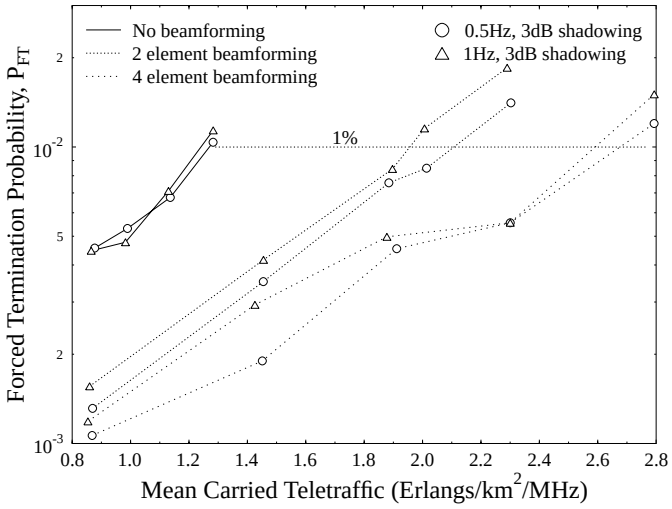

Figure 2.51: Call dropping probability versus mean carried traffic of a CDMA based cellular network using **relative received** E_c/I_o based soft handover thresholds both **with and without beamforming in conjunction with AQAM as well as with shadowing having a standard deviation of 3 dB** for SF=16. See Figure 2.46 for corresponding results without adaptive modulation.

interference, constituted by a user initiating a new call, results in an abrupt change in the gain of the antenna in the direction of the desired user. This in turn leads to low quality outages, which are more likely to occur for prolonged periods of time, when using a higher order modulation mode. Again, increasing the number of antenna elements from two to four results in an increased probability of a low quality outage due to the sharper antenna directivity. This results in a higher sensitivity to changes in the interference incident upon it.

The mean transmission power versus teletraffic performance is depicted in Figure 2.53, suggesting that the mean uplink transmission power was always significantly below the mean downlink transmission power, which can be attributed to the pilot power interference encountered by the mobiles in the downlink. This explanation can be confirmed by examining Figure 2.54, which demonstrates that the mean modem throughput in the downlink, without adaptive antenna arrays, was lower than that in the uplink even in conjunction with increased downlink transmission power. Invoking adaptive antenna arrays at the base stations reduced the mean uplink transmission power required in order to meet the service quality targets of the network. The attainable downlink power reduction increased as the number of antenna array elements increased, as a result of the superior interference rejection achieved with the aid of a higher number of array elements. A further advantage of employing a larger number of antenna array elements was the associated increase in the mean uplink modem

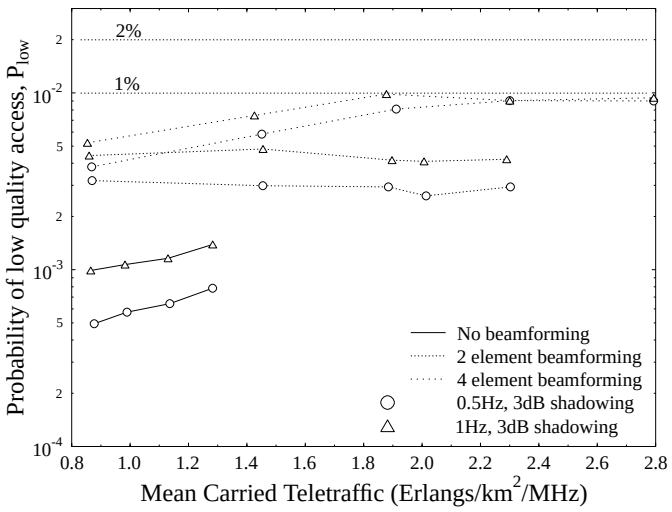

Figure 2.52: Probability of low quality access versus mean carried traffic of a CDMA based cellular network using **relative received** E_c/I_o based soft handover thresholds both **with and without beamforming in conjunction with AQAM as well as with shadowing having a standard deviation of 3 dB** for SF=16. See Figure 2.47 for corresponding results without adaptive modulation.

throughput, which became more significant at higher traffic loads. In the downlink scenario, however, increasing the number of adaptive antenna array elements led to an increased mean downlink transmission power, albeit with a substantially improved mean downlink modem throughput. This suggests that there was some interaction between the adaptive antenna arrays, the adaptive modulation mode switching algorithm and the maximal ratio combining performed at the mobiles. In contrast, simple switched diversity was performed by the base stations on the uplink, thus avoiding such a situation. However, the increase in the mean downlink transmission power resulted in a much more substantial increase in the mean downlink modem throughput, especially with the advent of the four element antenna arrays, which exhibited an approximately 0.5 BPS throughput gain over the two element arrays for identical high traffic loads which can be seen in Figure 2.54.

A summary of the maximum user capacities of the networks considered in this section in conjunction with log-normal shadowing having a standard deviation of 3 dB, with and without employing beamforming using two and four element arrays is given in Table 2.7. The teletraffic carried, the mean mobile and base station transmission powers required, and the mean up- and down-link modem data throughputs achieved are also shown in Table 2.7. Similarly, the lower bounds of the maximum network capacities obtained under identical scenarios in conjunction with a spreading factor of 256, leading to a bit rate of 15 kbps, suitable for speech-rate users are presented in

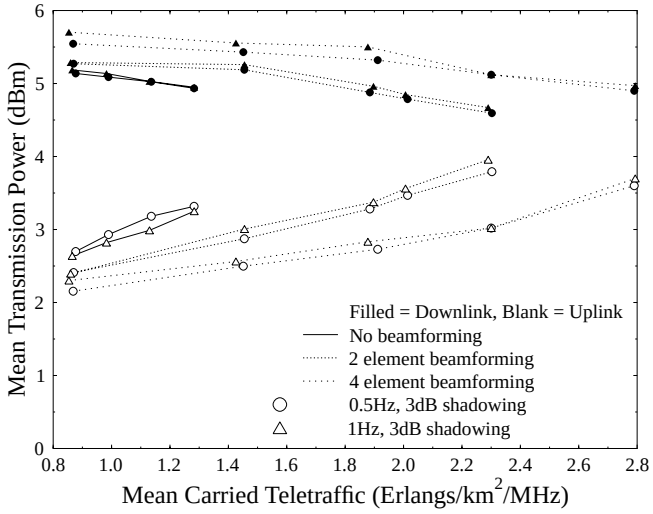

Figure 2.53: Mean transmission power versus mean carried traffic of a CDMA based cellular network using **relative received** E_c/I_o based soft handover thresholds both **with and without beamforming in conjunction with AQAM as well as with shadowing having a standard deviation of 3 dB** for SF=16. See Figure 2.48 for corresponding results without adaptive modulation.

Table 2.8. The network capacity calculations were performed by scaling the number of users supported, as presented in Table 2.7, by the ratio of their spreading factors, i.e. by 256/16=16.

2.5 Summary and Conclusions

We commenced this chapter with a brief overview of the background behind the 3G UTRA standard. This was followed in Sections 2.2 and 2.3 by an introduction to CDMA and the techniques invoked in the UTRA standard.

Network capacity studies were then conducted in Section 2.4, which evaluated the performance of four different soft handover algorithms in the context of both non-shadowed and log-normal shadow faded propagation environments. The algorithm using relative received pilot-to-interference ratio measurements at the mobile, in order to determine the most suitable base stations for soft handover, was found to offer the highest network capacity when subjected to shadow fading propagation conditions. Hence, this algorithm and its associated parameters, were selected for use in our further investigations. The impact of adaptive antenna arrays upon the network capacity was then considered in Section 2.4.5 in both non-shadowed and log-normal shadow faded propagation environments. Considerable network capacity gains were achieved, employing both two and four element adaptive antenna arrays. This

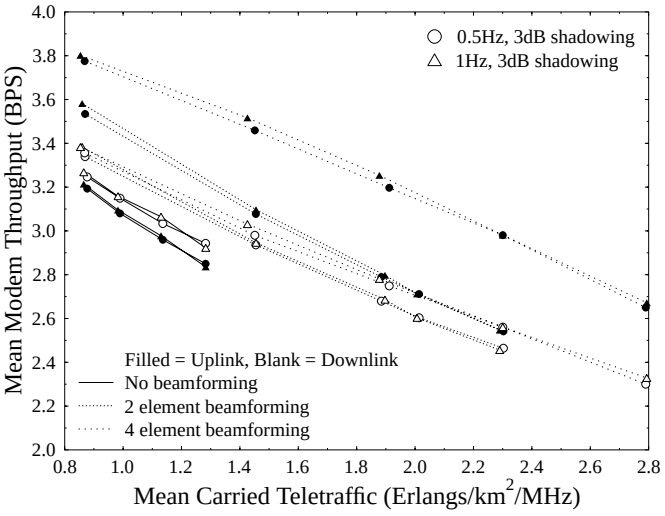

Figure 2.54: Mean modem throughput versus mean carried traffic of a CDMA based cellular network using **relative received** E_c/I_o based soft handover thresholds both **with and without beamforming in conjunction with AQAM as well as with shadowing having a standard deviation of 3 dB** for SF=16.

		Conservative scenario					
			Traffic (Erlangs	Power (dBm)		Throughput (BPS)	
Shadowing	Beamforming	Users	/km^2/MHz)	MS	BS	Uplink	Downlink
0.5 Hz, 3 dB	No	223	1.27	3.25	4.95	2.86	2.95
0.5 Hz, 3 dB	2 elements	366	2.11	3.55	4.7	2.56	2.66
0.5 Hz, 3 dB	4 elements	476	2.68	3.4	5.0	2.35	2.72
1.0 Hz, 3 dB	No	218	1.24	3.3	4.95	2.87	2.96
1.0 Hz, 3 dB	2 elements	341	1.98	3.5	4.9	2.62	2.73
1.0 Hz, 3 dB	4 elements	460	2.59	3.5	4.95	2.4	2.8

Table 2.7: Maximum mean carried traffic and maximum number of mobile users that can be supported by the network, whilst meeting the conservative quality constraints. The carried traffic is expressed in terms of normalised Erlangs (Erlang/km^2/MHz), for the network described in Table 2.2 both **with and without beamforming (using independent up/down-link beamforming), in conjunction with shadow fading having a standard deviation of 3 dB, whilst employing adaptive modulation techniques** for SF=16.

Shadowing	Beamforming	Conservative scenario Users	Conservative scenario Traffic (Erlangs /km^2/MHz)
0.5 Hz, 3 dB	No	3568	20.3
0.5 Hz, 3 dB	2 elements	5856	33.8
0.5 Hz, 3 dB	4 elements	7616	42.9
1.0 Hz, 3 dB	No	3488	19.8
1.0 Hz, 3 dB	2 elements	5456	31.7
1.0 Hz, 3 dB	4 elements	7360	41.4

Table 2.8: A lower bound estimate of the maximum mean carried traffic and maximum number of mobile **speech-rate** users that can be supported by the network, whilst meeting the conservative quality constraints. The carried traffic is expressed in terms of normalised Erlangs (Erlang/km^2/MHz), for the network described in Table 2.2 both **with and without beamforming (using independent up/down-link beamforming), in conjunction with shadow fading having a standard deviation of 3 dB, whilst employing adaptive modulation techniques** for SF=256. The number of users supported in conjunction with a spreading factor of 256 was calculated by multiplying the capacities obtained in Table 2.7 by 256/16=16.

work was then extended in Section 2.4.6 by the application of adaptive modulation techniques in conjunction with the previously studied adaptive antenna arrays in a log-normal shadow faded propagation environment, which elicited further significant network capacity gains.

Chapter 3

Conclusions and Further Research

3.1 Summary and Conclusions

In this book we have discussed the performance implications of adaptive antenna arrays and adaptive modulation techniques in both FDMA/TDMA and CDMA cellular mobile communications networks.

In Chapter ?? we investigated antenna arrays and adaptive beamforming algorithms. We commenced, in Section ??, by considering the possible applications of antenna arrays and their related benefits. The signal model used was then described in Section ?? and a rudimentary example of how beamforming operates was presented. Section ?? highlighted the process of adaptive beamforming using several different temporal reference techniques, along with the approaches used in spatial reference techniques. The challenges that must be overcome before beamforming for the downlink becomes feasible were also discussed in Section ??. Results were presented showing how the SMI, ULMS and NLMS beamforming algorithms behaved for a two element adaptive antenna in conjunction with varying eigenvalue spread and reference signal length. The SMI algorithm was shown to converge rapidly, irrespective of the eigenvalue spread. The performance of the ULMS beamformer was shown to be highly dependent upon the input signal power presented to the antenna, rendering it impractical. However, the NLMS algorithm was found to be far superior in this respect and it was later shown to approach the performance of the SMI beamformer for a three element adaptive array. A low SNR gives a poor estimate of the received signal's cross-correlation matrix, resulting in similar performance for all three algorithms. However, as the SNR improves, the SMI technique guarantees a stronger interference rejection. The SMI algorithm is more complex for a large number of antenna elements, but for a realistic number of elements, such as four, its complexity is below that of the LMS routines.

In Chapter ?? the performance gains achieved using adaptive antenna arrays at

the base stations in a cellular network were investigated for both LOS and multipath environments. A exposure to modelling an adaptive array was provided in Section ??, before an overview of fixed and dynamic channel allocation schemes was conducted in Section ?? . Section ?? then reviewed some of the different models available for simulating multipath environments, followed by a more detailed portrayal of the Geometrically Based Single-Bounce Elliptical Model (GBSBEM). The metrics used for characterising the performance of mobile cellular networks were presented under both LOS and multipath propagation conditions, with and without adaptive antenna arrays. The network capacity was found to increase, when using adaptive antenna arrays, with further increases achieved due to the adoption of power control. An adaptive modulation mode switching algorithm with combined power control was developed and network capacity investigations were conducted. Employing adaptive modulation using adaptive antenna arrays was found to increase the network's capacity significantly, whilst providing a superior call quality and a higher mean modem throughput.

Our investigations in Chapter ?? initially focused on the non-wraparound or "desert island" type networks, where the outer cells of the simulation area are subjected to lower levels of co-channel interference, a scenario that may be encountered in the suburbs of large conurbations. Simulations were carried out for the FCA algorithm, and the LOLIA using nearest base station constraints of 7 and 19, when exposed to LOS propagation conditions. The FCA algorithm offered the lowest network capacity, but benefited the most from employing adaptive antenna arrays. Specifically, the network capacity of FCA increased by 67%, when employing two element antenna arrays at the base stations, and 144%, when using four element arrays. The LOLIA using a nearest base station constraint of 7 cells supported a higher number of users, but the adaptive antenna arrays did not result in such dramatic improvements in network capacity. Explicitly, a 22% increase was observed for the two element case, and a 58% when using four elements. However, the network capacity supported by the LOLIA in conjunction with $n = 7$ always exceeded that of the FCA algorithm. When using a 19 base station constraint, the LOLIA resulted in the highest network capacity without employing adaptive antenna arrays, although the large frequency reuse distance of this algorithm led to a negligible increase in network capacity through.

We then conducted further simulations in Section ?? using a more realistic 3-ray multipath propagation environment. Again, the FCA algorithm supported the lowest number of users, and gained the most from invoking adaptive antenna arrays. Using a four element array instead of a two element array led to a network capacity increase of 35%, and replacing the four element array with one employing eight elements resulted in a 24-34% increase in the number of users supported. The LOLIA employing $n = 7$ supported the greatest number of users, but did not benefit from the same capacity increases as the FCA algorithm with the advent of adaptive antenna arrays. The number of users supported increased by 18% upon upgrading the system from two to four element adaptive antenna arrays, and by between 5% and 15% upon using eight element arrays in place of the four element arrays. Using a frequency reuse constraint of 19 in conjunction with the LOLIA resulted in a network whose capacity was restricted by the high new call blocking probability associated with its large frequency reuse distance. This large frequency reuse distance led to low levels of co-

channel interference, which could not be nulled effectively by the adaptive antenna arrays, and hence the network capacity did not increase by more than 5% upon doubling the number of antenna elements comprising the array. Hence, our future studies only considered the FCA algorithm and the LOLIA in conjunction with $n = 7$.

The network capacity gains accruing from the implementation of power control over the same 3-ray multipath channel, as in the previous section, were then investigated for the FCA algorithm and the LOLIA using $n = 7$. Significant network capacity increases were observed for all of the scenarios considered. Specifically, the network capacity without power control and using a given number of antenna elements, was frequently exceeded by that of an identical scenario using power control and half the number of antenna elements. On comparing otherwise identical scenarios, an increase in the network capacity of between 28% and 72% was attributed to the implementation of power control, whilst using the FCA algorithm. When employing the LOLIA and power control, the number of users supported increased by between 8.5% and 15%. The network capacity gains resulting from increasing the number of elements in the adaptive antenna arrays were reduced however, to 11% and 17% for the FCA algorithm. In contrast, the adaptive nature of the LOLIA enabled it to maintain the network capacity increases of 12-17%, achieved due to increasing the number of elements comprising the adaptive arrays.

The implementation of adaptive modulation techniques was then investigated in Section ??, since they allow the exploitation of good near-instantaneous channel conditions, whilst providing resilience when subjected to poor quality channels. The network capacity of the FCA algorithm was found to increase by 6-12%, when invoking adaptive modulation in conjunction with two element adaptive antenna arrays. However, when using four element adaptive antenna arrays the network capacity was reduced upon invoking adaptive modulation. This was due to the improved call dropping probability accruing from employing adaptive modulation, leading in turn to a lower number of frequency/timeslot combinations available for new calls. Since the new call blocking probability was the factor limiting the network's capacity, the capacity was reduced. This phenomenon was not observed, when employing the LOLIA, which supported 43% more users on average upon invoking adaptive modulation techniques. Doubling the number of antenna elements led to an extra 20% supported users.

In summary, the network using the FCA algorithm supported 2400 users, or 14 Er-langs/km^2/MHz, in the conservative scenario, and approximately 2735 users, or 15.6 Erlangs-/km^2/MHz, in the lenient scenario. When using the LOLIA 7 channel allocation algorithm and two element adaptive antenna arrays, 3675 users (23.1 Erlangs/km^2/MHz) were carried under the conservative conditions, and 4115 users (25.4 Erlangs/km^2/MHz) under the lenient specifications. When invoking four element adaptive antenna arrays, 4460 users (27.4 Erlangs/km^2/MHz) and 4940 users (29.6 Erlangs/km^2/MHz) were supported under the conservative and lenient scenarios, respectively.

In Section ?? our investigations then led us to consider results obtained for an infinite network using the so-called "wraparound" technique, which allows a cellular network to be simulated as if part of a much larger network, thus inflicting similar levels of co-channel interference upon all cells within the network. The FCA algo-

rithm again supported the lowest number of users, but benefited the most from the employment of adaptive antenna arrays, resulting in network capacity increases of between 46 and 70%, when employing adaptive antenna arrays, or when using four rather than two elements. The LOLIA using a nearest base station constraint of 7, supported an extra 17-23% of users due to the application of adaptive antenna arrays at the base stations. As in the "desert island" scenarios, the LOLIA in conjunction with a frequency reuse constraint of 19 base stations, offered the greatest network capacity without adaptive antenna arrays. However, when using two element arrays, the network capacity grew by almost 20%, since the limiting factor was the co-channel interference, not the new call blocking probability. The extra interference rejection potential offered by the four element arrays was also exploited, but was also somewhat limited, since the new call blocking probability became the capacity limiting constraint once again.

Under 3-ray multipath propagation conditions the network capacities of both the FCA algorithm and the LOLIAs were limited by the probability of low quality access, and hence invoking adaptive beamforming techniques increased the number of users supported. For an adaptive antenna array consisting of a given number of elements, the FCA algorithm supported the least number of users, and although exhibiting the greatest capacity gains due to the adaptive antenna arrays, the LOLIA 7 employing two element arrays exceeded the capacity of the FCA algorithm using eight element arrays. The LOLIA in conjunction with a frequency reuse of 19 base stations benefited from doubling the number of antenna elements from two, to four, and from four, to eight, but the network capacity was then limited by the new call blocking probability, and hence further increases in the number of antenna array elements would have had no impact on the network's capacity.

The addition of power control in the "infinite" network was then considered under the above 3-ray multipath conditions. The capacity gains were significant for both the FCA algorithm and the LOLIA 7, when compared to our identical investigations conducted without power control. Again, the network capacity when using the FCA algorithm benefited the most, with the number of users supported increasing by between 38 and 82%, exhibiting a mean increase of 61%. However, the LOLIA 7 based network still supported the greatest number of users, although the capacity gains of the power control were limited to around 12%.

The employment of adaptive modulation techniques led to the saturation of network resources for the FCA algorithm, with the network capacity limited by the number of frequency/timeslot combinations available for new calls. Hence, increasing the number of antenna elements from two to four resulted in an increase in the mean modem throughput from 2.4 BPS to 2.7 BPS, and a small reduction in the mean transmission power. The adaptive nature of the LOLIA allowed it to fully exploit the potential of adaptive modulation and supported more than 32% extra users. The limiting factor of the LOLIA's network capacity was the requirement of a minimum mean modem throughput of 2.0 BPS.

Therefore, the FCA algorithm supported 1400 users, and carried a teletraffic load of 13.8 Erlangs/km^2/MHz in the conservative scenario and 1570 users, or 15.2 Erlangs/km^2/MHz of traffic under the lenient conditions. The LOLIA however supported an extra 35% of users, giving a network capacity of 1910 users, or 19.75

Erlangs/km^2/MHz, when using two element adaptive antenna arrays for both the conservative and lenient scenarios. Utilising four element antenna arrays at the base stations allowed 2245 users, or 23.25 Erlangs/km^2/MHz of network traffic to be supported at the required quality levels of the conservative and lenient scenarios.

Thus, the network capacity was found to substantially increase, when using adaptive antenna arrays, with further increases achieved through the adoption of power control. An adaptive modulation mode switching algorithm combined with power control was developed and network simulations were conducted. Employing adaptive modulation in conjunction with adaptive antenna arrays was found to increase the network capacity significantly, whilst providing superior call quality and a greater mean modem throughput.

Chapter 2 examined the performance of a CDMA based cellular mobile network, very similar in its nature to the FDD-mode of the proposed UTRA standard. A comparison of various soft handover algorithms was conducted in both non-shadowed and shadowed propagation environments. The algorithm that was found to offer the highest network capacity, i.e. the highest number of users supported at a given quality of service, used the relative received E_c/I_o for determining cell ownership. The impact of using adaptive antenna arrays at the base stations was then investigated, in both non-shadowed and shadowed environments for high data rate users. This work was then extended by the application of adaptive modulation techniques, in conjunction with adaptive antenna arrays.

The network capacity in terms of the number of users supported, was 256 when experiencing no log-normal shadow fading and using no adaptive antenna arrays. However, with the application of two element adaptive antenna arrays the network capacity increased by 27% to 325 users, and when upgrading the system to four element arrays, the capacity of the network increased by a further 47% to 480 users. When subjected to log-normal shadow fading having a standard deviation of 3 dB in conjunction with a maximum fading frequency of 0.5 Hz, the network capacity without adaptive antennas was reduced to about 150 users. Again, invoking adaptive antenna arrays at the base stations increased the network capacity to 203 users, and 349 users, when employing two and four array elements, respectively.

We then applied independent up- and down-link beamforming. This implied determining separately the optimum weights for both the up- and the down-link, rather than re-using the antenna array weights calculated for the uplink scenario in the downlink. This measure led to further network capacity gains. Specifically, employing independent up- and down-link beamforming resulted in 15% and 7% network capacity increases, for the two and four element arrays, respectively, giving total network capacities of 349 and 375 users. Increasing the maximum shadow fading frequency from 0.5 Hz to 1.0 Hz slightly reduced the maximum number of users supported by the network, resulting in a network capacity of 144 users without beamforming, and capacities of 201 and 333 users, when invoking two and four element arrays, respectively. These absolute network capacity increases corresponded to relative network capacity gains of 40% and 131%, respectively. Again, performing independent up- and down-link beamforming increased the network capacities, with 225 and 365 users supported by the two and four element adaptive antenna arrays, respectively. Hence, these results show that applying both two and four element adaptive antenna arrays

have led to significant network capacity increases both with and without log-normal shadow fading. Furthermore, the capacity of the network was found to be reduced by approximately 40%, when subjected to log-normal shadow fading having a standard deviation of 3 dB. However, increasing the maximum log-normal fading frequency from 0.5 Hz to 1.0 Hz had little impact on the total network capacity.

These results were then extended by applying adaptive modulation techniques, both with and without adaptive antenna arrays, which were performing independent up- and down-link beamforming in conjunction with log-normal shadow fading having a standard deviation of 3 dB as well as maximum fading frequencies of 0.5 Hz and 1.0 Hz. Without adaptive antenna arrays the network supported 223 users, at a mean uplink modem throughput of 2.86 BPS. The mean throughput of the downlink was 2.95 BPS. Upon increasing the maximum shadowing frequency from 0.5 Hz to 1.0 Hz the network capacity fell slightly to 218 users, whilst the mean modem throughputs remained essentially unchanged. However, invoking two element adaptive antenna arrays enhanced the network capacities by 64% upon encountering 0.5 Hz shadow fading, and by 56% when subjected to 1.0 Hz shadowing. In both cases the mean modem throughput dropped by approximately 0.3 BPS. A further 0.2 BPS reduction of the mean modem throughput occurred, when applying four element adaptive antenna arrays. However, this allowed an extra 30% of users to be supported, when subjected to shadow fading fluctuating at a maximum frequency of 0.5 Hz and 35% in conjunction with 1.0 Hz frequency shadowing. Therefore, these results have shown the significant network capacity increases achieved by invoking adaptive modulation techniques. These network capacity improvements have been achieved in conjunction with a higher mean modem throughput, albeit at a slightly higher mean transmission power.

The performance results obtained for the UTRA-type network of Chapter 2 were obtained for high data rate users communicating at a raw data rate of 240 kbps, using a spreading factor of 16. However, as described in Section 2.4, some exploratory investigations not presented in this book demonstrated that the increase in the number of users supported by the network, was up to a factor of two higher than expected on the basis of simple spreading factor proportionate scaling. Specifically, the expected increase in switching from a spreading factor of 16 to 256 was a factor of 256/16=16, and hence Tables 2.5 and 2.8 were presented showing the potential worst-case network capacities achieved by multiplying the high data rate results by 16. Even when considering these user capacities, the teletraffic carried by the network normalised with respect to both the occupied bandwidth and the network's area, was found to be higher than that achieved by the FDMA/TDMA based networks considered in Chapter ??.

3.2 Further Research

Future research that builds upon the investigations considered here includes applying beamforming techniques to the pilot signals, or developing a method by which the pilot signals received at the mobile may be cancelled. In future systems the carrier frequency may be sufficiently high so that two antenna elements may be incorpo-

rated into the mobile handset, thus enabling beamforming to be performed at both ends of the data link. Further research is required for optimising the AQAM mode switching criteria, which could amalgamate the power control and beamforming algorithms. This could be further developed to a joint optimisation of the adaptive modulation mode switching, power control and beamforming, and potentially could also be incorporated into multi-user detection algorithms. Additionally, the performance of multi-rate networks is worthy of investigation, especially when combined with adaptive modulation and adaptive beam-forming techniques, which are particularly suitable for mitigating the significant levels of interference inflicted by the high data rate users. Since the high rate users impose the majority of interference on the numerous low rate users, the employment of interference reduction techniques is of vital importance. This book has only considered the employment of uniform linear antenna arrays having an antenna element spacing of $\lambda/2$. However, other antenna geometries, exhibiting no symmetry and possibly relying on antenna elements, which are not omni-directional may result is higher network capacity gains. More sophisticated propagation models tailored for different environments, such as macro- and pico-cells also have to be considered. The TDD mode of UTRA offers a further rich ground for system optimisation in conjunction with various time-slot allocation techniques, whilst endeavouring to maintain the advantages of the asymmetric uplink/downlink data rate nature of the TDD mode.

As a further topic, the network performance of High Altitude Platform Stations (HAPS) [103] remains to be investigated, especially in the context of adaptive modulation, and finally, future networks may be ad-hoc [103] in nature, which currently is a promising unexplored region of research.

Glossary

AWGN	Additive White Gaussian Noise
BS	A common abbreviation for Base Station
CDMA	Code Division Multiple Access
CMA	Constant Modulus Algorithm
DCS1800	A digital mobile radio system standard, based on GSM, but operates at 1.8GHz at a lower power.
DOA	Direction Of Arrival
FDD	Frequency Division Duplex
GSM	A Pan-European digital mobile radio standard, operating at 900MHz.
HIPERLAN	High Performance Radio Local Area Network
IF	Intermediate Frequency
LMS	Least Mean Square, a stochastic gradient algorithm used in adapting coefficients of a system
MS	A common abbreviation for Mobile Station
MSE	Mean Square Error, a criterion used to optimised the coefficients of a system such that the noise contained in the received signal is minimised.
PDF	Probability Density Function
RF	Radio Frequency
RLS	Recursive Least Square

SDMA	Spatial Division Multiple Access
SINR	Signal to Interference plus Noise ratio, same as signal to noise ratio (SNR) when there is no interference.
SIR	Signal to Interference ratio
SNR	Signal to Noise Ratio, noise energy compared to the signal energy
TDD	Time Division Duplex
TDMA	Time Division Multiple Access
UMTS	Universal Mobile Telecommunication System

Bibliography

[1] M. Barrett and R. Arnott, "Adaptive antennas for mobile communications," *IEE Electronics & Communications Engineering Journal*, pp. 203–214, August 1994.

[2] S. C. Swales, M. A. Beach, D. J. Edwards, and J. P. McGeehan, "The Performance Enhancement of Multibeam Adaptive Base-Station Antennas for Cellular Land Mobile Radio Systems," *IEEE Transactions on Vehicular Technology*, vol. 39, pp. 56–67, February 1990.

[3] J. Litva and T. Lo, *Digital Beamforming in Wireless Communications*. Artech House, London, 1996.

[4] A. B. Carlson, *Communication Systems*. McGraw-Hill, 1986.

[5] J. G. Proakis, *Digital Communications*. Mc-Graw Hill International Editions, 3 ed., 1995.

[6] L. C. Godara, "Applications of Antenna Arrays to Mobile Communications, Part I: Performance Improvement, Feasibility, and System Considerations," *Proceedings of the IEEE*, vol. 85, pp. 1029–1060, July 1997.

[7] G. V. Tsoulos and M. A. Beach, "Calibration and Linearity issues for an Adaptive Antenna System," in *IEEE Proceedings of Vehicular Technology Conference*, pp. 1597–1600, 1997.

[8] B. D. V. Veen and K. M. Buckley, "Beamforming: A Versatile Approach to Spatial Filtering," *IEEE ASSP Magazine*, pp. 4–24, April 1988.

[9] A. J. Paulraj and B. C. Ng, "Space-Time Modems for Wireless Personal Communications," *IEEE Personal Communications*, pp. 36–48, February 1998.

[10] A. J. Paulraj and E. Lindskog, "Taxonomy of space-time processing for wireless networks," *IEEE Proceedings on Radar, Sonar and Navigation*, vol. 145, pp. 25–31, February 1998.

[11] R. Steele and L. Hanzo, *Mobile Radio Communications*. IEEE Press - John Wiley, 2nd ed., 1999.

[12] W. T. Webb and L. Hanzo, *Modern Quadrature Amplitude Modulation: Principles and Applications for Wireless Communications*. IEEE Press-Pentech Press, 1994. ISBN 0-7273-1701-6.

[13] L. Hanzo, W. T. Webb, and T. Keller, *Single- and Multi-Carrier Quadrature Amplitude Modulation*. John-Wiley, IEEE Press, 2000.

[14] N. Anderson and P. Howard, "Technology and Transceiver Architecture Considerations for Adaptive Antenna Systems," in *Proceedings of ACTS Summit*, pp. 965–970, 1997.

[15] J. Strandell, M. Wennstrom, A. Rydberg, T. Oberg, O. Gladh, L. Rexberg, E. Sandberg, B. V. Andersson, and M. Appelgren, "Experimental Evaluation of an Adaptive Antenna for a TDMA Mobile Telephony System," in *Proceedings of PIMRC*, pp. 79–84, 1997.

[16] J. J. Monot, J. Thibault, P. Chevalier, F. Pipon, S. Mayrargue, and A. Levy, "A fully programmable prototype for the experimentation of the SDMA concept and and use of smart antennas for UMTS and GSM/DCS1800 networks," in *Proceedings of PIMRC*, (Helsinki, Finland), pp. 534–538, September 1997.

[17] M. Mizuno and T. Ohgane, "Application of Adaptive Array Antennas to Radio Communications," *Electronics and Communications in Japan, Part 1*, vol. 77, no. 2, pp. 48–56, 1994.

[18] Y. Ogawa and T. Ohgane, "Adaptive Antennas for Future Mobile Radio," *IEICE Trans. Fundamentals*, vol. E79-A, pp. 961–967, July 1996.

[19] G. V. Tsoulos, M. A. Beach, and S. C. Swales, "On the Sensitivity of the Capacity Enhancement of a TDMA system with Adaptive Multibeam Antennas," in *IEEE VTC Proceedings*, pp. 165–169, 1997.

[20] P. Leth-Espensen, P. E. Mogensen, F. Frederiksen, K. Olesen, and S. L. Larsen, "Performance of Different Combining Algorithms for a GSM System applying Antenna Arrays," in *Proceedings of ACTS Summit*, 1997.

[21] W. Jakes, ed., *Microwave Mobile Communications*. Wiley-Interscience, 1974.

[22] J. S. Blogh, P. J. Cherriman, and L. Hanzo, "Adaptive Beamforming Assisted Dynamic Channel Allocation," in *Proceedings of VTC*, (Houston, USA), pp. 199–203, May 1999.

[23] J. S. Blogh, P. J. Cherriman, and L. Hanzo, "Comparative Study of Dynamic Channel Allocation Algorithms," *IEEE Transactions on Vehicular Technology*, 2001.

[24] J. S. Blogh, P. J. Cherriman, and L. Hanzo, "Dynamic Channel Allocation Using Adaptive Antennas and Power Control," in *Proceedings of ACTS Mobile Communications Summit*, (Sorrento), pp. 943–948, June 1999.

[25] J. S. Blogh, P. J. Cherriman, and L. Hanzo, "Dynamic Channel Allocation Techniques using Adaptive Modulation and Adaptive Antennas," *Accepted for publication in IEEE Journal on Selected Areas in Communications*, 2001.

[26] J. S. Blogh, P. J. Cherriman, and L. Hanzo, "Dynamic Channel Allocation Techniques using Adaptive Modulation and Adaptive Antennas," in *Proceedings of VTC Fall*, (Amsterdam, The Netherlands), pp. 2348–2352, September 1999.

[27] L. Hanzo, "Bandwidth-efficient wireless multimedia communications," *Proceedings of the IEEE*, vol. 86, pp. 1342–1382, July 1998.

[28] S. Nanda, K. Balachandran, and S. Kumar, "Adaptation techniques in wireless packet data services," *IEEE Communications Magazine*, vol. 38, pp. 54–64, January 2000.

[29] L. Hanzo, P. Cherriman, and J. Streit, *Video Compression and Communications over Wireless Channels: From Second to Third Generation Systems and Beyond*. IEEE Press, 2001. (For detailed contents please refer to http://www-mobile.ecs.soton.ac.uk.).

[30] Research and Development Centre for Radio Systems, Japan, *Public Digital Cellular (PDC) Standard, RCR STD-27*.

[31] Telcomm. Industry Association (TIA), Washington, DC, USA, *Dual-mode subscriber equipment — Network equipment compatibility specification, Interim Standard IS-54*, 1989.

[32] Telcomm. Industry Association (TIA), Washington, DC, USA, *Mobile station — Base station compatibility standard for dual-mode wideband spread spectrum cellular system, EIA/TIA Interim Standard IS-95*, 1993.

[33] D. Knisely, S. Kumar, S. Laha, and S. Nanda, "Evolution of wireless data services : IS-95 to cdma2000," *IEEE Communications Magazine*, vol. 36, pp. 140–149, October 1998.

[34] T. Ojanperä and R. Prasad, *Wideband CDMA for Third Generation Mobile Communications*. Artech House, Inc., 1998.

[35] W. Webb and R. Steele, "Variable rate QAM for mobile radio," *IEEE Transactions on Communications*, vol. 43, no. 7, pp. 2223–2230, 1995.

[36] S. Sampei, S. Komaki, and N. Morinaga, "Adaptive Modulation/TDMA scheme for large capacity personal multimedia communications systems," *IEICE Transactions on Communications*, vol. E77-B, pp. 1096–1103, September 1994.

[37] J. M. Torrance and L. Hanzo, "Upper bound performance of adaptive modulation in a slow Rayleigh fading channel," *Electronics Letters*, vol. 32, pp. 718–719, 11 April 1996.

[38] C. Wong and L. Hanzo, "Upper-bound performance of a wideband burst-by-burst adaptive modem," *IEEE Transactions on Communications*, vol. 48, pp. 367–369, March 2000.

[39] J. M. Torrance and L. Hanzo, "Optimisation of switching levels for adaptive modulation in a slow Rayleigh fading channel," *Electronics Letters*, vol. 32, pp. 1167–1169, 20 June 1996.

[40] H. Matsuoka, S. Sampei, N. Morinaga, and Y. Kamio, "Adaptive modulation system with variable coding rate concatenated code for high quality multi-media communications systems," in *Proceedings of IEEE VTC '96* [105], pp. 487–491.

[41] A. J. Goldsmith and S. G. Chua, "Variable Rate Variable Power MQAM for Fading Channels," *IEEE Transactions on Communications*, vol. 45, pp. 1218–1230, October 1997.

[42] S. Otsuki, S. Sampei, and N. Morinaga, "Square-qam adaptive modulation/TDMA/TDD systems using modulation estimation level with walsh function," *IEE Electronics Letters*, vol. 31, pp. 169–171, February 1995.

[43] J. Torrance and L. Hanzo, "Demodulation level selection in adaptive modulation," *Electronics Letters*, vol. 32, pp. 1751–1752, 12 September 1996.

[44] Y. Kamio, S. Sampei, H. Sasaoka, and N. Morinaga, "Performance of modulation-level-control adaptive-modulation under limited transmission delay time for land mobile communications," in *Proceedings of IEEE Vehicular Technology Conference (VTC'95)*, (Chicago, USA), pp. 221–225, IEEE, 15–28 July 1995.

[45] J. M. Torrance and L. Hanzo, "Latency and Networking Aspects of Adaptive Modems over Slow Indoors Rayleigh Fading Channels," *IEEE Transactions on Vehicular Technology*, vol. 48, pp. 1237–1251, July 1999.

[46] T. Ue, S. Sampei, and N. Morinaga, "Symbol rate controlled adaptive modulation/TDMA/TDD for wireless personal communication systems," *IEICE Transactions on Communications*, vol. E78-B, pp. 1117–1124, August 1995.

[47] T. Suzuki, S. Sampei, and N. Morinaga, "Space and path diversity combining technique for 10 Mbits/s adaptive modulation/TDMA in wireless communications systems," in *Proceedings of IEEE VTC '96* [105], pp. 1003–1007.

[48] K. Arimochi, S. Sampei, and N. Morinaga, "Adaptive modulation system with discrete power control and predistortion-type non-linear compensation for high spectral efficient and high power efficient wireless communication systems," pp. 472–477.

[49] T. Ikeda, S. Sampei, and N. Morinaga, "TDMA-based adaptive modulation with dynamic channel assignment (AMDCA) for high capacity multi-media microcellular systems," in *Proceedings of IEEE Vehicular Technology Conference*, (Phoenix, USA), pp. 1479–1483, May 1997.

[50] T. Ue, S. Sampei, and N. Morinaga, "Adaptive modulation packet radio communication system using NP-CSMA/TDD scheme," in *Proceedings of IEEE VTC '96* [105], pp. 416–421.

[51] M. Naijoh, S. Sampei, N. Morinaga, and Y. Kamio, "ARQ schemes with adaptive modulation/TDMA/TDD systems for wireless multimedia communication systems," pp. 709–713.

[52] S. Sampei, T. Ue, N. Morinaga, and K. Hamguchi, "Laboratory experimental results of an adaptive modulation TDMA/TDD for wireless multimedia communication systems," pp. 467–471.

[53] J. Torrance and L. Hanzo, "Interference aspects of adaptive modems over slow Rayleigh fading channels," *IEEE Transactions on Vehicular Technology*, vol. 48, pp. 1527–1545, September 1999.

[54] C. Berrou and A. Glavieux, "Near optimum error correcting coding and decoding: turbo codes," *IEEE Transactions on Communications*, vol. 44, pp. 1261–1271, October 1996.

[55] J. Cheung and R. Steele, "Soft-decision feedback equalizer for continuous-phase modulated signals in wide-band mobile radio channels," *IEEE Transactions on Communications*, vol. 42, pp. 1628–1638, February/March/April 1994.

[56] M. Yee, T. Liew, and L. Hanzo, "Radial basis function decision feedback equalisation assisted block turbo burst-by-burst adaptive modems," in *Proceedings of VTC '99 Fall*, (Amsterdam, Holland), pp. 1600–1604, 19-22 September 1999.

[57] M. S. Yee, B. L. Yeap, and L. Hanzo, "Radial basis function assisted turbo equalisation," in *Proceedings of IEEE Vehicular Technology Conference*, (Japan, Tokyo), pp. 640–644, IEEE, 15-18 May 2000.

[58] L. Hanzo, F. Somerville, and J. Woodard, "Voice compression and communications: Principles and applications for fixed and wireless channels." 2001 (For detailed contents, please refer to http://www-mobile.ecs.soton.ac.uk.).

[59] ITU-T, *Recommendation H.263: Video coding for low bitrate communication*, March 1996.

[60] "COST 207: Digital land mobile radio communications, final report." Office for Official Publications of the European Communities, 1989. Luxembourg.

[61] A. Klein, R. Pirhonen, J. Skoeld, and R. Suoranta, "FRAMES multiple access mode 1 — wideband TDMA with and without spreading," vol. 1, pp. 37–41.

[62] P. Cherriman, C. Wong, and L. Hanzo, "Turbo- and BCH-coded wide-band burst-by-burst adaptive H.263-assisted wireless video telephony," *IEEE Transactions on Circuits and Systems for Video Technology*, vol. 10, pp. 1355–1363, December 2000.

[63] T. Keller and L. Hanzo, "Adaptive multicarrier modulation: A convenient framework for time-frequency processing in wireless communications," *Proceedings of the IEEE*, vol. 88, pp. 611–642, May 2000.

[64] A. Klein and P. Baier, "Linear unbiased data estimation in mobile radio sytems applying CDMA," *IEEE Journal on Selected Areas in Communications*, vol. 11, pp. 1058–1066, September 1993.

[65] K. Gilhousen, I. Jacobs, R. Padovani, A. Viterbi, L. Weaver Jr., and C. Wheatley III, "On the capacity of a cellular CDMA system," *IEEE Transactions on Vehicular Technology*, vol. 40, pp. 303–312, May 1991.

[66] S. Kim, "Adaptive rate and power DS/CDMA communications in fading channels," *IEEE Communications Letters*, vol. 3, pp. 85–87, April 1999.

[67] T. Ottosson and A. Svensson, "On schemes for multirate support in DS-CDMA systems," *Wireless Personal Communications (Kluwer)*, vol. 6, pp. 265–287, March 1998.

[68] S. Ramakrishna and J. Holtzman, "A comparison between single code and multiple code transmission schemes in a CDMA system," pp. 791–795.

[69] M. Saquib and R. Yates, "Decorrelating detectors for a dual rate synchronous DS/CDMAchannel," *Wireless Personal Communications (Kluwer)*, vol. 9, pp. 197–216, May 1999.

[70] A.-L. Johansson and A. Svensson, "Successive interference cancellation schemes in multi-rateDS/CDMA systems," in *Wireless Information Networks (Baltzer)*, pp. 265–279, 1996.

[71] S. Abeta, S. Sampei, and N. Morinaga, "Channel activation with adaptive coding rate and processing gain control for cellular DS/CDMA systems," in *Proceedings of IEEE VTC '96* [105], pp. 1115–1119.

[72] M. Hashimoto, S. Sampei, and N. Morinaga, "Forward and reverse link capacity enhancement of DS/CDMA cellular system using channel activation and soft power control techniques," pp. 246–250.

[73] T. Liew, C. Wong, and L. Hanzo, "Block turbo coded burst-by-burst adaptive modems," in *Proceedings of Microcoll'99, Budapest, Hungary*, pp. 59–62, 21–24 March 1999.

[74] L. Hanzo, P. Cherriman, and J. Streit, *Wireless Video Communications: From Second to Third Generation Systems, WLANs and Beyond.* IEEE Press-John Wiley, 2001. IEEE Press, 2001. (For detailed contents please refer to http://www-mobile.ecs.soton.ac.uk.).

[75] P. Cherriman and L. Hanzo, "Programmable H.263-based wireless video transceivers for interference-limited environments," *IEEE Trans. on Circuits and Systems for Video Technology*, vol. 8, pp. 275–286, June 1998.

[76] E. Kuan and L. Hanzo, "Joint detection CDMA techniques for third-generation transceivers," in *Proceeding of ACTS Mobile Communication Summit '98*, (Rhodes, Greece), pp. 727–732, ACTS, 8–11 June 1998.

[77] V. Tarokh, N. Seshadri, and A. Calderbank, "Space-time codes for high data rate wireless communication: Performance criterion and code construction," *IEEE Transactions on Information Theory*, vol. 44, pp. 744–765, March 1998.

[78] V. Tarokh, A. Naguib, N. Seshadri, and A. Calderbank, "Space-time codes for high data rate wireless communication: Performance criteria in the presence of channel estimation errors, mobility, and multiple paths," *IEEE Transactions on Communications*, vol. 47, pp. 199–207, February 1999.

[79] V. Tarokh, N. Seshadri, and A. Calderbank, "Space-time codes for high data rate wireless communications: Performance criterion and code construction," in *Proc IEEE International Conference on Communications '97*, (Montreal, Canada), pp. 299–303, 1997.

[80] V. Tarokh, H. Jafarkhani, and A. Calderbank, "Space-time block codes from orthogonal designs," *IEEE Transactions on Information Theory*, vol. 45, pp. 1456–1467, July 1999.

[81] H. Holma and A. Toskala, eds., *WCDMA for UMTS : Radio Access for Third Generation Mobile Communications.* John Wiley & Sons, Ltd., 2000.

[82] "3rd Generation Partnership Project; Technical Specification Group Radio Access Network; Spreading and modulation (FDD)." 3G TS 25.213 V3.2.0 (2000-03).

[83] F. Adachi, M. Sawahashi, and K. Okawa, "Tree-structured Generation of Orthogonal Spreading Codes with Different Lengths for Forward Link of DS-CDMA Mobile," *Electronics Letters*, vol. 33, no. 1, pp. 27–28, 1997.

[84] "3rd Generation Partnership Project; Technical Specification Group Radio Access Network; Physical layer procedures (FDD)." 3G TS 25.214 V3.2.0 (2000-03).

[85] S. Verdú, *Multiuser Detection*. Cambridge University Press, 1998.

[86] A. D. Whalen, *Detection of signals in noise*. Academic Press, 1971.

[87] W. T. Webb and L. Hanzo, *Modern Quadrature Amplitude Modulation : Principles and Applications for Fixed and Wireless Channels*. John Wiley and IEEE Press, 1994.

[88] M. Dell'Anna and A. H. Aghvami, "Performance of optimum and sub-optimum combining at the antenna array of a W-CDMA system," *IEEE Journal on Selected Areas in Communications*, pp. 2123–2137, December 1999.

[89] R. L. Pickholtz, L. B. Milstein, and D. L. Schilling, "Spread spectrum for mobile communications," *IEEE Transactions on Vehicular Technology*, vol. 40, pp. 313–322, May 1991.

[90] K. S. Gilhousen, I. M. Jacobs, R. Padovani, A. J. Viterbi, L. A. Weaver, and C. E. Wheatley, "On the capacity of a cellular CDMA system design," *IEEE Transactions on Vehicular Technology*, vol. 40, pp. 303–312, May 1991.

[91] L. Wang and A. H. Aghvami, "Optimal power allocation based on QoS balance for a multi-rate packet CDMA system with multi-media traffic," in *Proceedings of Globecom*, (Rio de Janeiro, Brazil), pp. 2778–2782, December 1999.

[92] D. Koulakiotis and A. H. Aghvami, "Data detection techniques for DS/CDMA mobile systems: A review," *IEEE Personal Communications*, pp. 24–34, June 2000.

[93] P. J. Cherriman, E. L. Kuan, and L. Hanzo, "Burst-by-burst adaptive joint-detection CDMA/H.263 based video telephony," in *Proceedings of the ACTS Mobile Communications Summit, Sorrento, Italy*, pp. 715–720, June 1999.

[94] J. Laiho-Steffens, A. Wacker, and P. Aikio, "The Impact of the Radio Network Planning and Site Configuration on the WCDMA Network Capacity and Quality of Service," in *IEEE Proceedings of Vehicular Technology Conference*, (Tokyo, Japan), pp. 1006–1010, 2000.

[95] R. D. Kimmo Hiltunen, "WCDMA Downlink Capacity Estimation," in *IEEE Proceedings of Vehicular Technology Conference*, (Tokyo, Japan), pp. 992–996, 2000.

[96] K. Sipilä, Z.-C. Honkasalo, J. Laiho-Steffens, and A. Wacker, "Estimation of Capacity and Required Transmission Power of WCDMA Downlink Based on a Downlink Pole Equation," in *IEEE Proceedings of Vehicular Technology Conference*, (Tokyo, Japan), pp. 1002–1005, 2000.

[97] M. L. Cheng and J. I. Chuang, "Performance evaluation of distributed measurement-based dynamic channel assignment in local wireless communications," *IEEE JSAC*, vol. 14, pp. 698–710, May 1996.

[98] "GSM 06.90: Digital cellular telecommunications system (Phase 2+)." Adaptive Multi-Rate (AMR) speech transcoding, version 7.0.0, Release 1998.

[99] S. Bruhn, E. Ekudden, and K. Hellwig, "Adaptive Multi-Rate: A new speech service for GSM and beyond," in *Proceedings of 3rd ITG Conference on Source and Channel Coding*, (Technical Univ. Munich, Germany), pp. 319–324, 17th-19th, January 2000.

[100] S. Bruhn, P. Blocher, K. Hellwig, and J. Sjoberg, "Concepts and Solutions for Link Adaptation and Inband Signalling for the GSM AMR Speech Coding Standard," in *Proceedings of VTC*, (Houston, Texas, USA), 16-20 May 1999.

[101] T. Ojanperä and R. Prasad, ed., *Wideband CDMA for 3rd Generation Mobile Communications*. Artech House Publishers, 1998.

[102] R. Owen, P. Jones, S. Dehgan, and D. Lister, "Uplink WCDMA capacity and range as a function of inter-to-intra cell interference: theory and practice," in *IEEE Proceedings of Vehicular Technology Conference*, vol. 1, (Tokyo, Japan), pp. 298–303, 2000.

[103] B. G. Evans and K. Baughan, "Visions of 4G," *IEE Electronics and Communication Engineering Journal*, vol. 12, pp. 293–303, December 2000.

[104] W. Tuttlebee, ed., *Cordless telecommunications in Europe : the evolution of personal communications*. London: Springer-Verlag, 1990. ISBN 3540196331.

[105] IEEE, *Proceedings of IEEE VTC '96*, (Atlanta, GA, USA), 1996.